IPL

escola superior de tecnologia e gestão
instituto politécnico de leiria

Process Parameter Optimization of FFF 3D Printed Parts

Project

Master's Degree in Mechanical Engineering – Industrial Production

Supervisors Professors: Joel Vasco, Dino Freitas and Miranda Fateri

Academic Year 2021/2022

Carolina Neves Cordeiro Coutinho da Costa
2201581@my.ipleiria.pt

Leiria, September 2022

Abstract

This work aimed to create a Metal Additive Manufacturing technique, namely Fused Filament Fabrication (FFF), to find the ideal parameters for the printing of 316L stainless steel. The work consisted of adapting and developing the process parameters of FFF to produce tensile specimens. These parameters included the infill pattern, density, printing angle and support structures. In addition, several tests were done, like tensile, surface roughness, and microscopic analysis, to validate the imposed parameters.

After gathering the best parameters, a part from the automotive industry was printed to optimise the parameters, and cost analysis was compared with SLM technology. Thus, in this dissertation, the process parameter optimization of the FFF technology was made.

Keywords: Fused Filament Fabrication, Additive Manufacturing, Stainless Steel, Infill, Support Structures.

Acknowledgements

Throughout this thesis, there were several people whose support was essential to me. Firstly, I want to thank the professor who made all this work and experience possible, Professor Joel Vasco. I want to thank him for being available to follow my work throughout the semester from the beginning and for all the method, rigour and ambition he transferred to me. Next, thanks to professor Dino Freitas who also contributed to this work and professor Miranda Fateri for coordinating practical component of this work, for all the knowledge she gave me and for the constant availability for any questions.

Colleagues were also important, so I want to thank Sebastian Uhl and Juan Carlos Palomares for all the help shown throughout this period. I would also like to thank my colleague Catarina Bento with whom I had the opportunity to share Erasmus's experience and part of the laboratory work done this semester.

I want to thank Aalen University and everyone who works there for being so well received and for the opportunity to do my thesis on their facilities.

Besides the people directly involved in this thesis, I also want to thank those in my personal life. Who contributed to this work in one way or another. Thus, I thank my boyfriend for understanding my ambition to do my thesis in another country, showing me the simplicity of things and my value in the most challenging moments. I thank my sister, who is and always will be my role model, and, even without knowing, inspires me to be a brave, warrior and independent woman just like her. Finally, I want to thank from the bottom of my heart to the people who made all my academic paths possible, my parents. Without a doubt, my parents are the reason I have come this far, either for all the investment they have put in me or for never having stopped believing in my capacities and dreams.

Table of contents

Figures List

Tables List

List of acronyms and abbreviations

AM	Additive Manufacturing
BJT	Binder Jetting
DLP	Digital Light Processing
DOD	Drop On Demand
EBM	Electron Beam Melting
ESTG	Escola Superior de Tecnologia e Gestão
FDM	Fused Deposition Modelling
FFF	Fused Filament Fabrication
MJT	Material Jetting
MJF	Multi Jet Fusion
NPJ	NanoParticle Jetting
SHL	Sheet Lamination
SLA	Stereolithography
SLM	Selective Laser Melting
SLS	Selective Laser Sintering
VPP	Vat Photopolymerization

1. **Introduction**

Currently, most worldwide research into additive manufacturing (AM) is towards a greener approach to avoid waste and create complex geometric parts. In addition, this type of manufacturing is progressive, replacing some conventional manufacturing processes since it is an excellent option to produce components in a sustainable and environmentally friendly way. Although AM is still much more widely used for polymeric materials, the use of ceramic and metallic materials is increasing significantly. Thus it becomes necessary for companies to keep up with the evolution of additive manufacturing.

The present work results from a curricular internship held at Aalen University in Germany. This university focuses heavily on engineering courses since the entire state of Baden-Württemberg is an industrialised zone with renowned companies. As a result, Aalen University offers excellence in both teaching and research. It also boasts several technically rich facilities, including advanced scientific laboratories.

This report is divided into six chapters, the first of which is the introduction. The second chapter is dedicated to an in-depth study of additive manufacturing, its categories and inherent processes with special focus on Fused Filament Fabrication technology for metal printing. The third chapter is dedicated to the presentation of the materials and equipment used, as well as the development of the methods used in the practical work. Moving on to chapter four where the results obtained from the tests performed in the previous chapter are discussed. Chapter five focuses on the printing of a part using the parameters used previously and also to understand the viability of the FFF technology in comparison with the SLM technology. And lastly chapter six is the conclusion.

This work will focus on the FFF (Fused Filament Fabrication) technology to manufacture stainless steel components. The main aim of this project is to find the ideal parameters to produce metallic parts through the FFF technology using BASF Ultrafuse 316L, a relatively new material in the market. The strategies to be used focus on the printing stage, where different densities, infill patterns, angles and types of support structures will be used to understand the impact of variation of these parameters on the properties of the final product.

So, after the parts are produced, microstructural and mechanical characterizations will be carried out to determine the combination of parameters that renders the best results. First, microstructure analysis was performed of the different infill patterns of the parts. Then tensile and surface roughness tests were performed to assess the mechanical properties of the parts. These tests' results made it possible to reach parameter optimisation.

Finally, with the parameters that obtained the best results, an industry part will be manufactured, a cost analysis will be made, and a comparison with the competitor, Selective Laser Melting.

2. Literature review

2.1. Additive Manufacturing

Additive manufacturing (AM), also known as 3D printing, is defined as the "process of joining materials to make 3D model data, usually layer upon layer, in contrast to subtractive manufacturing and formative manufacturing methodologies" (ISO/ASTM, 2021).

In 1983, Charles Hull invented the first Stereolithography (SLA) machine, and later in 1986, Hull was granted the first patent in 3D printing.

After SLA, in 1987 it was developed a new technology, Selective Laser Sintering (SLS), by Carl Deckard. This technology was based on SLA, which consists of using a high-power laser to sinter small particles of polymer powder into a solid structure based on a 3D model.

In 1989, Scott and Lisa Crump filed a patent for fused deposition modelling (FDM), an additive manufacturing method where layers of materials are fused in a pattern to create an object. Also, in 1989, Hans Langer established EOS GmbH in Germany and became an industry leader in laser sintering research (González, 2020).

Later, in 1995, SLM was initially developed at the Fraunhofer Institute for Laser Technology (ILT) in Aachen, Germany. Then, Dr Dieter Schwarze and Dr Matthias Fockele formed F&S Stereolithographietechnik GmbH and worked with other ILT research members to develop today's commercial technology. However, only in 1997 was first patented and applied to the German Patent and Trade Mark.

In 1997, AeroMat developed the first 3D printed metal process called laser additive manufacturing (LAM), which used a high-power laser and powdered titanium alloys (Gornet, 2017).

In 1999, the first 3D-printed organ was transplanted into a human. Created by scientists at Wake Forest Institute for Regenerative Medicine, a human bladder was printed, covered in the recipient's cells, and then implanted. It was a scientific breakthrough; because the device used the patient's cells; therefore, the possibility of implant rejection was minimal. Even today there is a possibility that the organ is rejected, but this possibility is minimal. Later in 2002, it was printed the first kidney.

In 2003, the first commercial Electron Beam Melting (EBM) System was launched. This system melts metal powder together, layer by layer, using an electron beam in a high-temperature vacuum. Still, this year, EOS introduced the first laser-based system for metal powder.

In 2005, Dr Adrian Bowyer invented the RepRap open-source concept to create a self-replicating 3D printer process. This event opened the doors for creating several new 3D printers (González, 2020).

In 2008, Shapeways rolled out its service to the world. The company gives consumers a relatively easy way to convert 3D designs into parts or products. In addition, Shapeways offers a range of "creator" tools that simplify designing custom consumer products (Gornet, 2017).

In 2011, in the United Kingdom, the university of Southampton designed and 3D printed the first unmanned 3D printed aircraft, and Kor Ecologic unveiled the Urbee, a prototype car with a 3D printed body, at the TEDXWinnipeg conference.

In 2015, Cellink, a Swedish company, introduced the first standardized commercial bio-ink derived from a seaweed material called non-cellulose alginate. The bio-ink can be used for printing tissue cartilage. Later in the year, Cellink releases the INKREDIBLE 3D printer for bioprinting services, creating an affordable market for bioprinting (González, 2020).

In 2019, with the expiration of patents and open-source projects, there were over 170 3D printer system manufacturers worldwide. This list includes 3D Systems, Stratasys, Fusion3, Formlabs, Desktop Metal, Prusa, and Voxel8, among many others (González, 2020).

Throughout the timeline of additive manufacturing, some technologies have marked the beginning and the development of AM. Thus, the best-known processes responsible for the rise of AM are those shown in Figure 1.
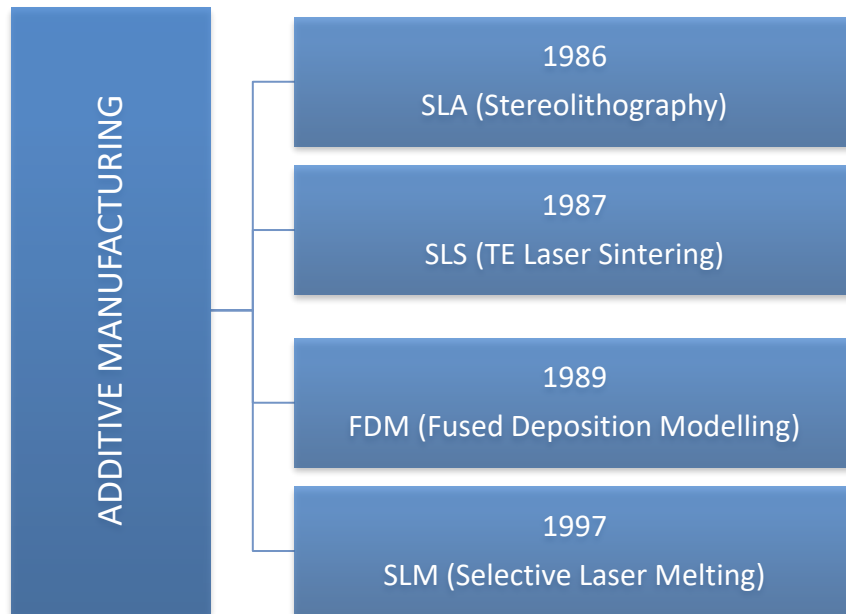
Figure 1 - Additive Manufacturing first processes

Nowadays, the costs of 3D printers are falling phenomenally. Thus, making the technology increasingly available to the average consumer and laying the foundations for a potential explosion in the home inventor and DIY (do it yourself) markets.

AM is evolving since it increasingly meets people's needs. Two professional groups influenced by 3D printing are designers and engineers since they have a new way of thinking about parts through DfAM (Design for Additive Manufacturing). DfAM is the practice of designing and optimizing a product together with its production system to reduce development time and cost and increase performance, quality, and profitability. This is done considering design goals and manufacturing constraints, for example, the user and market needs, materials, processes, and assembly and disassembly methods. It is an entirely new mindset for designers compared to conventional design thinking.

2.2. Additive manufacturing standards

The standards for additive manufacturing were developed in 2012 by the ASTM F42 and ISO TC261 subcommittees. These standards result from cooperation between the leading standardization organizations ASTM (the American Society for Testing and Materials) and ISO (International Organization for Standardization). Establishing standards and norms for relatively new additive manufacturing technology required an alliance between competing organizations (Dubert, 2020).

The International Standard ISO/ASTM 52900:2021 was created to provide a basic understanding of the fundamental principles of additive manufacturing processes, materials, and files. Based on this, it was given clear definitions for terms and nomenclature associated with additive manufacturing technology. This standardization of terminology for additive manufacturing aims to facilitate communication between people involved in this technology field worldwide (ISO/ASTM, 2021).

The introduced standards falling under the jurisdiction of the F42.07 subcommittee are:

- ISO / ASTM52942-20 Additive Manufacturing – Qualification Rules – Qualification of Powder Bed Fusion Machine and Equipment Operators for Metals and Additive Manufactured Components for Aerospace Applications
- ISO / ASTM52941-20 Additive Manufacturing – System Performance and Reliability – Laser Beam Powder Bed Fusion Machine Acceptance Testing for Aerospace Metallic Materials.

The additive manufacturing standard currently in effect is the "ISO/ASTM 52900:2021".

2.3. Additive manufacturing categories and processes

AM is constantly evolving, and new technologies are being created to meet the market's needs. For this reason, the standard "ISO/ASTM 52900:2021" had to create categories to distinguish all AM technologies. Thus, AM technologies can be split into two groups: direct and indirect 3D printing. The main difference lies in the fact that the design is directly made from 3D printing (direct), or 3D printing was used in the process of creating your model (indirect) (Experience, 2022).

The categories defined by the standard are as follows: Vat photopolymerization, Material extrusion, material jetting, binder jetting, powder bed fusion, direct energy deposition and sheet lamination. In Figure 2, it is possible to see the different groups.
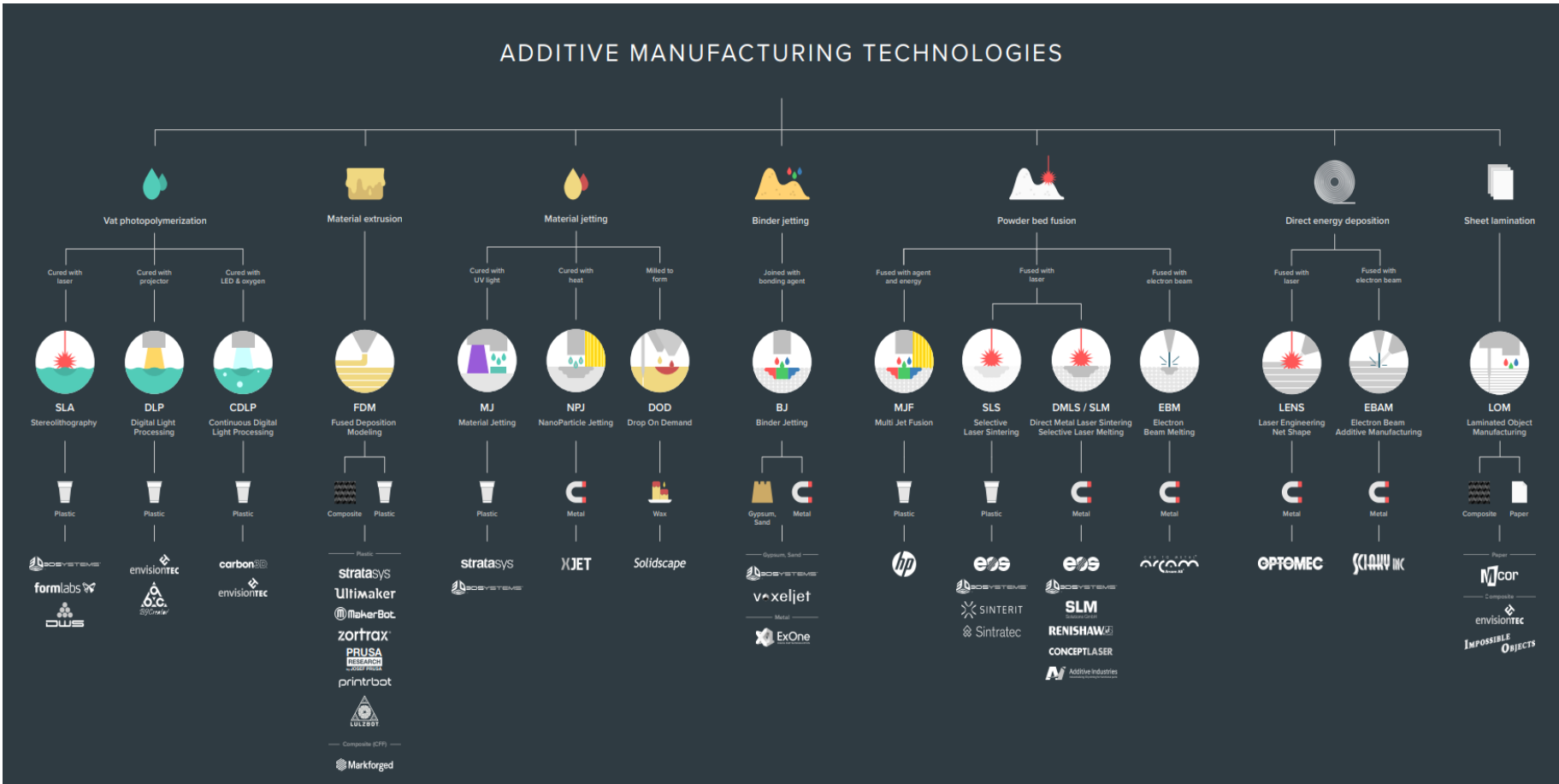
Figure 2 - Additive Manufacturing Technologies (HUBS, n.d.)

2.3.1. Vat-photopolymerization processes

Vat photopolymerization (VPP) is the oldest of the commercial AM processes, characterized by its use of curing light, normally UV or infrared radiation. The working principle of VPP is to cure a photopolymer, a light-curable resin in a vat, and create a solid preform by polymer chains or cross-linking. Figure 3 shows a representation of the vat-photopolymerization process.
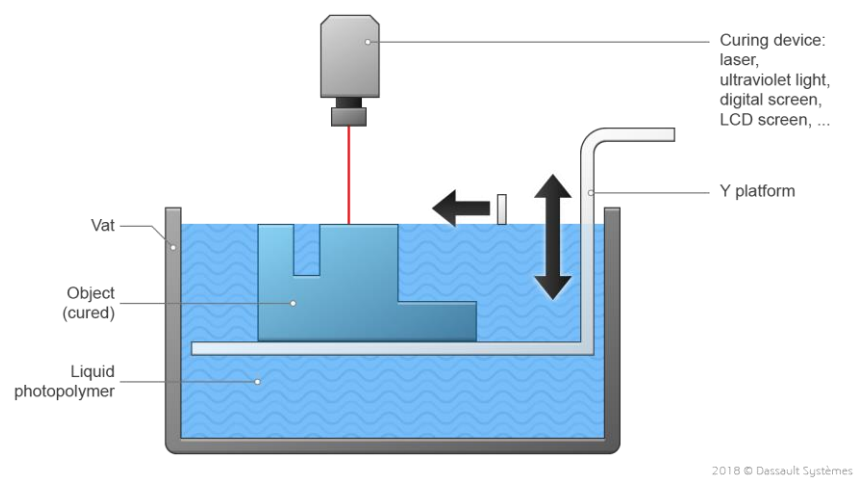
Figure 3 - Vat Photopolymerization Process (Experience, 2022)

This process provides a smooth surface finish to the parts created and high precision in part size with high-resolution detail and the ability to produce wall thicknesses from less than 50 µm to 150 µm (Nohut & Schwentenwein, 2022). Other advantages are that many materials are available since photopolymer resins are available in different colours and exhibit different physical properties, each corresponding to a specific use. The range of resins includes tough resin, low residue resin (for investment casting), transparent resin and flexible polyurethane resin.

Thus, VPP technologies are strong candidates for cost-effective, near-net shape production of multi-material and FGM components, which makes this the ideal technology for jewellery, investment casting and many dental and medical applications (Pagac et al.,

2021). Material developments have also allowed the printing of low-run injection moulds. The main limitations for vat polymerization are the build size and part strength.

The vat polymerisation technologies are Stereolithography, Digital Light Processing and Continuous Digital Light Processing, as shown in Figure 4.
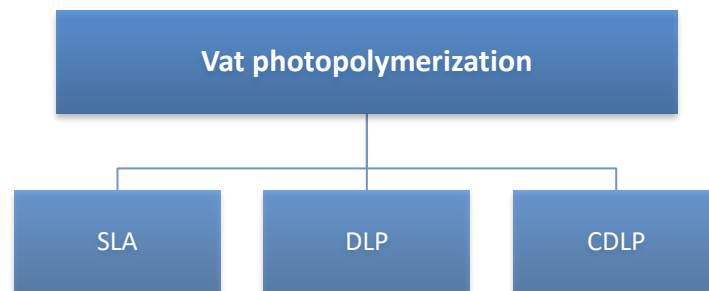
Figure 4 - Vat photopolymerization Technologies

Stereolithography (SLA)

The SLA technology uses a laser beam, there are several options for the laser some of which are UV, IR or other capable of curing the liquid resin in the reservoir to create the desired 3D shape. In short, the process uses the emitted light and the photopolymerization reaction to convert a photosensitive liquid layer by layer into a three-dimensional solid plastic. Therefore, it can only process epoxy-based materials (Alkaios Bournias Varotsis, 2022). Figure 5 shows how the SLA process works.
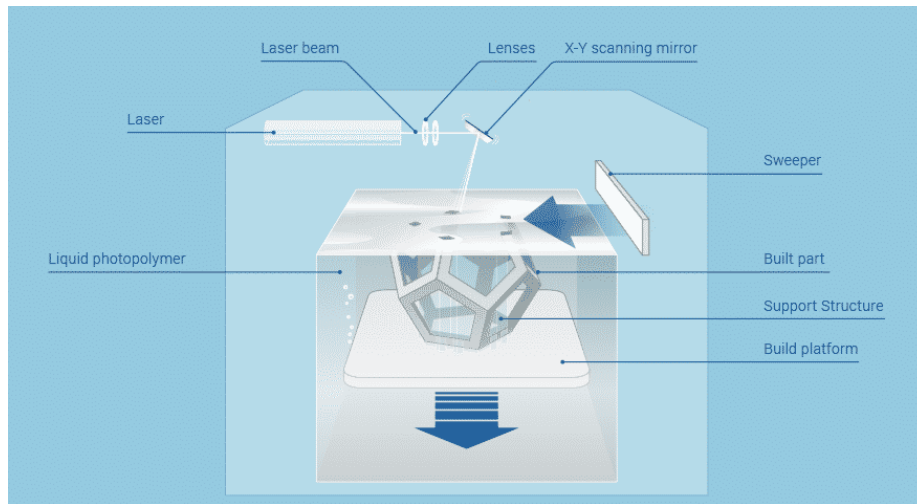
Figure 5 - Stereolithography Process (3m3drobotics, 2022b)

The material comes in the form of liquid resins. The specific resin is selected considering thermal resistance properties, a smooth surface finish or abrasion resistance (Alkaios Bournias Varotsis, 2022). As such, resin price depends on the part specifications and characteristics, ranging from 45€ for the standard material to 350€ per litre for speciality materials.

The most famous manufacturers of SLA printers are 3D Systems and Formlabs. 3D Systems was founded by Chuck Hull, the inventor and patent-holder of the first SLA rapid prototyping system. The company creates product concept models, precision and functional prototypes, master patterns for tooling, as well as production parts for direct digital manufacturing. This company has printers like the ProX 800, shown in Figure 6, ProX 950, ProJet 6000 HD and ProJet 7000 HD.

Figure 6 - SLA Printer ProX 800 by 3D Systems (3D Systems, 2022)

Formlabs was founded in 2011 by three MIT Media Lab students. This company created the first printer in 2012, the Form 1 3D printer, a printer that uses SLA technology, and later the Form1+ and Form 2. Nowadays, Formlabs has the 4th Generation of their SLA printers, the Form 3 and Form 3L, designed for artists, designers, and other professionals. The Form 3 offers a larger print area than Form 2, a smoother surface finish, and more detailed prints.

The following table, Table 1, shows the advantages and disadvantages of SLA technology compared to other AM technologies.

Table 1 - Advantages and disadvantages of SLA Technology

SLA Advantages	SLA Disadvantages
Manufactured simple and complex	Expensive equipment and materials
Fast and good resolution	Limited range of materials
Smooth Finish	Post-curing is required

Digital Light Processing (DLP)

DLP is an SLA derivative technology created by Chuck Hull of 3D Systems. The only significant difference is the light source used to cure the resin. In DLP printers, a specially developed digital light projector screen defines the layer section exposed to UV light, in contrast with SLA technology which uses lasers combined with galvanometers to cure the resin. This difference makes DLP a faster technology than SLA since the laser has to individually cure the resin in a "point to point" technique. In DLP, the projector screen flashes an image of a layer at once. Thus all points of a layer can be cured simultaneously. This way, the printing speed is increased compared to SLA since it takes less time to cure a single layer (B FOXDOC, 2022).

Since DLP is a digital technology, the 2D image that is projected is composed of pixels. When translated into three dimensions, they become voxels. The key part of DLP technology is the digital micromirror device (DMD), Figure 7. This component contains hundreds of thousands or even millions of tiny micromirrors that direct light and create the pattern of a layer on the bottom of the resin tank (B FOXDOC, 2022). The resolution of a part printed using a DLP 3D printer typically corresponds to the number of micromirrors within a DMD device.

Digital Micromirror Device
(DMD)

Array of micromirrors
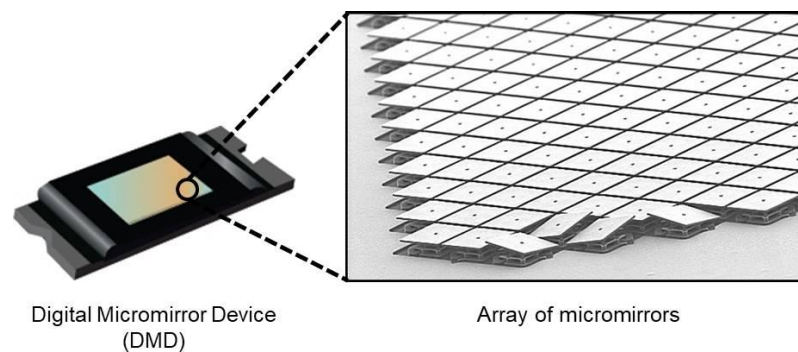
Figure 7 - Digital micromirror device (Ibsen, 2022)

DLP 3D can only print polymer-like parts such as SLA. DLP printers use liquid photopolymers in the form of resin. 3D Systems and Formlabs, like in SLA technology, and EnvisionTEC, Stratasys and Carbon are the best-known manufacturers of printers for DLP technology.

EnvisionTEC was one of the first 3D printing vendors to use DLP technology and has since introduced variations to speed the build process even more. It has existed since 2002 and has grown a lot, creating products for different AM technologies. DLP printers manufactured by EnvisionTEC specialise in jewellery, dentistry, and hearing aid manufacturing. Some of the DLP printers from this company are VIDA and MICRO PLUS desktop range shown in Figure 8.

Figure 8 - Printer MICRO PLUS by EnvisionTEC (Treatstock, 2022a)

Continuous Digital Light Processing (CDLP)

CDLP is a vat-polymerisation additive manufacturing process that enables high-volume and scalable part production. By combining the energy of light with long-chain material chemistry and industrial-grade materials, the CDLP 3D printing process is an effective way to produce complex end-use parts with the speed and economics comparable to traditional manufacturing methods like injection moulding (Proto, 2022)

In this technology, a 'dead zone' is formed by flowing a thin layer of oxygen above the film of the printing bed. Within this 'dead zone', the polymerization process is inhibited, ensuring the printed layer adheres to the layer above, not the printing bed film. This 'dead zone' is what enables continuous printing, where the build plate can continually move in the Z axis, leading to faster, more reliable prints.

The company that created this technology was EnvisionTEC. Envision One is one of the machines this company sells that uses CDLP technology. This technology brings advantages like printing speed, multi-cure resins, isotropic proportions, high accuracy and detail, and surface finish. In Figure 9 is it shown the Envision One printer.

Figure 9 - Envision One printer (ETEC, 2021)

2.3.2. Material Jetting Processes

The Material Jetting (MJT) technique is often compared to the standard 2D ink jetting process. However, they utilize photopolymers, metals, or wax that solidify when exposed to light or heat, ensuring that physical objects are built up one layer at a time. In addition, the MJT manufacturing process allows for different materials to be 3D printed within the same part. In MJT, droplets deposited by a single or multiple nozzles of the build material are selectively deposited into a platform. Usually, photosensitive thermoset polymers are used to allow for hardening after deposition (Prata, 2019). Figure 10 shows how MJT processes work.
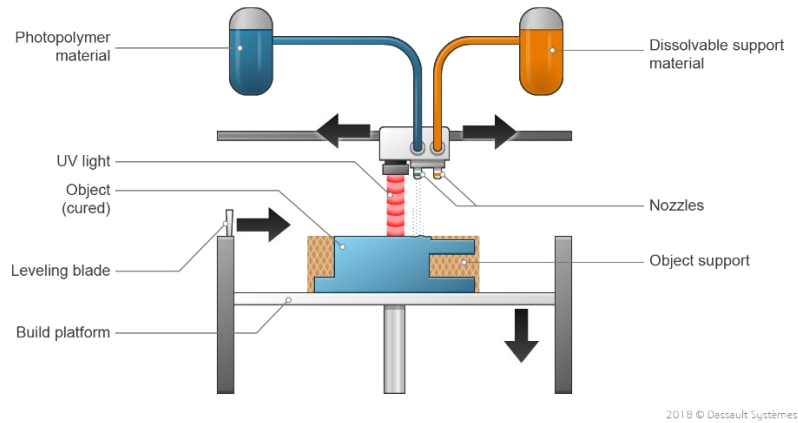
Figure 10 - Material Jetting Process (Experience, 2022)

This process is widely used in the prototyping environment since the build speed, flexibility, and availability of the used materials are quite satisfying. In addition, MJT allows printing a design in multiple colours and with several materials in a single print. It is possible to designate a different material or colour to particular areas of the part. The main disadvantages to printing with MJT technologies are the high cost and UV-activated photopolymers losing mechanical properties over time and can become brittle.

There are three types of MJT processes: Material Jetting (MJ) or PolyJet (PJ), Nanoparticle Jetting and Drop On Demand (DOP), as shown in Figure 11.
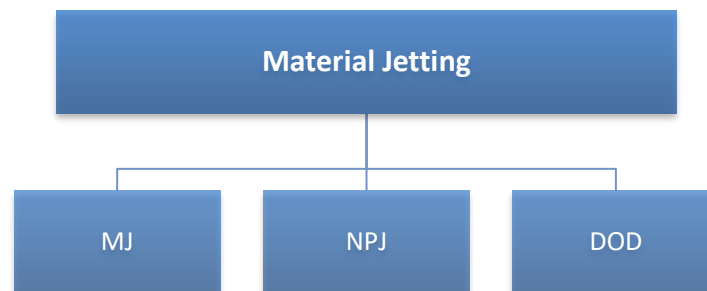
Figure 11 - Material Jetting Technologies

PolyJet - Material Jetting (MJ)

MJ is an AM method that creates objects similar to a two-dimensional inkjet printer. This technology uses droplets of the liquid feedstock jetted through spatial control over the desired component cross-section following a curing mechanism using a UV lamp. Then, the build platform moves down to be prepared for a new layer deposition onto a previously cured layer, and this process continues to achieve the final desired part (Razavykia, Brusa, Delprete, & Yavari, 2020).

MJ fabrication can be accomplished by applying adequate material with proper surface tension and viscosity. There are constraints to jet molten metals or thermal plastics. Droplet ejection from the printer head and landing control on the substrates is critical to MJ.

This technology can use polymers, metals and ceramics. The critical determinant parameter is the material capability to be deposited as a droplet through the jetting print head. Multi-Material Jetting (MMJ) through several individual nozzles enables local specification of colour. However, porosity and anisotropy could arise during the layer-by-layer printing process, resulting in imperfect or weak interlayer bonding (Razavykia et al., 2020).

This technology is known for having two names. "Polyjet" is the name used by the company Stratasys and "Material Jetting" is the name given by the company 3D Systems.

PolyJet, from Stratasys, uses dissolvable support material, which is usually made of polyethene, propylene, and glycerin. After printing, parts are removed from the build platform and exposed to pressurized water to remove the support material. Afterwards, the parts are submerged in a chemical solution, where the rest of the supports dissolves, leaving a clean part. In Figure 12, it is possible to see the Stratasys J850, a multi-material printer.

On the other hand, MultiJet 3D printers utilize paraffin wax as a support material. Therefore, after a part is printed on a MultiJet 3D printer, supports have to be melted away in an oven.

Figure 12 - Stratasys J850 printer multi-material (Stratasys, 2022)

NanoParticle Jetting (NPJ)

NPJ is a 3D printing process developed by XJET. It is an MJT technology that uses suspensions of powdered material to build up parts. NPJ jets a liquid containing nanoparticles of metal or ceramic material in suspension to build the part, simultaneously jetting a support material. The layers are very thin and can be almost as fine as 10 μm. The process takes place in a heated bed held at 250°C, which allows the liquid to evaporate upon jetting so that the particles adhere in all directions. The resulting 3D object has only a small amount of bonding agent in its body and supports (Hendrixson, 2022) .

This technology's advantages are design freedom due to its soluble support material and the absence of vat. Since the material is directly in the liquid, there is no need for a separate vat of powder or resin material as in the case of other Jetting or Vat Photopolymerisation technologies.

The company XJET founded in 2005, is responsible for NPJ Technology. One of the most known models of XJET printers is XJet's Carmel 1400 NanoParticle Jetting system, which is presented in Figure 13.

Figure 13 - XJET's Carmel 1400 NanoParticle Jetting system (3druck, 2021)

Drop On Demand (DOD)

DOD technology is similar to NPJ. However, DOD printers have two print jets: one to deposit the build material and another for dissolvable support material. In front of the nozzle is a chamber that is filled with ink. By reducing the volume of this chamber, the ink is ejected through the nozzle. This principle is the same for both thermal and piezo inkjet printing (ANDY, 2022). The difference only lies in the technique used to achieve the volume reduction. The Figure 14 shows how the DOD processes work.
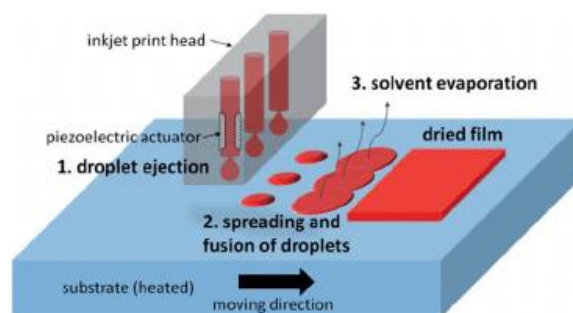
Figure 14 - Drop on Demand Process (Burgués-Ceballos, Stella, Lacharmoise, & Martínez-Ferrero, 2014)

The material used in this technology is a pigment ink and dye ink. With the former, pigments are suspended into a liquid, which gives the ink its colour. Pigment ink is particularly long-lasting and achieves stronger colour results that are more resistant to water.

In return, dye-based ink offers a more comprehensive colour range. The inks consist of dye molecules that are dissolved in the ink fluid.

Solidscape created this technology, which is part of the Stratasys group. This company created this technology using wax as the material.

2.3.3. Binder Jetting Processes (BJT)

For the binder jetting processes, the only one is the actual Binder Jetting. Figure 15 shows the processes of binder jetting.
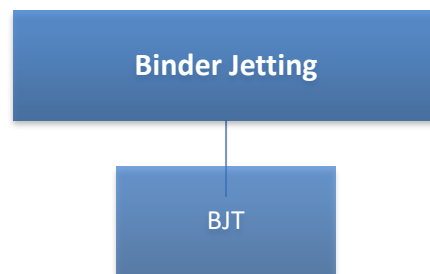
Figure 15 - Binder Jetting Processes

The BJT technique uses liquid droplet deposition, and adhesive properties are needed for the binder. It joins the processes of powder bed and materials jetting. Initially, a layer of powder is laid on a platform. Then a printing head using single or multiple nozzles passes above the powder bed and deposits droplets of the binder material in order to join the powder particles (Tan, Wong, & Dalgarno, 2017), as shown in Figure 16. The process is repeated vertically to build the component. Regarding structural materials, post-processing is required to remove the binder and densify the powder.
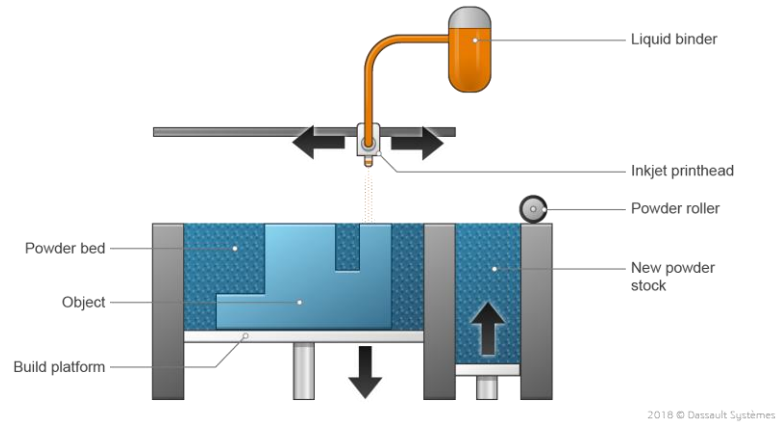
Figure 16 - Binder Jetting Process (Experience, 2022)

The binder is printed above the powder, enabling the use of any material. Thus, different companies commercialize the different materials. In the case of polymeric powder, it can be obtained from companies such as Voxeljet and HP. The ceramic and metal materials can be acquired in ExOne, HP, Desktop Metal, and 3D Systems. In terms of machines, the companies mentioned above also have options in the market, like ExOne's M-Flex, shown in Figure 17.

Figure 17 - ExOne's M-Flex (3Dnatives, 2022)

BJT is great for applications that require good aesthetics and form, such as architectural models, packaging, toys and figurines. However, it is generally not suited for functional applications due to the brittle nature of the parts.

Metal-based binder jetting parts have relatively good mechanical properties thanks to the infiltration process. Thanks to the infiltration process, they can be used as functional components and have relatively good mechanical properties (Experience, 2022).

2.3.4. Material Extrusion Processes (MEX)

Material Extrusion is one of the most used AM technologies, which can use two kinds of material, wire or feedstock, which is extruded through a nozzle. For the material to form a part, the part before the nozzle must be heated. There is the need to use a combination of post-processing procedures, such as binder removal and sintering. Figure 18 shows the technologies that belong to MEX processes.
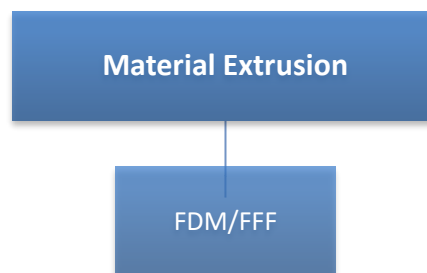
Figure 18 - Material Extrusion Processes

Fused Deposition Modeling (FDM)

FDM was invented in 1988 by S. Scott Crump, co-founder of Stratasys. This company commercialized the technology with a series of 3D printers, including the FDM 300, FDM Maxum, and FDM Titan. As a result, FDM had different patents created by Stratasys. However, all these patents were stopping the development of the technology, so in 2009, when the patents were about to expire, the RepRap community members had to come up with a new name for a similar technology so all the makers could use and speak about it without infringing the copyright before the patent has expired (Top 3D Blog, 2022). The solution found was the creation of Fused Filament Fabrication (FFF), which is based on producing objects with a complex design without the need to use expensive tools.

The following steps describe the printing process of FFF: a computer-controlled driving wheel is used to unwind the filament from its coil and feed it to the hot end. The filament is then melted and extruded through a small printing nozzle to be deposited in fine flattened lines along a defined extrusion path (Riecker et al., 2018). Once one complete layer is printed, the nozzle height is increased, or the build platform is lowered to apply the next layer. These steps are repeated until the desired geometry is printed layer by layer. The process of FDM is shown in Figure 19.
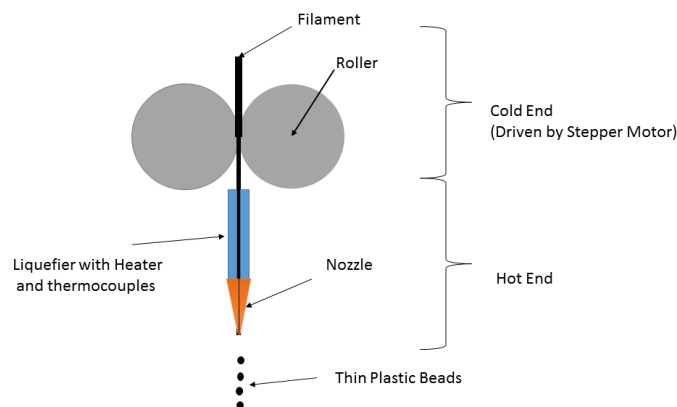
Figure 19 - Fused Deposition Modeling Process (Wikipedia, 2022)

The benefits of FFF include a wide choice of materials, fast print times, multiple printer manufacturers, and an affordable option compared with the other AM technologies. In addition, printing with FFF is very flexible, and the technique allows small overhangs to be achieved using supports from the underlying layers.

To produce metal parts using FFF technology it is necessary to follow some steps, starting with the 3D model, then the printing, the debinding, the sintering and finally the mechanical post-processing. In Figure 20, it is possible to see the different stages needed to have a part with good properties.
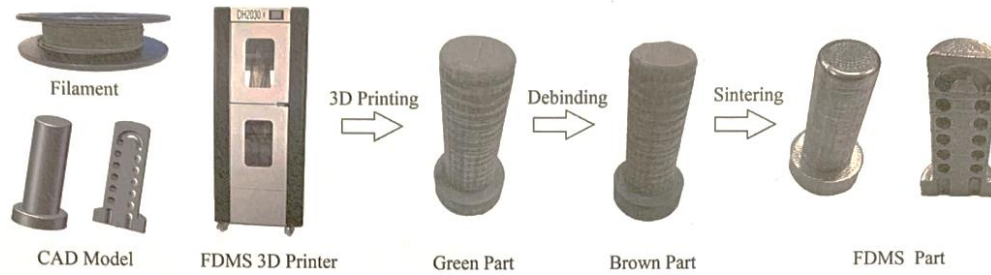
Figure 20 - Stages of Fused Deposition Modeling (Liu, Wang, Lin, & Zhang, 2020)

FFF printers are divided into three parts: the extrusion mechanism, the cold-end, and the hot-end. The extrusion mechanism is composed of the filament and the rollers. In this part, the rollers are responsible for applying pressure while winding the filament, causing the filament to go down.

The cold-end should have a heat sink capable of limiting any heat from the hot-end to the other parts of the extrusion system.

The hot end is an extrusion head to which the fabrication material is supplied by unwinding plastic filament or a metal wire of a coil. The wire or filament is fed to the head's nozzle at a controlled rate in a worm-drive. As the filament or wire enters the extrusion nozzle, it is heated past its glass transition temperature and melted. When the molten filament or wire exits from the extrusion nozzle, either exposed to air or an inert gas chamber, it solidifies immediately on a base or onto a preceding layer. In Figure 21 it is shown the printer mechanism.
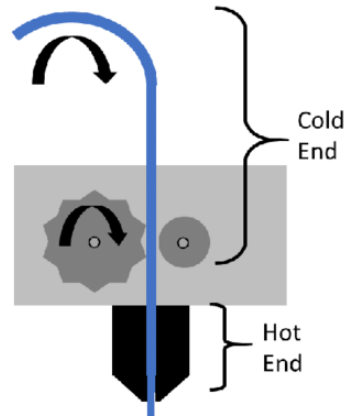
Figure 21 - Fused Deposition Modeling Printer Mechanism (Lahaie, 2020)

FFF technology can use polymers, ceramics, or metal materials. Material for FFF 3D printers is typically sold as spools of filament, each containing from 250 g to 3 kg of material.

To properly function the printer, specific filament requirements must be met. To the filament being extruded, the filament itself acts as a piston for the extrusion through the printing nozzle. Therefore, the filament must have sufficient strength to be processed in the printing machine without buckling between the driving wheel and the nozzle. Typically, filaments have 1,75 mm or 3 mm in diameter. However, when coming out of the printer nozzle, the diameter of the filament is between 0,30mm a 0,35mm. At the same time, it must be sufficiently flexible to get coiled. Further, low melt viscosity is favourable for the extrusion through the small printing nozzle. The requirement for successfully extruded is defined differently and depends on the printing machine and process parameters. To achieve metal parts, the feedstock material must contain a high-volume loading of metal powder (>45 vol%), and the polymer components must allow for debinding and sintering after printing (Riecker et al., 2018).

FFF Technology is used in manufacturing industries. 3D printers provide quick tooling and replacement parts to maintain maximum uptime and productivity on the production line. They are used to flexibly create end-use parts, such as custom quality meters or small batch first runs, to speed time-to-market. It is also used for prototyping. Cheap materials and short print times make FFF 3D printing ideal for iterative design processes. 3D printed prototypes can be used to visualize concepts or perform functional testing of technical parts.

Some companies with FDM/FFF printers are 3D Systems, Stratasys, Prusa, Ultimaker and others. For example, in Figure 22, it is possible to see Stratasys J55.
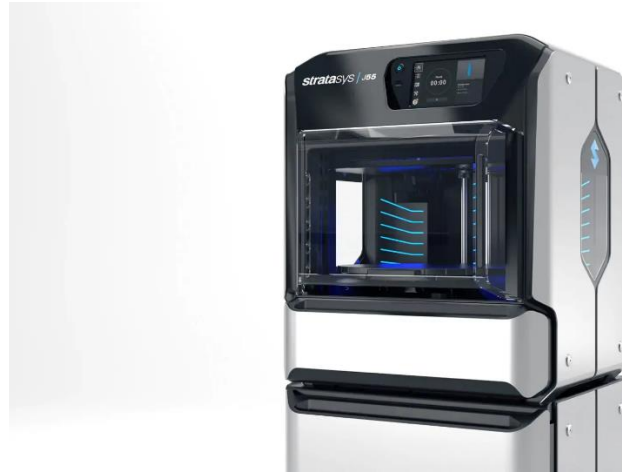
Figure 22 - Stratasys J55 (Clevercreations, 2022)

Like every AM technology, FFF has advantages and disadvantages. In Table 2, it is possible to see it.

Table 2 - Fused Filament Fabrication Advantages and Disadvantages

FFF Advantages	FFF Disadvantages
Cheapest available technology	Rough surface finish
Strong parts	Slow speed
Cheap material	The size of the nozzle limits the detail of finished prints
Easy to switch materials	The strength of finished parts is limited because each layer is joined to the layer below it
Fast printing	

2.3.5. Powder Bed Fusion processes (PBF)

Powder-bed Fusion is a 3D printing technology that enables the manufacturing of a vast array of geometrically complex products using a heat source, mainly laser or electron beams, to fuse powder particles layer-by-layer, forming a solid part. Because of the minimal constraints on feedstock, it is mainly used for parts manufacturing for service applications (Prata, 2019). Figure 23 shows how the PBF processes work.
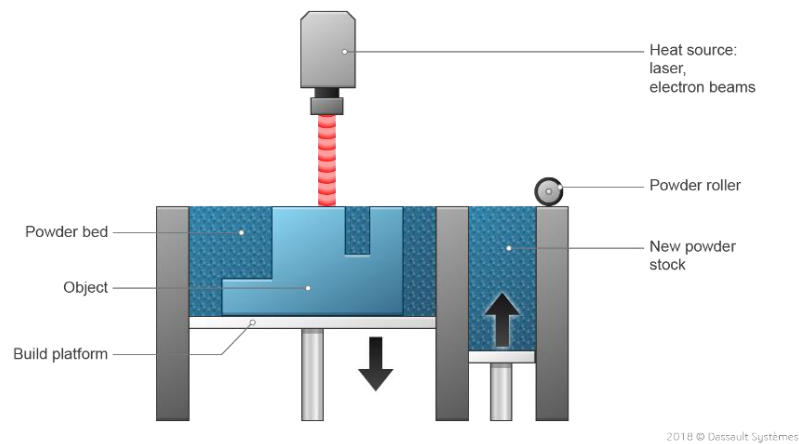
Figure 23 - Power Bed Fusion Process (Experience, 2022)

One of the most significant advantages of this category is that it has several viable technologies and materials. This category has four different technologies: Multi Jet Fusion (MJF), Selective Laser Sintering (SLS), Selective Laser Melting (SLM) and Electron Beam Melting (EBM). In Figure 24, it is possible to see the PBF technologies.
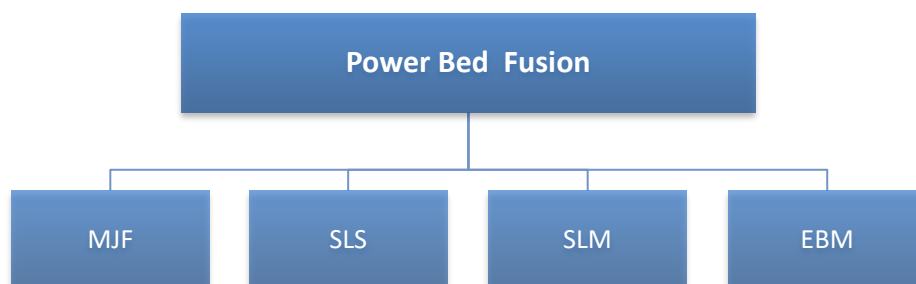
Figure 24 - Power Bed Fusion Technologies

Selective Laser Sintering (SLS)

SLS was invented in 1988 by Dr Carl Deckard and academic adviser Dr Joe Beaman at the University of Texas at Austin (Robinson, 2022). SLS is an additive manufacturing process based on joining consecutive layers of powder using a laser beam, and it only uses polymers as a material. This process takes place in the working chamber of a machine equipped with a computer that controls the production process. Through software, it is possible to control the pressure value and atmosphere inside the chamber, depending on the material used. This process is performed using infrared laser radiation.

SLS technology starts spreading a thin layer of powder on a table. Then the laser beam over the surface of the powder according to pre-input and properly configured information concerning consecutive layers in the cross-section of the 3D model image. Excess powder is diverted into a collection box found outside of the platform on which objects are constructed. The laser scans the cross-section once again. This process is repeated until a cohesive object is obtained according to the data contained in the generated digital file (Mierzejewska & Markowicz, 2015). One main advantage of SLS is creating a part without bringing the material to a liquid state. Figure 25 shows the SLS process.
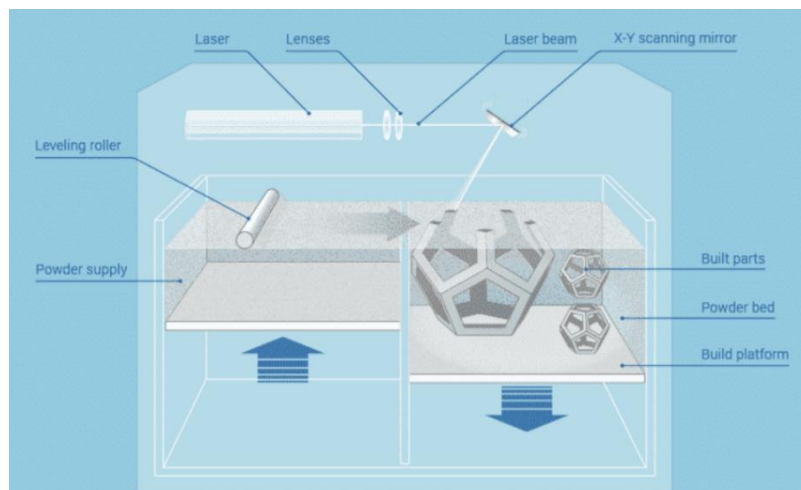
Figure 25 - Selective Laser Sintering Process (3m3drobotics, 2022)

Some companies that use this technology are EOS, 3D Systems and Shinning. One example of one printer of EOS is the INTEGRA P 450 presented in Figure 26.

Figure 26 - INTEGRA P450 EOS (EOS, 2022)

Selective Laser Melting (SLM)

SLM was invented in 1995 at the Fraunhofer Institute ILT in Aachen, Germany, with a German research project. This technology is an additive manufacturing process that uses high-power laser beams to build 3D objects. SLM technology is considered the reference technology in AM and a significant competitor for FFF technology since both can print plastic or metal.

An SLM machine has a chamber filled with metal powder. A coater blade spreads this metal powder across the substrate or build plate in very thin layers. Next, a high-power laser fuses a 2D slice of the part by selectively melting the powdered material. The build plate then drops by the height of one layer, and the coater finely spreads another layer of fresh powder across the surface. The process is repeated until the part has finished (Ile Kauppila, 2022). In Figure 27, it is possible to see how the SLM process works.
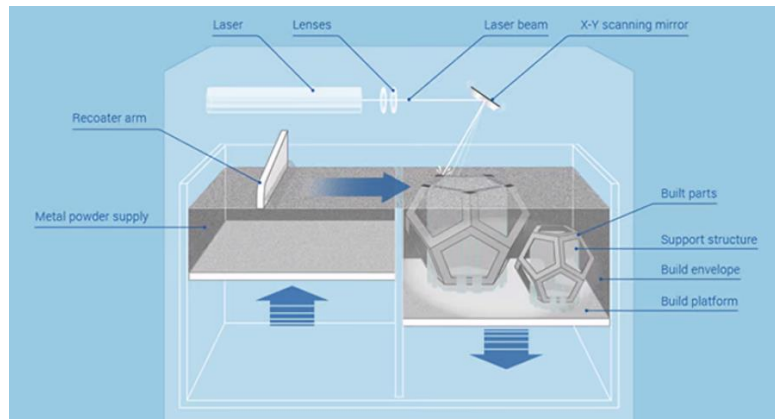
Figure 27 - Selective Laser Melting Process (FACFOX, 2022)

This process is performed inside the machine, avoiding any disturbances. Once the part is built, it can be removed from the machine. SLM parts must be removed from the build plate, often done with a bandsaw. After that, it is necessary to remove the supports. This process can be complicated and lengthy since the support material is the same as the part material. Depending on the part requirements, the surface finish of the sintered parts is rough and may need some post-processing. Therefore, machine parts undergo post-processes steps to achieve acceptable tolerances and finish fine features, surfaces, and holes (FACFOX, 2022).

The companies commercialising this technology are SLM Solutions, EOS, GE Additive, and Trumpf, among others. SLM Solutions has a variety of SLM machines with LASER outputs from 100 to 2800 Watt. The devices can machine different materials such as Aluminium, Steel, titanium and Inconel. The newest machine model on SLM Solution is the *THE 12-LASER FUTURE DRIVER - NXG XII 600,* presented in Figure 28.
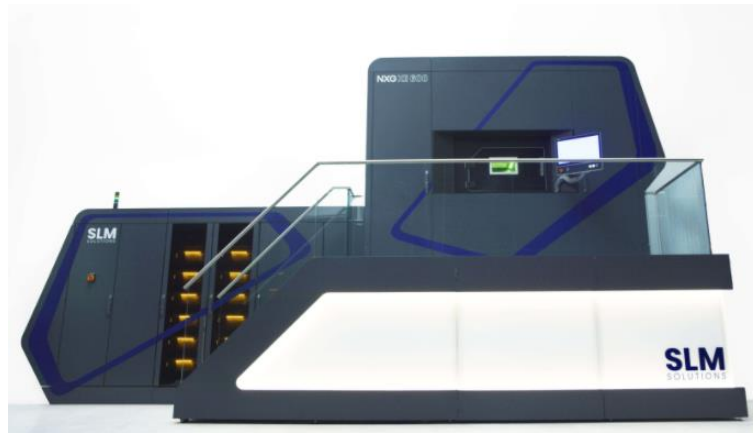
Figure 28 - NGX XII 600 (SLM Solutions, 2022)

Table 3 shows the advantages and disadvantages of SLM technology.

Table 3 - Selective Laser Melting Advantages and Disadvantages

SLM Advantages	SLM Disadvantages
Good material properties	Requires complex post-processing
No distinct binder and melt phases	Not suitable for large objects
Long durability of the material	Expensive equipment and materials
Dense functional parts made of various metallic materials such as tool steel, stainless steel, aluminium, copper, and titanium	Melt pool instabilities and higher residual stress

Electron Beam Melting (EBM)

EBM is a Power Bed Fusion process that uses a high-energy electron beam to melt powder metals creating a stream of electrons that are guided by a magnetic field and melt metal powder layer by layer to create objects that conform to the precise specifications of the CAD model. The EBM process can build a minimum layer thickness of 0.05 mm and it has a tolerance capability of ± 0.4 mm (L.E. Murr, 2014).

EBM is similar to SLM since both processes use powder from a powder bed, but EBM uses an electron beam instead of a laser. Another difference is that the electron beam scanning trajectory on the work plane can only be governed by magnetic fields, enabling high scanning speeds. In addition, high-strength parts made by EBM take advantage of the natural properties of the metals used in the process and eliminate contamination that can build up when using cast metals or other manufacturing processes. As a result, it is widely used to produce aerospace, automotive, defence, petrochemical, and medical components. In Figure 29 shows how the EBM process works.
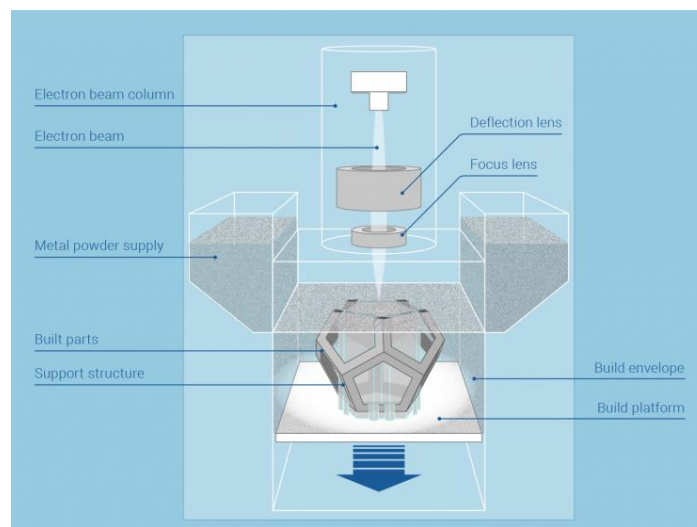
Figure 29 - Electron Beam Melting Process (ArtiBoyut, 2022)

GE Additive is one of the companies with this technology, such as Freemelt. One of the most know 3D printer models of GE Additive is the Arcam Q10 Plus, Figure 30 since this company bought Arcam in 2016.

Figure 30 - Arcam Q10 Plus (GE Additive, 2022)

2.3.6. Sheet Lamination processes (SHL)

In Sheet Lamination technique, more specifically Laminated Object Manufacturing (LOM), the material used is in the shape of a sheet, one of the layers belonging to the final component. Here the sheet can be cut into the desired shape and then adhered into layers. It can be bounded into layers and then cut to form the final geometry, combining additive and subtractive technologies to produce a 3D component (Prata, 2019). First, the process binds the sheets (polymer, composites, metals, paper) in a stack using pressure- or heat-activated adhesives and then it is laser cut into the desired shape. Figure 31 shows the Sheet Lamination technology.
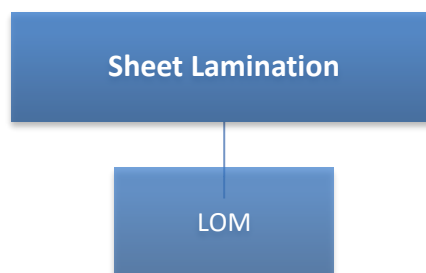
Figure 31 - Sheet Lamination Technologies

However, this technology is practically in disuse since the company Stratasys conditioned its development due to several patents on FFF technology. In FFF, there are

advantages far superior to LOM, such as the possibility of having equipment that works with polymeric filament or ceramic or metallic feedstocks. In 2009 the patent on FDM 3D Printing expired, paving the way for new, lower-cost 3D printers using a similar printing process called FFF. With the advent of these low-cost printers, 3D printing became tangible and accessible to everyone, making it possible for consumers to own their 3D printers.

The latest manufacturer of LOM technology is the company Mcor. One of the models commercialized is Mcor IRIS HD Benefits, Figure 32.

Figure 32 - Mcor IRIS HD Benefits (Treatstock, 2022b)

2.3.7. Directed Energy Deposition processes (DED)

DED uses thermal energy to melt and bind the materials. The heat source is an electron or a laser beam where the raw material is directed into a platform. This technique is mainly used when large volume deposition rates are required. The process is similar in principle to the material extrusion 3D printing technique (Prata, 2019). However, with DED, a nozzle can move in multiple directions, with up to five different axes, compared to only three for most FFF machines. The Figure 33 shows how the DED process works.
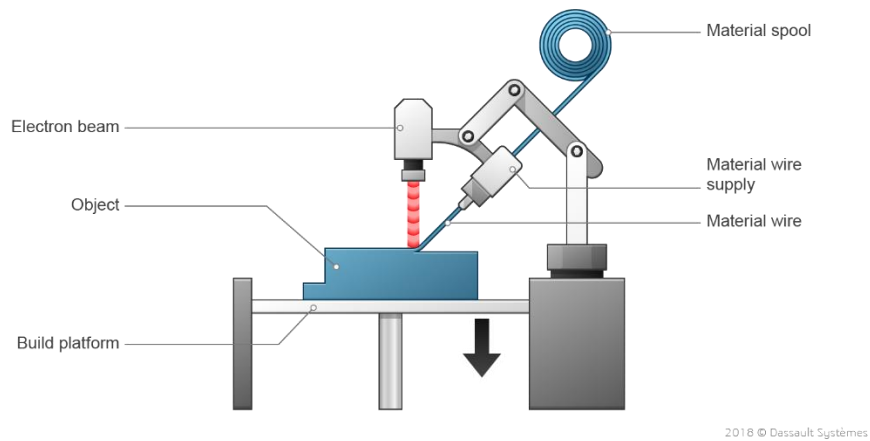
Figure 33 - Directed Energy Deposition process (Experience, 2022)

Some of the advantages of this category are the capacity to fix complex damaged parts, such as turbine blades or propellers and the capacity to use a variety of metals, including aluminium, copper, titanium, stainless steel, tool steel, copper-nickel alloys, and several steel alloys.

DED category has three processes: Laser Engineering Net Shape (LENS) and Electron Beam Additive Manufacturing (EBAM), and Wire Arc Additive Manufacturing (WAAM), as shown in Figure 34.
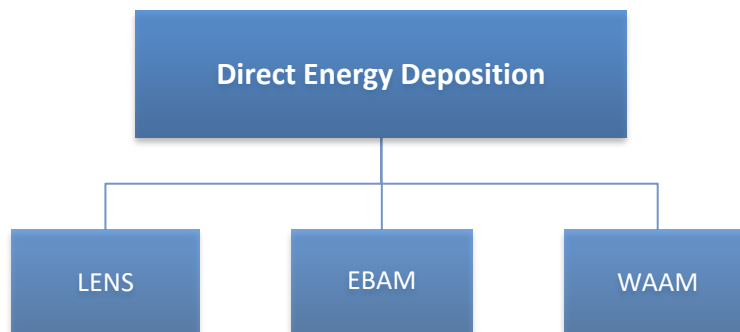
Figure 34 - Directed Energy Deposition technologies

Laser Engineering Net Shape (LENS®)

The process is a laser fabrication technique, similar to traditional laser-initiated rapid prototyping technologies such as SLA and SLS in that layer additive techniques are used to

fabricate physical parts directly from CAD data (Palčič, 2009). This method creates parts from powder through nozzle injection and irradiates a laser beam with high energy density to melt and deposit over a built base plate in a layer-by-layer scheme. After the deposition of each layer, the build platform moves down in a controlled manner (Kumar, 2021). This process repeats until an expected component is realized.

LENS® was created in response to the need to create complex geometries. This method enables the production of complex prototypes, tooling, and small-lot production parts.

Some of the companies that use this technology are Optomec and Trumpf, and one of the most known printers is Optomec LENS® 450, Figure 35.

Figure 35 - Optomec LENS® 450 (OPTOMEC, 2020)

Electron Beam Additive Manufacturing (EBAM)

EBAM technology belongs to the company Sciaky. This technology began with a layer of powder spread on the build plate and preheated. EBAM can use heated tungsten filament also, instead of powder. After preheating, helium is dispersed to avoid electrostatic charging of the powder. Subsequently, the powder melts on the required path for material consolidation. The same electron beam energy source does both preheating and melting. For preheating, the beam is defocused with a high scanning speed. After completion of the process, the building part is cooled (Negi et al., 2020).

One advantage of this process is that it produces denser and higher quality parts than powder processes (ThomasNet, 2022). Moreover, it prints large-scale metal structures, and the supporting materials are titanium, titanium alloys, stainless steel (300 series), inconel, tantalum, tungsten and niobium.

Sciaky is the company that owns the printer EBAM 300 Series shown in Figure 36.
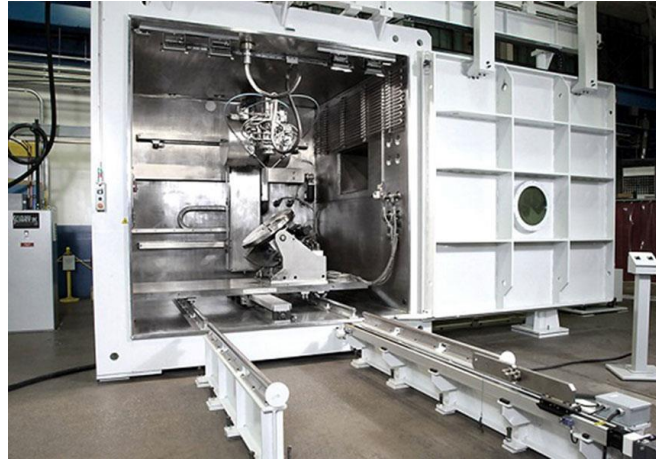
Figure 36 - EBAM 300 Series (Aniwaa, 2022)

Wire Arc Additive Manufacturing (WAAM)

WAAM is executed by depositing layers of metal on top of each other until a desired 3d shape is created. It combines two production processes: Gas Metal Arc Welding (GMAW) and additive manufacturing. GMAW is a welding process for joining metal parts using an electric arc, and additive manufacturing is the industrial term for 3D printing. The production of parts using WAAM is carried out by a welding robot integrated with a power source (RAMLAB, 2022). A welding torch attached to the robot is used to melt the wire feedstock to build 3D parts.

The process has been used to perform local repairs on damaged or worn components and to manufacture round components and pressure vessels for decades. Some advantages include large size, additional design freedom, low star-up cost and wide material availability.

Ramlab is a company that produces machines for this technology. Figure 37 is presented MaxQ for WAAM.
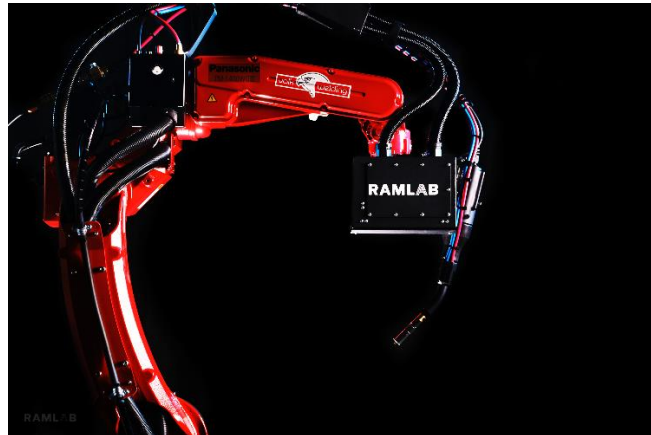
Figure 37 - MaxQ for WAAM (RAMLAB, 2022)

2.4. Subtractive Manufacturing *versus* Additive Manufacturing

Additive manufacturing is a process that adds successive layers of material to create an object, often referred to as 3D printing. Subtractive manufacturing is the opposite; it removes sections of material by machining or cutting it away. It can be carried out manually but generally by a Computer Numerical Control (CNC) machining. In Figure 38, the significant differences between these two types of manufacturing are shown.
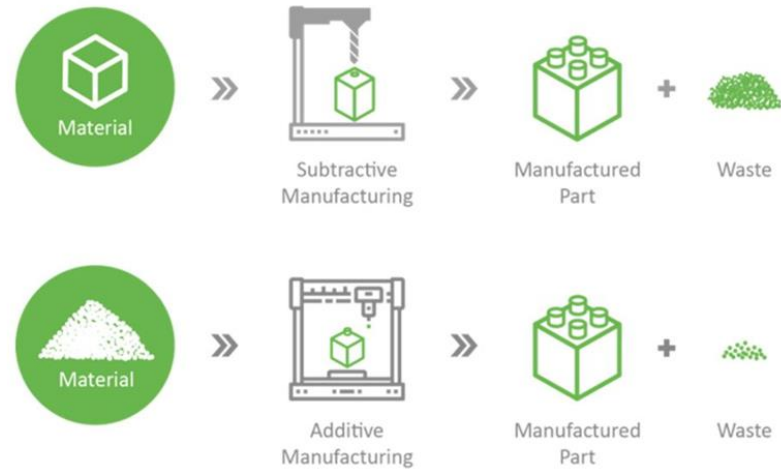
Figure 38 - Subtractive Manufacturing and Additive Manufacturing Process Differences (Advanced Additive Manufacturing, 2018)

The differences between the two types of manufacturing are shown in Table 4. It is also displayed the way of creating parts, the cost of the equipment, the finishing required in the parts, the waste, the possible materials to use, the necessary setup, the accuracy of the processes and the mechanical properties that each type of manufacturing provides to the pieces.

Table 4 - Comparison between Subtractive Manufacturing and Additive Manufacturing

	Additive Manufacturing	Subtractive Manufacturing
Process	Involves adding layers of material to create an object (bottom-up approach)	Removes material from a blank to produce an object (top-down approach)
Equipment Costs	Depends on the type of equipment and technology used. In the case of FFF equipment, they are reasonably cheap. In the case of laser-based technologies, the value can range from €80000 to close to €1000000	Small CNC machines for workshops start around 2000€. More advanced workshop tools go well beyond, around 100000€ that depending on the number of axes, features, part size, and tooling needed for specific materials (Formlabs, 2022).
Finishing	It needs post-processing in the end	A smooth surface finish is obtainable
Waste	It is highly efficient since it adds only the required material	These processes are associated with material wastage in the form of chips, scraps, dissolved ions, vapors, etc (Machining, 2022)
Production Materials	There is a wide variety of materials (Machining, 2022). However, supplying the raw material affects its use a lot.	Variety of materials (metals, plastics, plastic composites and even wood)
Setup	Faster to go from the design stage to production	More time per part than additive manufacturing methods
Accuracy	It can achieve less dimensional accuracy. Typical tolerances as 0.100 mm (Xometry, 2022)	Can achieve greater dimensional accuracy. Typical tolerances as 0.025 mm (Xometry, 2022)
Mechanical Properties	Parts produced may have insufficient mechanical properties	Parts produced may have excellent mechanical and thermal properties (Xometry, 2022)

Some machines combine 3D printing and CNC machining during one production process. For example, a CNC machine was used every 10th layer of 3D printing to drill highly accurate canals. This solution means a shorter lead time, consequently bringing down production costs. In addition, this combination allows for new design solutions. Parts that had to be put together now can be produced as one, eliminating the assembly time and lowering the costs.

When talking about precision in terms of tolerances, AM stands out for the quality and thinness of the layers, but the surface of the parts can still sometimes be porous. This is precisely why traditional machining methods can improve the built parts. For example, they can give them a smooth surface finish or provide additional details. AM gives new design freedom to reinvent mechanical parts. As also improves tools by hollowing complex geometries and achieving even smaller parts. When combined with CNC machining, it will produce high-quality, complex parts with the exact details needed.

It is possible to achieve lower-costs, faster manufacturing processes, and less material waste in production. Regarding new design solutions, 3D printing and CNC machining will provide better details, higher accuracy, and precision. All those benefits will result in improved productivity, surpassing what is possible with Subtractive and Additive technologies separately.

2.5. FFF Metals

Fused Filament Fabrication can print polymers, ceramics, and metal. However, in this work, the material used is metal. One of the most economical options to print metallic parts in AM is to use FFF combined with debinding and sintering. This combination was first introduced as FDMet in the 1990s.

2.5.1. FFF Metals Stages

In FFF technology, there are specific steps to compress. These are represented in Figure 39.
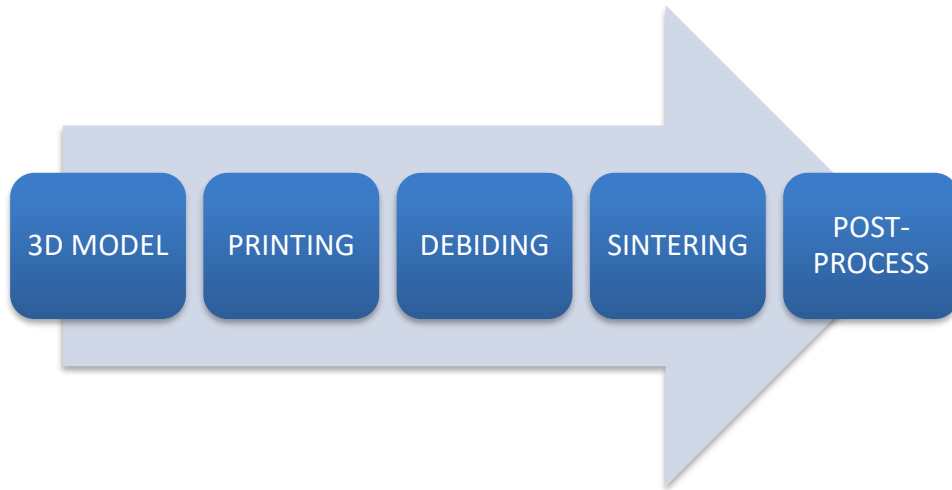
Figure 39 - Fused Filament Fabrication stages for metals

The process starts using a 3D Model. Typically, that only describes the face figure of a three-dimensional object without any representation of colour, texture, or other common CAD model attributes. In this technology, support structures are needed when the orientation or shape of a part makes it impossible to print from bottom to top, for example, a part with a large overhang.

The next step in FFF is to print the part. The software imports the 3D model and adds material to create an object, enabling the user to select the printing parameters. The nozzle speed, the extrusion rate, and other parameters such as the infill percentage, printing speed, printing temperature, supports, and layer height will determine the quality of the printed part. During the printing step, the printer creates the green sample by extruding the feedstock or filament along a precise path, layer-by-layer, directly onto a built plate. Figure 40 shows an example of a green part where it is possible to see the layers of filament created by the printer.

Figure 40 - FFF printed part/ Green part (i.materialise, 2022)

When the green part is created, it is necessary to perform a debinding process. This is a required post-processing procedure when a part is made of a feedstock/filament containing a binding agent and the part material. First, the green sample must be debonded to go into the furnace with as little binder as possible. Then, the binders are progressively removed to avoid deformation, cracking, and contamination during the sintering stage. If the green part is not binder-free, the binder will melt when it is put into the furnace, and the component will lose its shape.

There are different types of debinding methods: thermal and solvent. Thermal debinding consists of heating the component to decompose the binder. It is performed in a furnace, set at the melting temperature of the material used in the binder. The binder material must always have a lower melting temperature than the melting temperature of the material part. This way, the binder will evaporate, keeping only the final part's material, commonly known as the brown part. In solvent debinding, the binder composition is dissolved in a liquid when the components are immersed (Valérie, 2021). Figure 41 shows the two types of debinding processes.
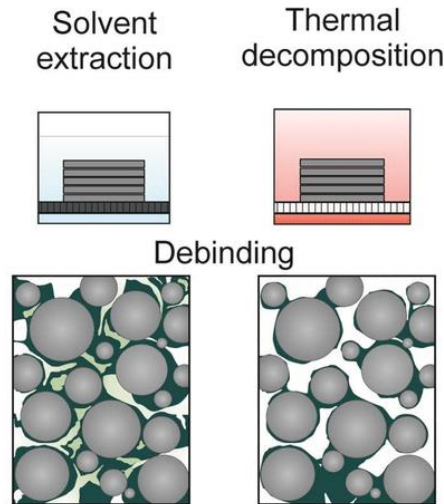
Figure 41 - Solvent debinding versus Thermal debinding (Gonzalez-Gutierrez et al., 2018)

After the debinding process, the part proceeds to the sintering stage. It is imperative because it is a process that modifies mechanical properties, physical and chemical properties, but also the dimensions of the component under temperature and pressure that will activate mechanisms to decrease the system's free energy. In this transformation, the component keeps its shape, but its volume decreases. Pressure is also applied simultaneously with heating for materials that are difficult to sinter. The sintering stage is done in a furnace, such as the debinding stage. Sintering qualities can be influenced by specific parameters, such as the sintering time, the sintering temperature, the sintering pressure, or the particle size of the raw material. During the sintering process, bonds between powder particles, also known as sinter neck, are created by the diffusion of atoms under temperature and pressure. Figure 42 shows the formation of the sinter necks between contacting particles.
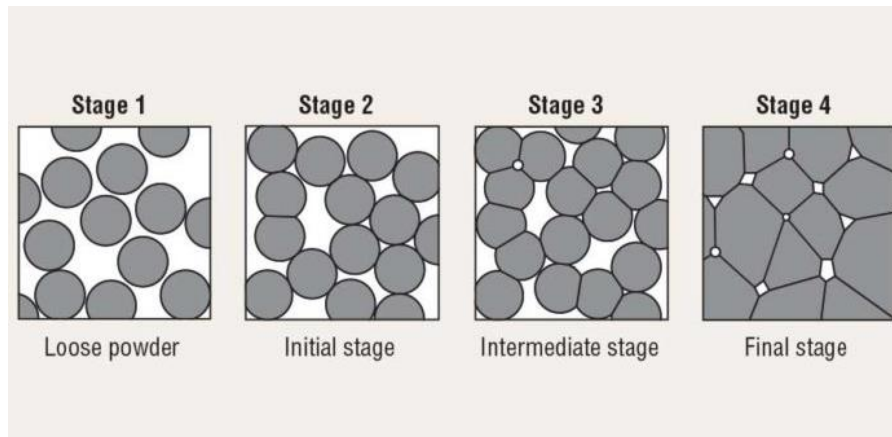
Figure 42 - Sintering process (Industrial Heating, 2022)

The last stage is post-processing. This stage is not mandatory for all parts. The goal of this stage is to finish the surface of the 3D part since these parts usually require some degree of post-production treatment. Post-processing is any process that needs to be performed on a printed part or any technique used to enhance the object further. The options for post-processing 3D printed parts include removing support or excess material, washing, curing, sanding, or polishing a model to painting or colouring (Beamler, 2019).

2.5.2. FFF Metals - Stainless Steel

In 1996 a study was carried out on a metal-polymer filament, in which the metal part corresponded to 50-60%, allowing it to fabricate parts out of, e.g., stainless steel, WC–Co, and SiO_2. Other materials for FFF metals use iron-nylon composite or Sn-Bi alloys. One of the latest materials on the market for this technology is ("Ultrafuse 316LX") with high metal filler ratios of 80 vol%. This percentage reduces the volumetric shrinkage and integrates AM machines into existing metal injection moulding process chains using the same catalytic debinding parameters and similar sintering temperature profiles (Ait-Mansour, Kretzschmar, Chekurov, Salmi, & Rech, 2020)

After testing this material, a comparison was made with SLM technology. FFF technology with "Ultrafuse 316LX" proved to create successful 3D prints with x/y-shrinkages of 13–18% and z-shrinkages of 15–23%, reaching a yield strength of 167 MPa and ultimate tensile strength of 465 MPa (as expected, both tensile strength indicators below SLM (Ait-Mansour et al., 2020).

Some of the stainless-steel metals that can be used with FFF technology are: 17-PH stainless steel, a precipitation-hardened steel that maintains 95% wrought strength at high temperatures. Good corrosion resistance, widely used for pump shafts and mechanical seals.

2.5.3. Comparison of metal-based processes

Compared to other AM processes that can fabricate metal parts only at temperatures higher than the melting points. Printing metals, which are usually above 1000°C, the FFF can achieve the green part at temperatures slightly higher than the melting points of polymers, usually below 300°C. Additionally, although it is necessary to sinter the Brown Parts at a relatively high temperature, the sintering and debinding processes can be in batches. Thus, FFF is a more energy-saving process to fabricate metal parts compared to other AM techniques.

Besides energy, the monetary part is also different from other additive manufacturing technologies. The FFF equipment is much more affordable since it is a significantly lower investment to own and operate than other metal printers.

In terms of safety, it is also a technology that stands out from the rest. The fact that the raw material is filament or feedstock and not powder makes the use of the machines easier so that the machines can be used effectively with minimal training and PPE.

When it comes to materials FFF printers accept a wide range of filament materials, and they're often budget-friendly (Fast Radius, 2022).One of the significant advantages of FFF metals over other technologies is the material used. Not only because it is affordable and in its physical state, but also because of its variety. Several types of metals can be printed using this technology, such as aluminium, copper, gallium, cobalt-chrome, titanium, and iron. In the future, there is potential for even broader future state compatibility. For example, industrial 3D printer metal types may include exotics and alloys.

In Table 5, it is possible to compare the different categories of AM that use metal, Binder Jetting, Directed Energy Deposition, Material Extrusion, Powder-bed Fusion and Nano Particle Jetting. The comparison parameters are the build plate size, resolution, equipment, and raw material cost.

Table 5 - Comparison between Additive Manufacturing categories

	Build plate Size	Resolution	Equipment Cost	Raw Material Cost
Binder Jetting	up to 2200 x 1200 x 600 mm (HUBS, 2022b)	0,03 mm - 0,12 mm	114.000€ - 500.000 €	119€/kg - 300€/kg
Directed Energy Deposition	100 x 100 x 100 - 5791 x 1219 x 1219	0,15 mm - 0,2 mm	40.000€ - 500.000€	200€/kg - 500€/kg
Material Extrusion	230 x 190 x 200 mm - 500 x 500 x 500 mm	0,02 mm – 0,6 mm	500€ - 30.000€	15€/kg - 55€/kg
Powder-bed Fusion	110 x 110 x 110 mm - 340 x 340 x 605 mm	0,02 mm - 0,15 mm	80.000€ - 600.000€	110€/kg - 260€/kg
Nano Particle Jetting	+/- 500 x 280 x 200 mm	+/- 0,01 mm	4000.00€ - 500.000€	75€/kg - 330€/kg

The AM category that stands out for the possible size of the parts built is Directed Energy Deposition. While for resolution, the Nano Particle Jetting category stands out. The "Material Extrusion" category that includes FFF technology is the one that shows cheaper values, making the technology more accessible to companies.

2.5.4. FFF Metal Applications

The metal parts produced with FFF commonly are for forming, cutting, and bonding, low-volume custom parts, maintenance tools/fixtures, and replacement parts. The main industries that use AM parts are automotive, aerospace, production, healthcare and consumer goods.

Additive manufacturing is increasingly a choice to produce aerospace parts as it provides weight reductions, significant cost reduction compared to conventional manufacturing processes, and it is better to produce complex parts. In addition, the weight factor leads to a

reduction in fuel consumption and CO_2 emissions. For this reason, leading aerospace companies have long been integrating additive manufacturing technology when planning their production strategies for the future. Some parts that can be produced for this industry are engine and turbine parts like valve blocks and landing gear harness brackets.

In manufacturing parts for the energy sector, functional integration and heat resistance are the decisive factors of longevity and process selection. For these factors, industrial 3D printing opens opportunities beyond the reach of conventional manufacturing processes. Thus, it is possible to print parts like blades, fuel injectors, burners and combustion chambers, cladding, seals and housings (Peels, 2020). For example, Figure 43 is presented a solar metal clamp printed through FFF technology.

Figure 43 - Solar panel clamp printed with FFF technology (Peels, 2020)

2.6. Support Material

With the evolution of additive manufacturing, more and more difficulties have appeared in manufacturing parts with complex geometries. For example, a 3D model with overhanging, hole or edge features will need support structures for successful fabrication as printed materials will not be able to stand in a position "in the air" (Jiang, Xu, & Stringer, 2018).

For this reason, the support material was developed to solve the existing problem. This material has a lower melting temperature than the part material, which is placed underneath the workpiece, overhanging the lower layers to create an angled surface. However, when

that angle exceeds 45°, the overhanging element generally requires support, or the weight of the unsupported material will cause the element to collapse and the print to fail (Radius, 2022), as shown in Figure 44.

Figure 44 - Cases where it is necessary to use support material (HUBS, 2022a)

The support material is integrated into the part design and printed into the part when it is produced. When it is used, it must be taken into consideration that it has to be removed after the printing. This leads to higher material and energy consumption and longer post-processing time. All these factors affect the manufacturing costs, which increase.

2.6.1. When to use support material

One technique to know when to use support material in manufacturing is the letters Y, H, and T useful to illustrate the need for support structures in additive manufacturing (Radius, 2022). This method is explained in Table 6.

Table 6 - YHT Principle / Support material requirement

The YHT Principle	
	Two arms extend from the letter Y at 45° – the angle of their overhang does not necessitate support structures. The further the overhang angle exceeds 45°, the more likely it is that support structures will be needed

	The letter H is a little more complicated, but if the centre bridge is under 5mm, it can be printed without support or sagging. However, over 5mm and support will be required. For this example, the centre bridge is over 5mm and support is needed (Perry Cain, 2022).
	The two arms of the letter T extend from the vertical element at 90°, requiring support structures. There is nothing for the outer arms to be printed on, and the material will fall down without support.

2.6.2. Types of Structures

There are several possibilities of support structures for manufacturing parts in FDM: lattice supports, unit cell supports, honeycomb supports, tree-like supports, and linear/PIN supports. The most common are the last two.

The tree support replicates the structure of a tree and encloses the print around its "trunk" with "branches". It can be designed, applied and tested quickly as part of a 3D printing project, enabling rapid iteration. In addition, this structure has less contact with the print surface, resulting in a better surface finish post-processing. In Figure 45 a) this structure is shown.

Linear support is the most common type of support used in 3D printing, consisting of vertical pillars touching the entire overhang. This 3D printing support works for just about every overhang and bridge. However, they are much harder to remove and much more likely to cause damage to the model surface.

The block supports resemble walls, and with various mounting points, fence supports are printed perpendicular to a part's surface, often with a lattice structure (Radius, 2022). This type of support is more durable and accessible to remove than tree supports and is the most common and best suited for most FDM prints. Figure 45 shows the tree-like structure a) and the block structure b).
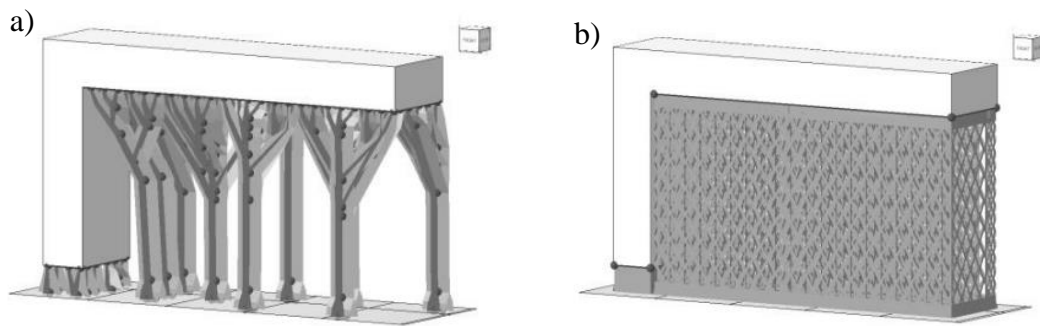
Figure 45 - Tree-like structure and block structure (Weber, 2020)

2.6.3. Remove Support Material

There are two ways to remove the support material, either through physical means, as in the case of breakaway materials, or dissolved with soluble support.

Breakaway support is trimmed, sanded, or otherwise mechanically removed. Depending on the build material and shape of the printed object, removing support may be simple or laborious. Delicate details can make removal difficult without damaging the print, and complex voids or other internal structures are not possible with breakaway support. This is where soluble supports have an essential role (Team, 2022).

In printers with two print heads, the support material can be printed with a dissolvable material that does not tear away from the part but instead dissolves away in a chemical solution that does not affect the primary material of the printed model. Soluble support is removed by placing the printed object in a bath of water or solvent. The result of the chemical removal depends on the material and temperature; if needed, additional mechanical agitation is used. This chemical method will result in a better surface finish than breakaway supports. However, it can be an expensive and time-consuming solution.

2.6.4. Material supports optimization

It is essential to try as much as possible to reduce the amount of support material used in printing since the use of solvents implies material costs and production times.

One way to reduce the number of support structures needed is to choose the optimal part orientation. Depending on the part orientation, fewer or more support structures may be needed. For example, consider a part printed in the shape of the letter T. In its normal position, both branches of the letter will collapse without support structures. However, if the

part is oriented differently, then supports will not be required (Manufacturing, 2018). As a result, it is feasible to comprehend that a part can be constructed in various ways, implying that the need for supports might vary and be highly influenced by the part's orientation.

Another method is to optimise the support structures to use as little material as possible and to speed up the printing process. The correct choice of the type of structure used to build the support material can be advantageous. For example, creating tree-like support structures instead of straight vertical structures may be a viable alternative because they consume 75 % less material. Figure 46 shows an example of support material reduction through the type of structure choice, in image a) shows the part with an opaque support structure, while image b) shows a lattice support structure.
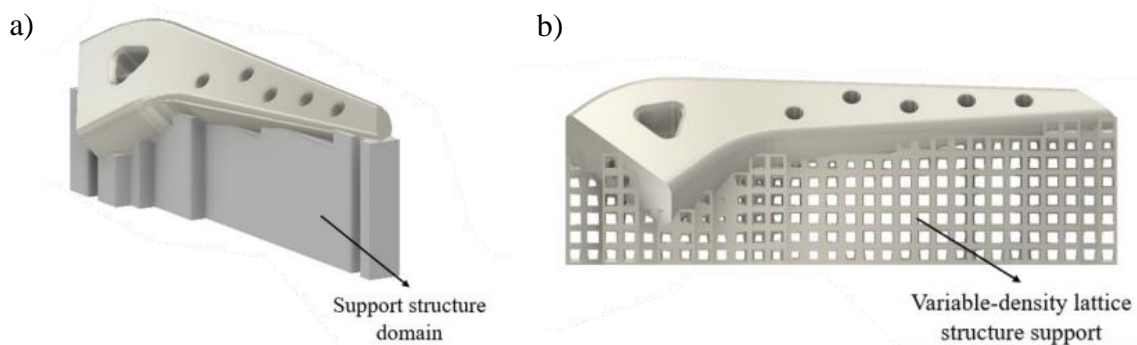
Figure 46 - Support material reduction through lattice structure (Cheng et al., 2019)

Another idea is to use fillets and chamfers instead of support structures for overhanging surfaces greater than 45 degrees. These features turn an angle greater than 45 degrees into an angle that is 45 degrees or less and can be added to either the interior or the exterior of a part (Manufacturing, 2018).

The final solution is to split the part, which will reduce the amount of support and speed up the printing process while saving material. In the end, it is possible to assemble the parts.

3. **Materials and Methods**

This work aims to study the mechanical properties of several metal specimens that will be produced. All these pieces will have variables: density, type of infill and construction orientation. When the mechanical properties of these parts are studied through tensile tests and other tests, it will be possible to compare the results obtained. This comparison will lead to a conclusion as to which combination of variables is the most effective for producing metallic parts using the FFF technology.

This chapter will present the experimental procedures in chronological order according to work done.

3.1. Materials

The material used in this study is "Ultrafuse 316L", composed of 90% 316L stainless steel and 10% BASF Polymer, allowing it to be used in any FDM/FFF printer. This material is typically used to create tooling, jigs and fixtures, series production, functional parts and prototypes (BASF 3D Printing Solutions, 2019b). Figure 47 shows a roll of this material.

Figure 47 – BASF Ultrafuse 316L – Quality (IGO3D, 2022)

This material is an affordable, easy-to-use metal 3D printing solution for mechanical and functional parts. Stainless steel 316L is corrosion-resistant, strong, and robust. After going through all the necessary steps, this material is an excellent choice to withstand pressure.

Ultrafuse 316L is a good material for prototyping and tooling, jigs and fixtures, moulds, and other functional parts where durability and resistance are essential. The main industries

where it can be used are the medical, automotive, or aerospace industries to create functional prototypes and mass production.

According to the datasheet of the material, specific parameters must be respected so that the printing happens fluidly. For example, as is possible to see in Table 8, there are temperature ranges to be respected for the nozzle and the platform. In addition, the nozzle diameter and print speed also have parameters that must be followed.

Table 7 -Print processing parameters of Ultrafuse 316L (BASF 3D Printing Solutions, 2019b)

Recommended 3D-Print processing parameters	
Nozzle Temperature	230 – 250 °C
Build Chamber Temperature	-
Bed Temperature	90 – 120 °C
Bed material	Glass + approved glues* / polyimide tape (*Dimafix® suggested)
Nozzle Diameter	≥ 0.4 mm
Print Speed	15 – 50 mm/s

The material has good mechanical properties and a low cost of production, making it one of the most affordable materials for metal 3D printing. Table 8 shows the mechanical properties in terms of tensile strength, yield strength, elongation at break, impact strength and Vickers hardness.

Table 8 - Mechanical properties of Ultrafuse 316L (BASF 3D Printing Solutions, 2019b)

	[1]Specimen shape Form E2x6x25 according to DIN 50125 [2]Undersized impact test specimen according to DIN EN ISO 148-1		
Print direction	Standard	XY	ZX
Orientation		Flat	Upright
Tensile strength	DIN EN ISO 6892-1[1]	561 MPa	521 MPa
Yield Strength, $R_{p\,0.2}$	DIN EN ISO 6892-1[1]	251 MPa	234 MPa
Elongation at Break	DIN EN ISO 6892-1[1]	53 %	36 %
Impact Strength Charpy (notched)	DIN EN ISO 148:2017-05[2] (2mm V-notch)	111 J/cm^2	-
Vickers Hardness	DIN EN ISO 6507-1	128 HV10	128 HV10

The printer used for this work was the Ultimaker S3. This printer belongs to 3D Dual Extrusion FDM which offers high quality and consistent performance in a compact size. This printer was intended initially to produce polymer parts. However, in this work, it has been adapted to be able to print metallic material by changing the nozzle from one AA0.4 mm to one CC0.6mm. In Figure 48, it is possible to see the machine used, the Ultimaker S3.
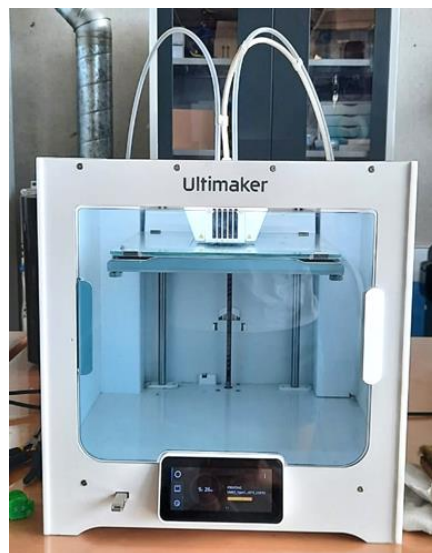
Figure 48 - Ultimaker S3

This printer has two print heads, one for the main material and one for the support material. When printing specimens that are horizontal to the build plate, there is no need for

support material, as the surface area can handle the printing independently. For the printing to run smoothly, it is necessary to maintain the printer, such as cleaning the plate and the nozzle. These two factors can influence the structure of the printed part.

3.2. Methods

The process used in the practical component of this thesis is FFF. Figure 49 is a summary of the steps of the practical component of this work.
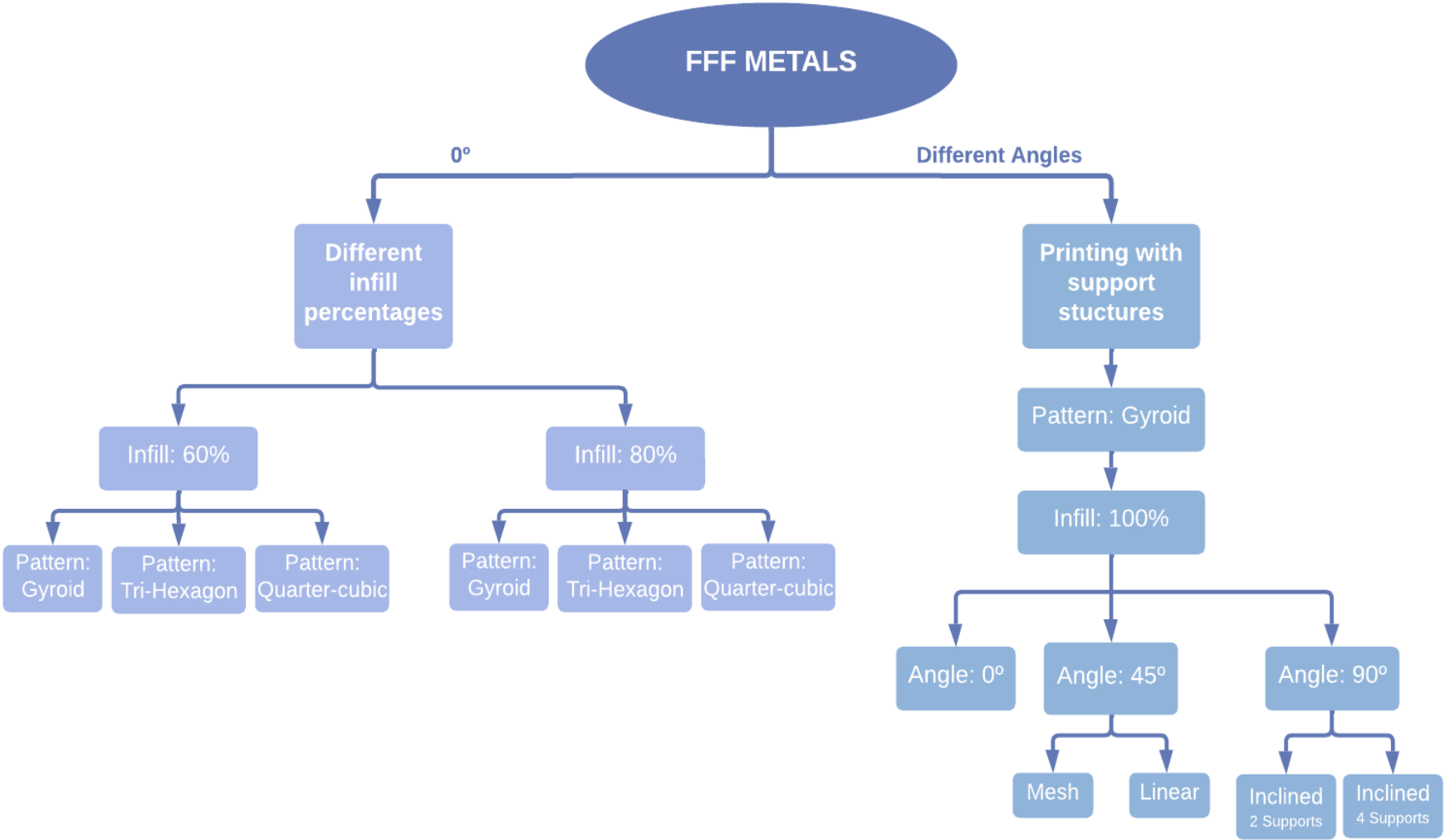
Figure 49 - Flowchart of the practical work

The initial part of the practical work refers to printing 0º specimens with different infills and patterns. Therefore, some parameters were defined to produce the specimens to carry out this work. Thus, the parameters chosen for the infill pattern were: gyroid, tri-hexagon and quarter cubic. In terms of density, the percentages used were: 60% and 80%. Therefore, it is necessary to produce seven specimens of each pattern with different densities.

For specimens to reach the correct size after being sintered, they must be sized to 119.8% in X and Y and 126.6% in Z. These dimensions were given by the BASF manufacturer, Figure 50.

	Component dimensions (mm) CAD	Shrinking	Scaling	Large Green Part (mm)	Large Printed Part (mm)	Large Sintered (mm)	New Scaling
X	20.00	16.5	1.20	24	24.25	20,33	1.198
Y	20.00	16.5	1.20	24	24.25	20.25	1.198
Z	20.00	20.7	1.26	25.20	25.10	19.90	1.266

Figure 50 - Percentage recommended for the BASF because of shrinkage (IGO3D, 2020)

This contraction happens because catalytic debinding removes the primary binding materials of Ultrafuse 316L, causing shrinkage. Once debonded, the part is referred to as "brown". Brown parts are comprised of tightly packed metal powder. During sintering, the metal particles fuse, reducing the part size (BASF 3D Printing Solutions, 2019a). For this reason, the following measures will be the oversizing factor, which consists in the amount to scale up the green part to produce the desired sintered part.

In Table 9, it is possible to see all the parameters to follow, and in Attachment I, it is possible to consult in a more detailed way all the parameters used.

Table 9 - Data of the printed specimens

3D PRINTING DATA											
% INFILL	PATTERN	QTD	WALLS	BOTTOM	TOP	NOZZLE TEMP.	BED TEMP.	INFILL LINE DIRECTIONS	X	Y	Z
60%	Gyroid	7	2	6	6	240ºC	100ºC	-	119,80%	119,80%	126,60%
	Tri Hexagon	7						0			
	Quatercubic	7						0			
80%	Gyroid	7	2	6	6	240ºC	100ºC	-	119,80%	119,80%	126,60%
	Tri Hexagon	7						0			
	Quatercubic	7						0			

3.2.1. 0º Specimens – Different infill patterns and density

It is not common to print solid objects in Additive Manufacturing. This is mainly because printing solid parts use a lot of material, and the printing time is much longer. The standard form to avoid printing solid parts is the inside (infill) printed with less than 100% density. The infill pattern is a structure repeated to fill a 3D object and is typically not visible. The infill can have different patterns, such as gyroid, triangles, lines, tri-hexagon, cubic, and quarter cubic, among many other options.

Varying the infill percentage and the pattern can affect strength, material usage, print time, and other aspects of the object's performance. Every increase in strength usually means the cost and the print time are higher. In addition, the number of parameters can influence the final product. For example, this parameter has no influence when the fibres are oriented in the same direction as the raster angle (0◦). On the contrary, in other cases, the number of perimeters positively influences strength. For example, a raster angle perpendicular negatively influences strength to the direction of tensile and is positively influenced by a raster angle in the same direction of loading (Silva et al., 2021). The infills used in this work are gyroid, tri-hexagon and quarter cubic.

The gyroid infill creates a series of waves in alternating directions. It is a structure that allows excellent rigidity and resistance in every direction associated with low density, therefore less weight. It is known for being fast at printing, saving material, and not crossing

itself. Gyroid infill is an excellent fit to produce rigid and functional parts that need to withstand multiaxial stresses. In Figure 51 a) it is possible to see the unit cell of the gyroid infill and in b) the look of the specimen with the infill pattern on the right.
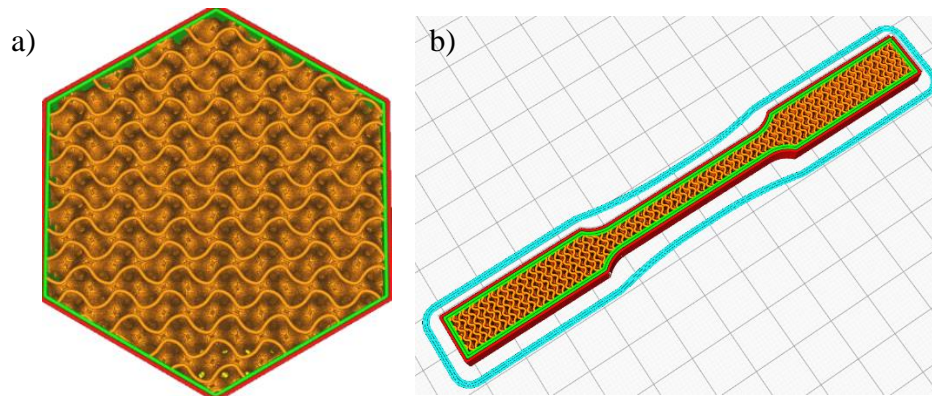
Figure 51 - Gyroid - unit cell and specimen with the infill (Michael Dwamena, 2022)

The tri-hexagon infill pattern consists of hexagons connected by triangles. It does this by creating three sets of lines in three different directions, but in a way that they do not intersect in the same position (Michael Dwamena, 2022). It provides high stability in X and Y directions, and moderate stability in Z. Hexagonal structures are generally very stable. They are often used in architecture, engineering and packaging materials to increase mechanical stability with as little material consumption and weight as possible (Martin, 2022). This principle is also very advantageous in 3D printing, as it needs less filament and time for a more stable object. In Figure 52 a), it is possible to see the unit cell of tri-hexagon infill and in b) the look of the specimen with the infill pattern on the right.
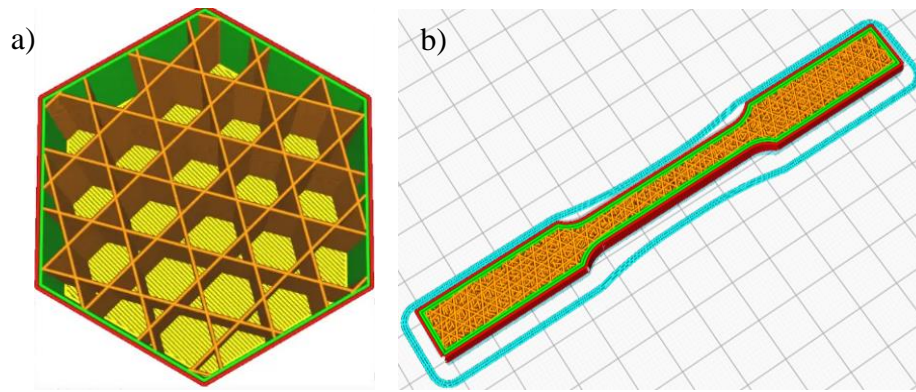
Figure 52 - Tri-hexagon - unit cell and specimen with the infill (Michael Dwamena, 2022)

The 3D pattern quarter-cubic has a close arrangement of shapes, consisting of tetrahedral and shortened tetrahedral forms. It places alternated multiple infill lines adjacent to the previous ones. This infill pattern is recommended to produce rigid and functional parts that need to withstand multiaxial stresses, such as a shelf bracket (Pollen, 2022). In Figure 53 on the left, it is possible to see the unit cell of the quarter-cubic infill and the look of the specimen with the infill pattern on the right.
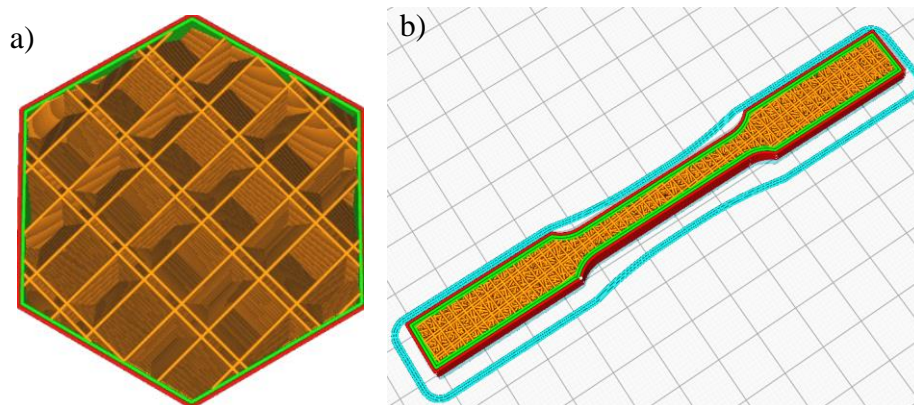
Figure 53 - Quarter-cubic - unit cell and specimen with the infill (Michael Dwamena, 2022)

After seeing all the parameters used in this process, the practical component begins. The first step is to import the CAD model of a tensile into the CURA software. In this software, it is possible to adapt the printing parameters to achieve the desired product. For example, it is possible to change the amount of printed tensile, the infill patterns, the percentage density,

the layer thickness, the type of material, the number of walls, the diameter of the nozzle, and other properties of the software. Figure 54 shows one specimen on CURA software.
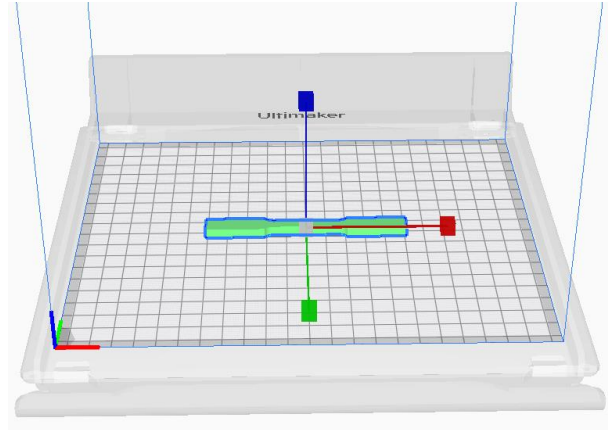
Figure 54 - CURA parameterisation

After the features are changed in the software, information is exported from the software to the printer, Ultimaker S3. Before it is put to print, it is necessary to pay attention to the condition and cleanliness of the machine. Check if the nozzle and plate are clean and if there is enough material to start printing.

If the conditions are right, glue on the platform is necessary so that it can stick to the platform when the material is deposited. The next step is printing, where the platform is warmed up in the first minutes, followed by the machine's calibration. After these two steps, the printer starts printing. Throughout this process, if there is material outside this area, the printing is not occurring correctly.

Throughout this process, the material is pulled through the printer, passing through the heating zone being extruded through the nozzle. Here, the material becomes more moldable, and as it leaves the nozzle, it is deposited layer by layer on the machine platform. After the printing is done, the result is shown in Figure 55.

When the printing process ends, the plate is removed from the machine and placed in a washing tank where the parts peel off from the plate. Then, the process is repeated for the other tensiles with different infill patterns and density percentages.

Figure 55 - Specimens printed with FFF technology

At the end of all the parts are made, the company responsible for the debinding and sintering process is *Conspir3D.*

This company performs the debinding process following the BASF method at 110 ° C with HNO3> 98%. Formaldehyde develops from the parts during debinding and can react with an oxidizing agent. The limit of oxygen to not explode is 4.5 vol %. There is evidence of a slow reaction between formaldehyde and nitric acid. For this reason is not used a high dose of nitric acid (Conspir3D, 2022)

This process is done in a 50 litre debinding oven. For this process to be carried out safely, specific parameters are respected. As is the case with the nitric acid, which must be at 30ml/h, and the nitrogen with an inflow of 500l/h. Furthermore, the value of the gas cannot be higher than 39ml/h. In addition to the previous steps, some preventive measures were taken to ensure the oven's correct operation and process. Thus, maintenance intervals were observed, especially for the door seals and the recirculation fan bearings.

When a minimum debinding loss of 7.10% is reached, the debinding process is finished. After this process, the sintering process begins.

The sintering process is done in a 100% clean and dry hydrogen atmosphere (dew point <- 40°C). Aluminium oxide (Al2O3) must have a purity of 99,6%, and a Frialit® Al2O3 (Friatec AG) is used to carry out the sinter transport operation.

The parameters to be followed for the sintering process to run as expected start with the room temperature of 600°C and hold it for one hour (5K/min), then increase to 1380°C

and keep it for three hours and finally, the cooling down of the at the oven. The burnt binder components remain early in the sintering process, and the pyrolysis products are extracted using a fan (Conspir3D, 2022).

At the end of the process, specific care must be taken in the oven cleaning operation as oxide of manganese (MnO) deposit may form during sintering. This compound may also present a fibrous morphology which may represent a health hazard and requires special care when cleaning the furnace (Conspir3D, 2022). These precautions include using an FFP3 mask and laboratory gloves and avoiding dust accumulation. The final appearance of the parts after this process is shown in Figure 56.
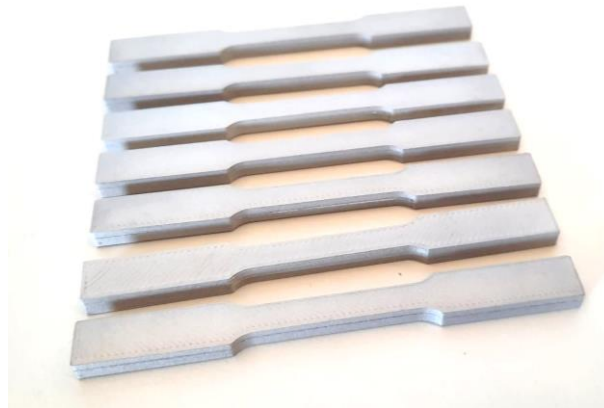
Figure 56 - Sintered specimens

3.2.2. 45º and 90º Speciemens - Support Stuctures

One of the purposes of this study is to compare the tensile strength of metal specimens created through additive manufacturing, specifically through the FFF technology. For this same reason, in addition to the 0º metal specimens already printed, specimens of the same material were produced with different degrees of construction, 45º and 90º, Figure 57.
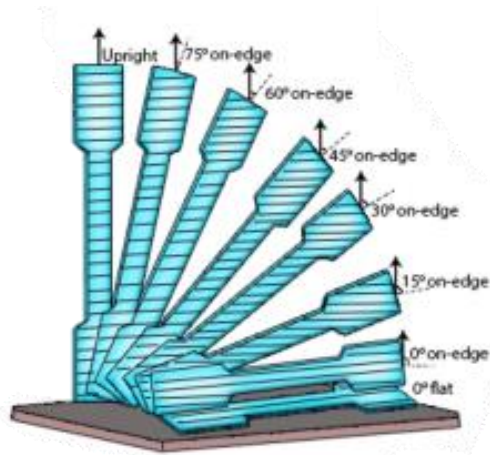
Figure 57 - Printing specimens with angles (Gonabadi, Yadav, & Bull, 2020)

In order to be able to print 45º and 90º specimens, it is necessary to create support structures. The CURA software automatically creates PVA support structures to hold the part, making removing the supports easier because this material is soluble in water. However, in this case, this type of support will not be sufficient since, for the sintering process to be correctly done, the parts must be sintered at the same angle as they were printed. For this same reason, it is necessary to create metal support structures like the central part. These are initially created through *Solidworks* software, then converted to an STL file and finally inserted in the *CURA* software where all the necessary parameterization for printing.

Several support structure types were created in Solidworks software to understand which type would be most suitable for printing the specimens. For the specimens created at 45º, three different types were designed. The first type consists of a simple linear structure with a 2mm thickness. In Figure 58, it is possible to see the designed structures; a) overall view; b) front view.
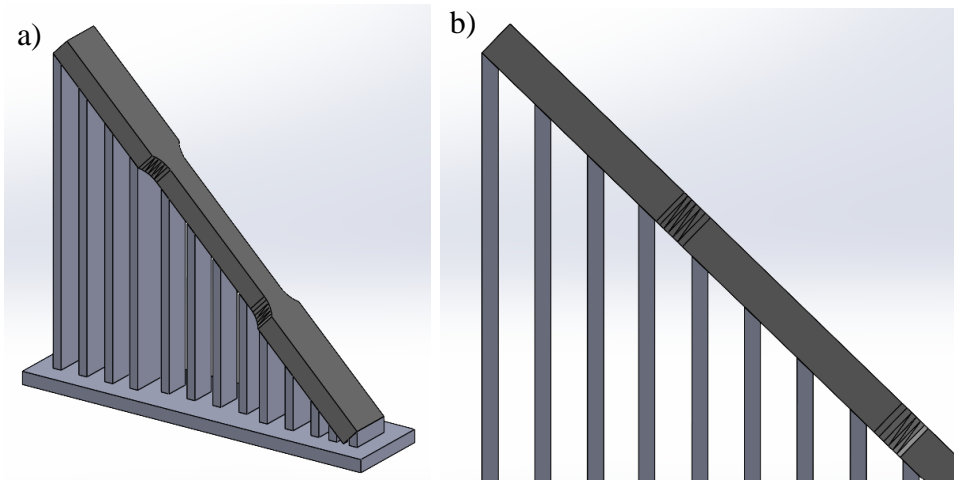
Figure 58 - 45º specimen - linear support structures

The second support structure was also linear with 1 mm of thickness. However, in this type, the ends of the support columns are narrowed to make it easier to remove the support structures at the end of the sintering process. In Figure 59, it is possible to see the designed structures; a) overall view; b) front view.
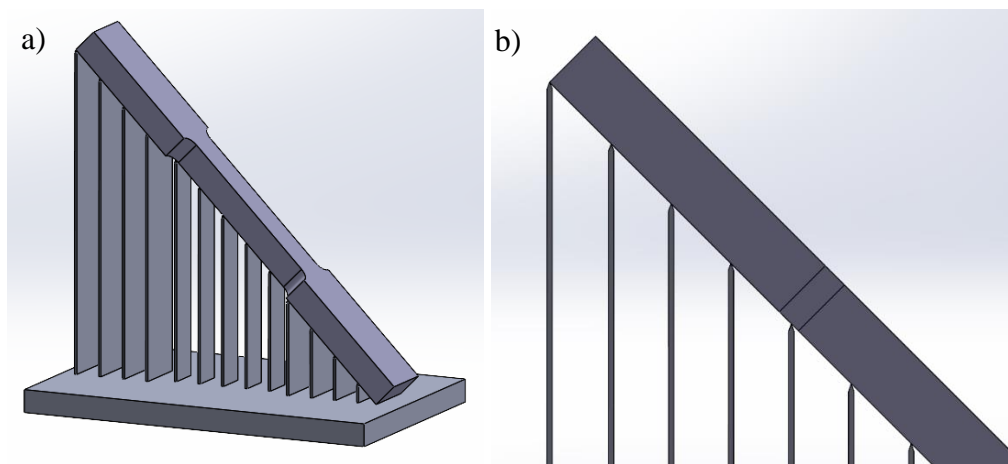
Figure 59 - 45º specimen - linear support structures with narrow tips

The last support structure to be created was the mesh structure, where each column is 2 mm thick. This support offers more structural support to the central part because it has columns vertically and horizontally. Figure 60 presents the mesh structure designed; a) overall view; b) front view.
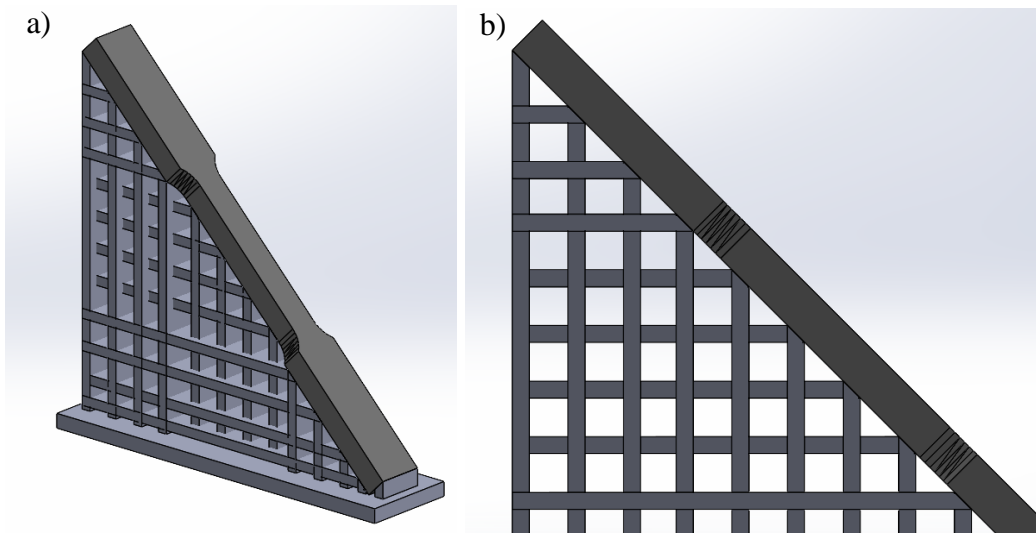
Figure 60 - 45º specimen - mesh support structure

Although it is not strictly necessary to print the 90° specimen with support structures, in this work, these are used so that in the sintering process, it is guaranteed that the parts are sintered at 90°. Therefore, two options of support structures have been designed for the specimens that will be created at 90º. The first option consists of only one column with 45º on each side of the part, positioned in the middle. These columns are 4mm wide at the bottom (contact with the base) and 3mm at the top (contact with the specimen). In addition, a circular base with holes was chosen because, with this geometry, we use less material and save material. In Figure 61, the designed structure can be seen; a) overall view; b) front view.
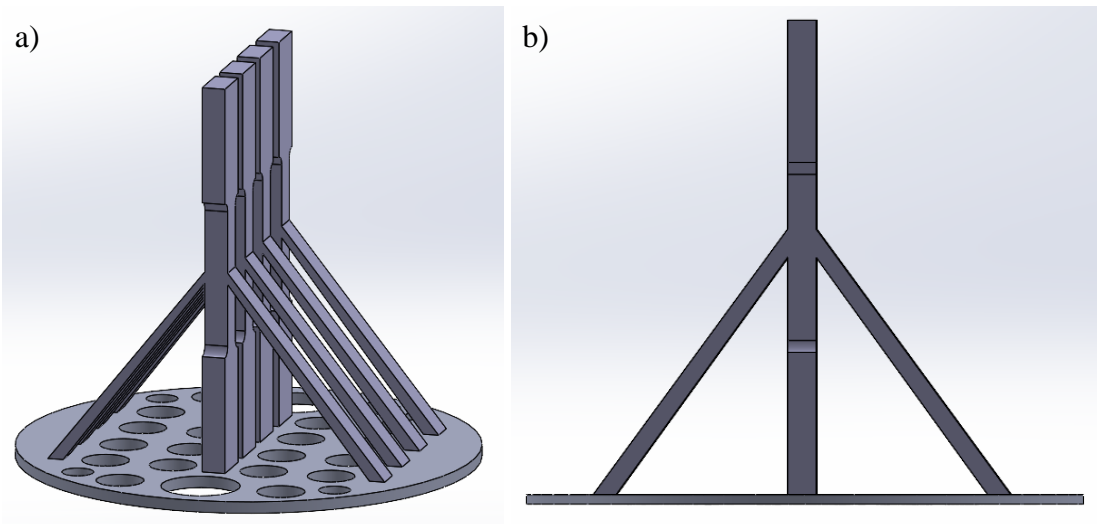
Figure 61 - 90º specimens - one support

The second type of structure created features two 45° columns, one at the top of the specimen and one at the bottom, on both sides. These supports were not placed in the narrow area of the part so that at the end of the sintering, it is easier to remove the support structures. These columns are 4 mm wide at the bottom (contact with the base) and 3 mm at the top (contact with the specimen). In Figure 62, it is possible to see the structure designed; a) overall view; b) front view.
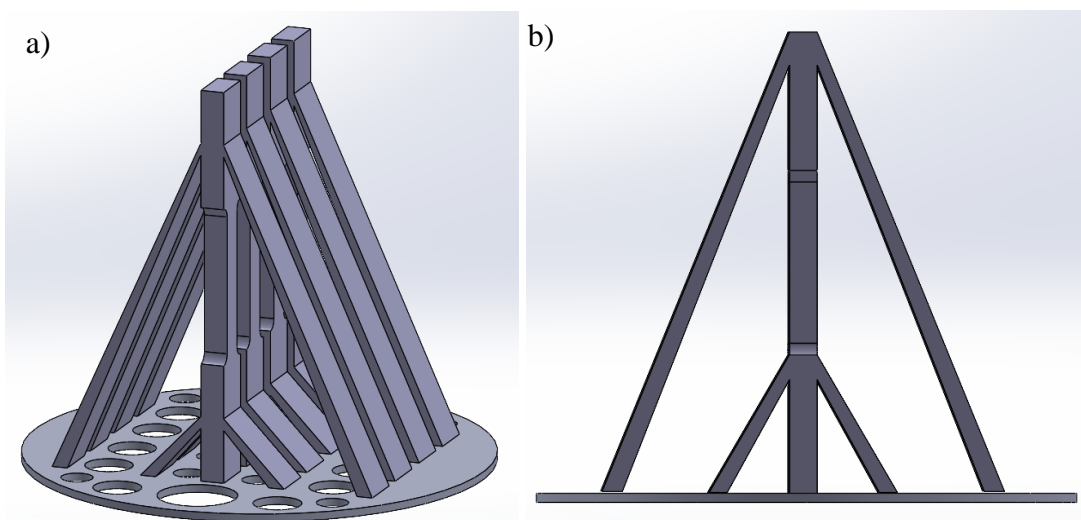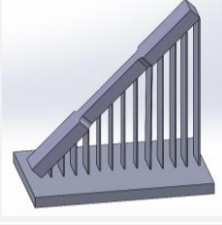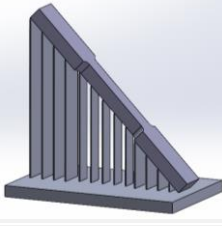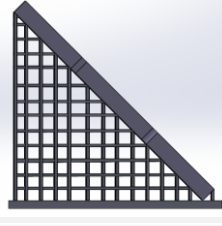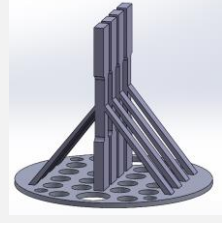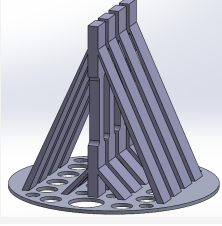
Figure 62 - 90º specimens - two supports

After all the support structures options have been created, it is necessary to analyse the advantages and disadvantages of each of them and then compare them. Hence, obtaining the most viable options for printing the specimens is possible. Table 10 presents each support's advantages and disadvantages and the final choice for printing.

Table 10 - Design support structures

				DESIGN SUPPORT STRUCTURES			
DESIGN	TYPES	Nº	ANGLE	IMAGE	ADVANTAGES	DISADVANTAGES	CHOSEN DESIGN
1	**Linear**	13 lines	45º		- use of few material - provides good support to the main part	- harder to remove the support material at the tips, compared to design 2	✓
2	**Linear** with narrow ends	13 lines	45º		- use of few material - easier removal of support material due to narrow tips	- does not provide as much support for speciemen	
3	**Mesh**	14 lines 13 rows	45º		- gives more support to the speciemen than designs 1 and 2	- uses more material than design 1 and 2	✓
4	**Inclined** 45º	2 columns	90º		- less support material than design 5 - easier to remove	- does not provide as much support for speciemen as design 5	
5	**Inclined** 45º	4 columns	90º		- gives more support to the speciemen than design 4	- uses more material than designs 4	✓

As it is possible to see in Table 11, the option chosen for printing the 45º specimen was designed 1, and for the 90º specimen, design 5. Design 1 proved to be an option that

provides good support to the specimen without using much material. On the other hand, design 5, despite using more material than design 4, provides more support in more vital areas of the specimen, making it less likely to break.

After the types of structures have been chosen, the next step is the printing part. All the support structures created in metal have an infill of 60%, and the infill pattern is gyroid. This infill pattern was chosen since it was the one with the best results in the tensile test done in the specimens printed with 0º. The appearance of the printing in *CURA* software is shown in Figure 63.
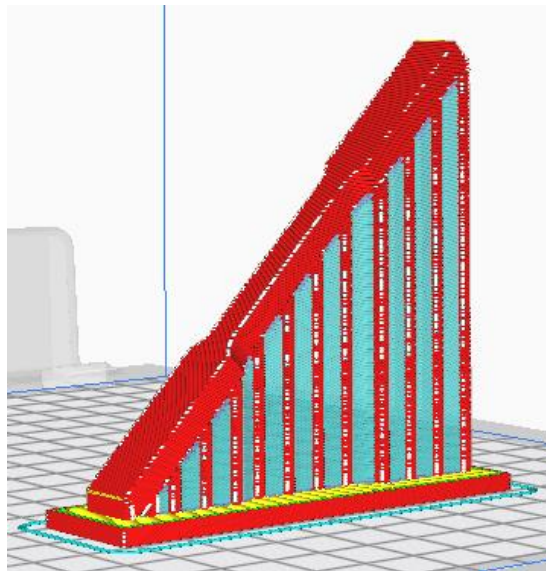
Figure 63 - Appearance of the 45º specimen in CURA

The first design to be printed is design 1. In printing this design, the PVA support material was used to provide extra reinforcement to the specimen. However, in the first attempts to print these parts, the printing did not go as it should have. In Figure 64 it is possible to see that when the printing with the PVA starts, the printing does not go as expected.

Figure 64 - Printing of the 45º specimens failed

After this situation, some changes were made, like printing only one sample instead of four, to see if the PVA problem was related to the amount of material used. In addition, the PVA material was changed by a new roll. After these changes were made, the final result is shown in Figure 65.

Figure 65 - 45º specimen printed with PVA structures

After this second attempt, it was realized that the problem would be that the PVA when extracted from the nozzle, could not stick to the metal platform already created. For

this reason, it was decided to print the specimen at 45º only with metal. The result of this change is presented in Figure 66.

Figure 66 - 45º specimen correctly printed without PVA

For the printing of the 90º specimens, the same process was followed for printing the 45º specimens, printing without PVA support structures, only with the structures created in *Solidworks* in metal.

Design 5 was printed without any PVA structures like in the other cases. Again, the result was positive, and the part was stable without any fragile zone, as had happened with the previous design. This may be because it has more support columns and because they are located in wider areas of the specimen. Figure 67 shows the final result.

Figure 67 - 90º specimens with two supports

Unfortunately, the specimens printed with 45° and 90° angles were neither debinded nor sintered, due to the unavailability of the company which Aalen University works. For this reason, only specimens made with 0° were tested for tensile, surface roughness and microscopic analysis. So, it will not be possible to understand whether the angle of construction of the parts through the FFF technology influences their mechanical properties or not.

3.3. Laboratory procedures

In order to verify the mechanical properties, the following tests will be performed: tensile strength, microscopic analysis and surface roughness. These tests were performed only for the 0° printed specimens and the cubes built for the microscopic analysis.

3.3.1. Tensile test

When the parts return, the mechanical properties of all the specimens are studied. The first test to be performed is the tensile test. This test is performed on the metal specimens is done in order to find their axial tensile modulus, ultimate strength and failure strain, according to DIN EN ISO 6892-1. The machine used is Zwick Z100.

All the specimens were numbered and measured the thickness and width. These measurements were entered into the test programme. The specimen to be tested is mounted on the machine, Figure 68.
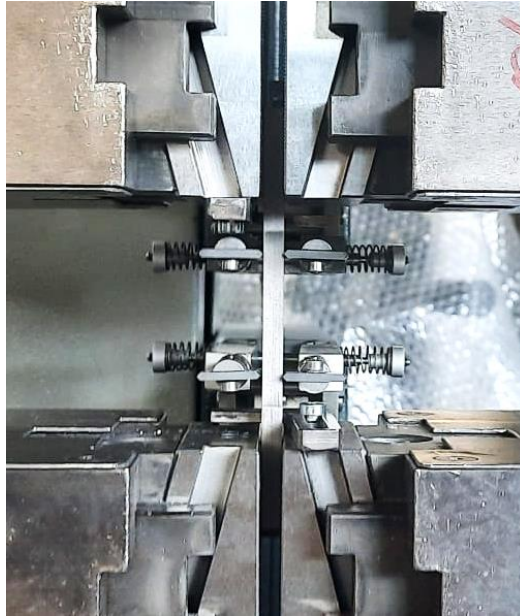
Figure 68 - Tensile placed in the tensile machine

Much care was taken to ensure the axis of the specimen was aligned with the axis of the cross-head. This process is vital in performing a uniform stress condition over the specimen's cross-section. Finally, the force is scaled to 0 N, and it is possible to start. The specimen is tensioned on both ends, and the chart records the test load and elongation until the specimen fails Figure 69. A total of 42 specimens are tested.

Figure 69 - Broken tensile

3.3.2. Microscopic Analysis

The microscopic analysis aims to understand the transformation that occurs to the infill before and after being sintered. For this purpose, cubes were printed with the different infills, Figure 70, used in this work, gyroid, quarter cubic and tri-hexagon, with a density percentage of 100%. Each cube measures X in length and width and Y in height, having no upper walls so that the analysis can be done. All the printed cubes were sintered except for one cube from each infill. In Attachment VI, it is possible to see all of the printing parameters of the cubes.
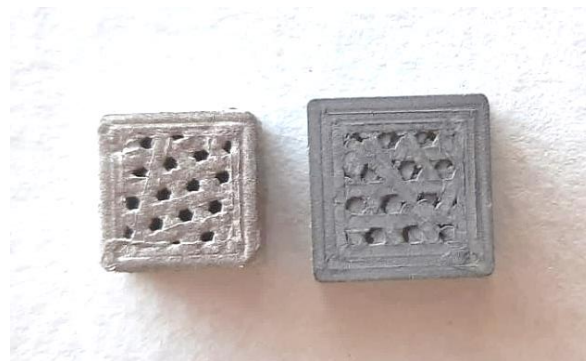
Figure 70 - Sintered cube on the left and only printed on the right

The microscope used was a Dino-Lite microscope, Figure 71. The process started by placing the cube on the plate under the microscope and adjusting the distance from the microscope to the part so that the image in the software appears focused. Then, using the software tools, measure the wall thickness of the cube and the diameter and thickness between the infill holes.

Figure 71 - Dino-Lite microscope for microscopic analysis

3.3.3. Surface roughness measurement

The surface roughness was measured with a contact profilometer, Zeiss Surfcom Touch 50, Figure 72. The measurements were done in tree samples of each category. The tests were performed under 4.0 mm of evaluation length, 0.3 mm/s of velocity, with cut-off (λs) of 0,08 mm and λs Filter of 2,5 μm. This test is based on the standard ISO 1997/2009.

To perform this test it was used the SupportWarrell software. The specimen was placed in the clamp. Then the needle was adjusted in height and horizontal distance to touch the pieces. The horizontal distance must be positioned at 0. This is how the test begins. Then the needle passes through the test piece horizontally for a few seconds, and the software displays the graph corresponding to its surface roughness.

This process is repeated three times for each specimen and is done in three specimens of each category (infill+density). Figure 73 shows the surface roughness test being dome.

Figure 72 - Zeiss Surfcom Touch 50

Figure 73 - Surface roughness test

4. **Results and Discussion**

4.1. Weight

When the specimens were printed, they were all weighed, and the same happened after they were sintered. Using this information it was possible to understand the consequence of the dibinding and sintering processes that causes the shrinkage of the part through the release of the polymeric component in the filament. The averages of the weights for each category (infill+density) were made, and Figure 74 was obtained through these values.
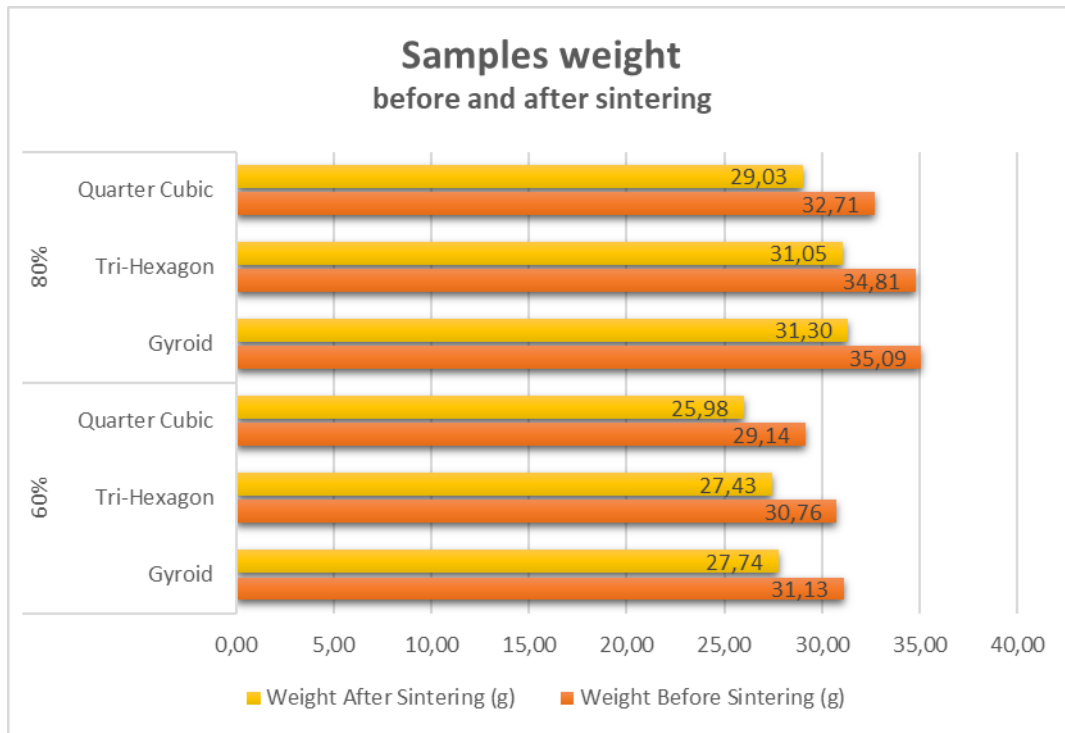
Figure 74 - Comparison between samples weight sintered and non-sintered

Figure 75 shows that the weight of the parts is reduced in all categories. The average difference in grams is 3,74g for the specimens with 80% infill and 3,29g for the specimens with 60%. In terms of infill pattern, the gyroid is the one that presents the most significant weight reduction and quarter cubic, the smallest, after the sintering process.

4.2. Shrinkage

As mentioned in sub-chapter "2.5.2. FFF Metals - Stainless Steel", the material "Ultrafuse 316L" used for producing the specimens presents a range of values concerning the shrinkage of the parts after the sintering process. For x/y, this range is 13-18%, while for z, it is 15-23%.

An analysis will verify if the shrinkage percentage of the sintered specimens corresponds to the theoretical values. The values of the non-sintered specimens were used to reference the values marked for the specimens in the CURA software. For y = 11.98 mm (width), and for z = 6.33 mm. The sintered specimens' measurements were obtained with an analogue micrometre. The obtained values can be consulted in Attachment IV in graphics and

attachment V in a table. The graph shown in Figure 75 was made with the results obtained from the table in the attachment.
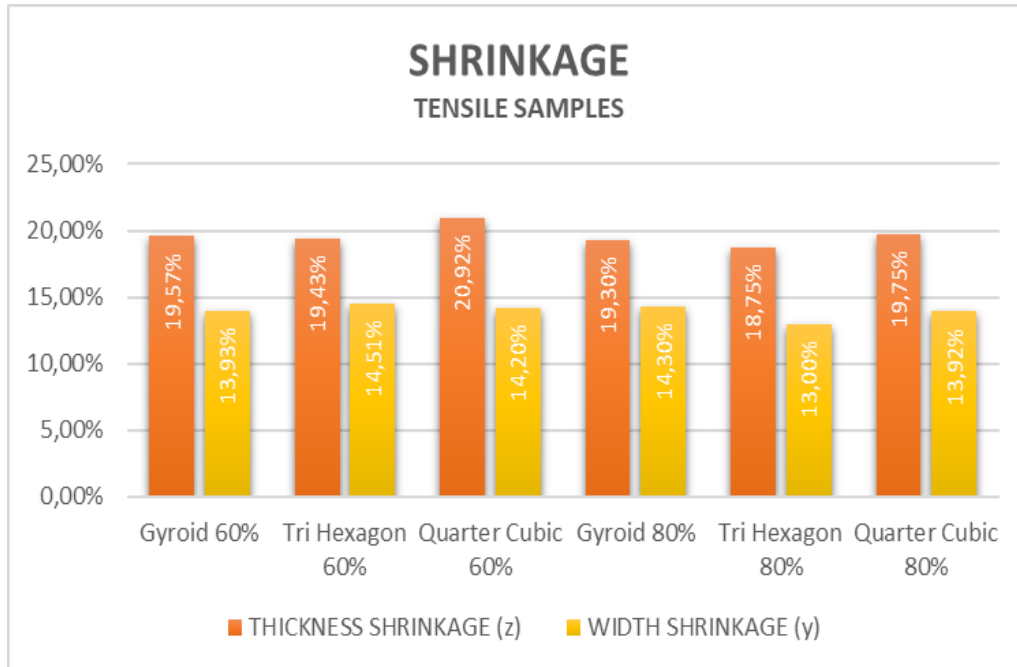
Figure 75 - Shrinkage in tensile samples

By analysing the graph, the shrinkage values corresponding to the width (y) are distributed between 13,00% and 14,51%, complying with the theoretical range of 13% - 18%. On the other hand, the shrinkage values for thickness (z) range from 18,75% to 20,92%, also complying with the theoretical range of 15% - 23%.

Visualizing the graph, it is also possible to see that the type of infill pattern does not influence the shrinkage behaviour of the parts.

4.3. Printing Time

A comparison was made between the time it took for each group of specimens to be printed to understand if the chosen infill pattern could delay the printing. As can be seen from Figure 76, the type of infill does not have a significant influence on the printing time.
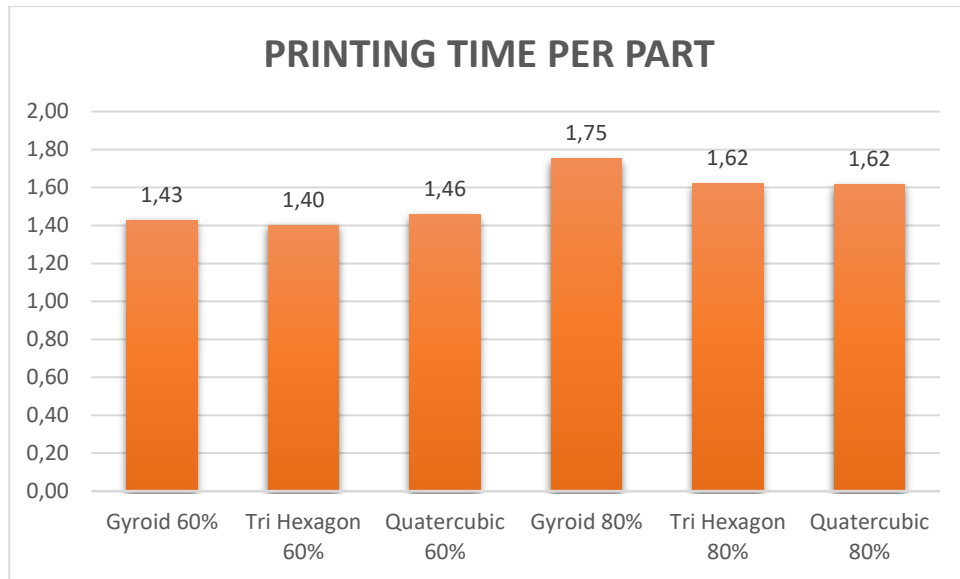
Figure 76 - Printing time per specimen for different infill patterns

4.4. Tensile Test

Seven specimens of each infill, gyroid, tri-hexagon and quarter cubic, with two different densities, 60% and 80%, were tested for the tensile test. In Figure 77, it is possible to see the result obtained for specimen AA with a gyroid pattern and 60% density. Attachments II, III and IV are presented with all the graphics obtained.
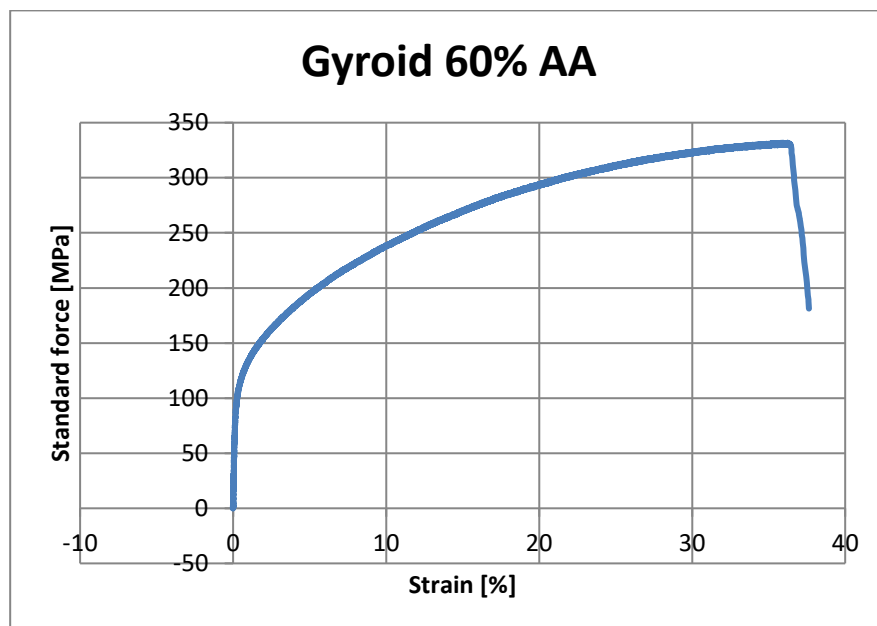
Figure 77 – Graph of the tensile test preformed on gyroid 60% infill specimen

As more test pieces are tested, the software of the Zwick Z100 machine generates a graph comparing the tensile stress-strain curve results obtained by the various test parts, Figure 78.
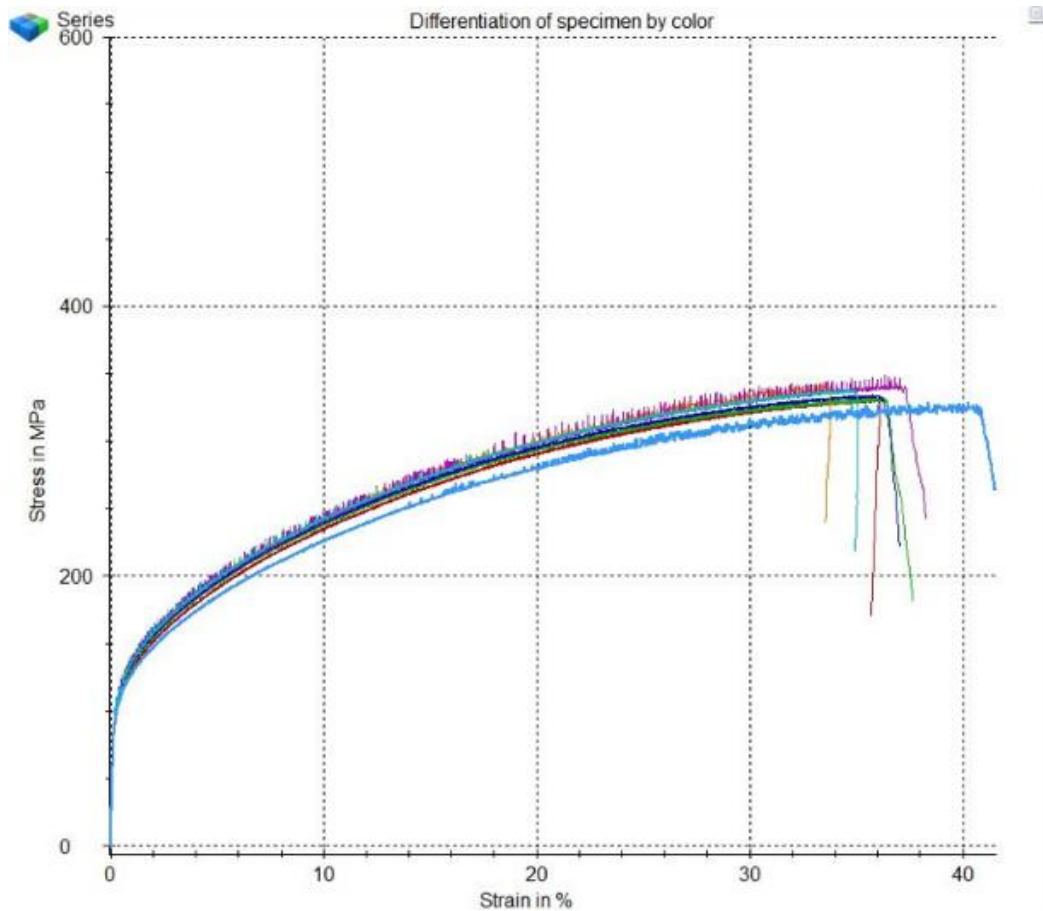
Figure 78 - Tensile stress-strain curve results Gyroid 60%

After performing all the tests on the various specimens, the tensile test program created reports for each sample. In these reports, the most relevant result to obtain conclusions is the Rm (Tensile strength), whose formula is the one presented below.

$$Rm \ (tensile \ stregth) = \frac{Fm \ (maximum \ tensile \ force)}{Specimen \ cross-sectional \ area \ S0}$$

The other result to be studied is the Rp 0.2 (Yield Strength). The calculation formula is the following:

$$\varepsilon = 0.20 \times (1^{-06}) \times \sigma + 0.20 \times (1^{-12}) \times \sigma^3$$

The results were organized in a table, and the average Rm values and standard deviation were obtained. The same procedure was applied to Rp 0.2 parameters. In Table 11, it is possible to see the averages obtained, and Attachment V presents all the values.

Table 11 - Averages of tensile test results

TENSILE TEST RESULTS - AVERAGES				
DENSITY	PARAMETER	GYROID	TRI-HEXAGON	QUARTER CUBIC
60%	Rm Average (Mpa)	336,583	278,181	323,01
	Rp 0.2 Average (Mpa)	109,156	113,367	104,485
80%	Rm Average (Mpa)	369,928	302,529	388,745
	Rp 0.2 Average (Mpa)	121,575	121,765	116,592

After each specimen category's averages and standard deviations were calculated, a graph was created (Figure 79), where it is possible to compare it. Thus, through the graph, it is possible to conclude that for the 60% infill density, the gyroid infill showed to be the most resistant to the tensile test since it presents the highest Rm value of 336,56 MPa. However, for the density of 80%, the infill that showed more tensile strength was the quarter cubic Rm with 388.745 MPa.
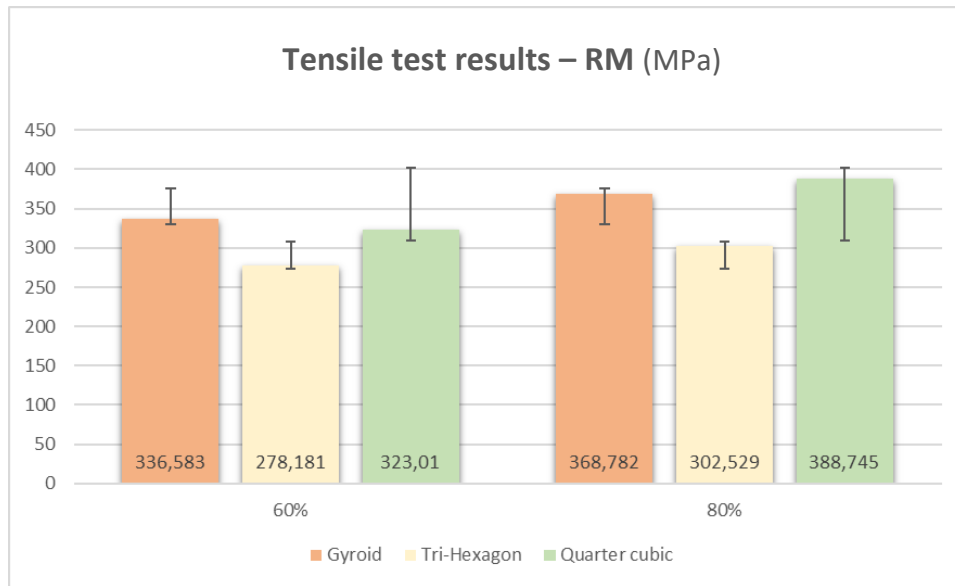
Figure 79 - Comparison between the tensile strength of different patterns and infill density (60% and 80%)

Since it is impossible to understand from these results which infill has the best performance, comparing the results of other tensile tests performed by other colleagues was necessary. Thus, the values obtained by other colleagues were added to the graph in Figure 80. They performed the tensile test for specimens with 10%, 25%, 50% and 100% with the same infill patterns. In the new graph (Figure 80), all of the values obtained for the different infill densities can be compared. The demarcated bars correspond to the specimens tested by the author of this work.
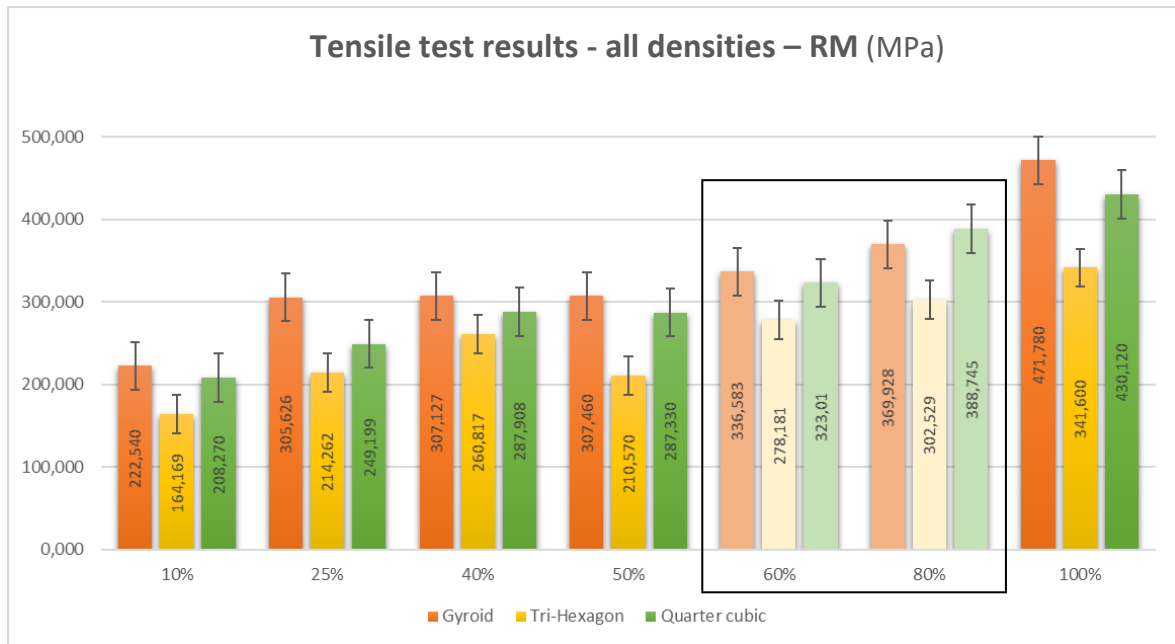
Figure 80 - Comparison between the tensile strength of different patterns and infill density

Through the analysis of Figure 80, it can be seen that the infill pattern that mainly shows better results in terms of traction is the gyroid and the one with lower values is tri-hexagon. Thus, it is possible to realize that there may have been some error in printing the gyroid tensiles with 80%, causing them not to have the expected performance in the tensile test. Despite this, gyroid is considered the infill pattern with the best tensile strength.

Also, in Figure 80, it is possible to verify that the 100% specimens obtained value was slightly below the theoretically expected value. Since the 100% specimens reached the maximum value of 471,78 Mpa tensile strength, the expected value presented in Table 9 was 561 MPa.

4.5. Microscopic Analyses

Through microscopic analysis, the following images were obtained by analysing the cubes printed at 100% density, with the three different infill patterns. Figures 81, 83 and 85 represent the non-sintered cubes, and Figures 82, 84 and 86 represent the ones that went through the sintering process. All these images were obtained with a microscope magnification factor of 60.7x.

Figure 81 - Gyroid microstructure non-sintered cube

Figure 82 - Gyroid microstructure sintered cube

.

Figure 83 - Tri-hexagon microstructure non-sintered cube
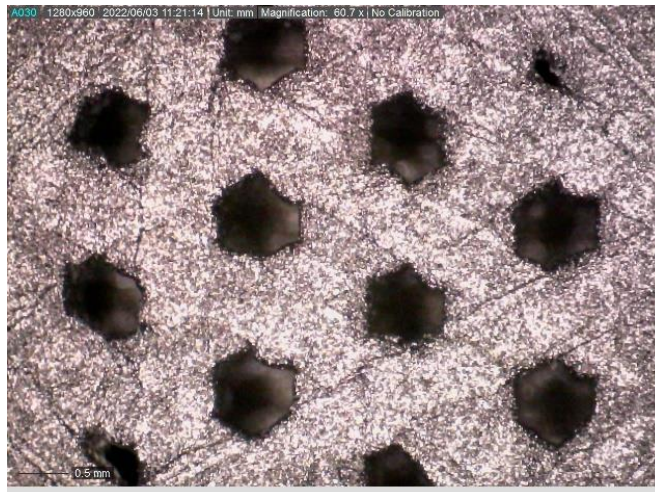
Figure 84 - Tri-hexagon microstructure sintered cube

Figure 85 - Quarter cubic microstructure non-sintered cube
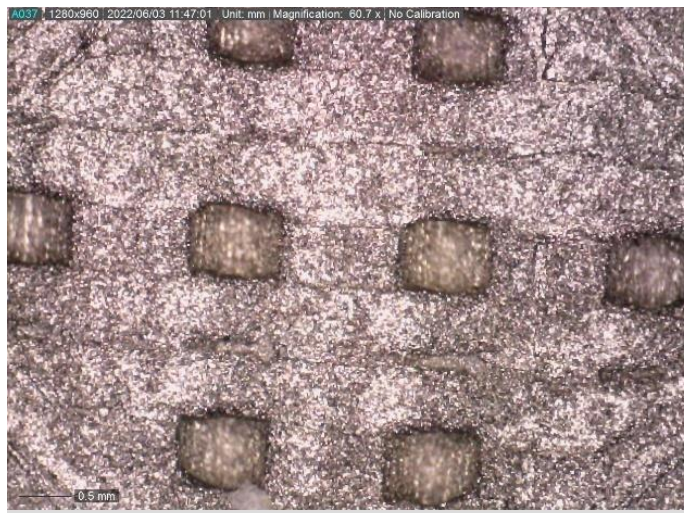
Figure 86 - Quarter cubic microstructure sintered cube

In order to understand what the differences in the infill are, some measurements were made, Figure 87. The first two measurements were the wall thickness and the dimension of the orifice of the non-sintered and sintered cubes. Attachment VII presents all of the measurements done.
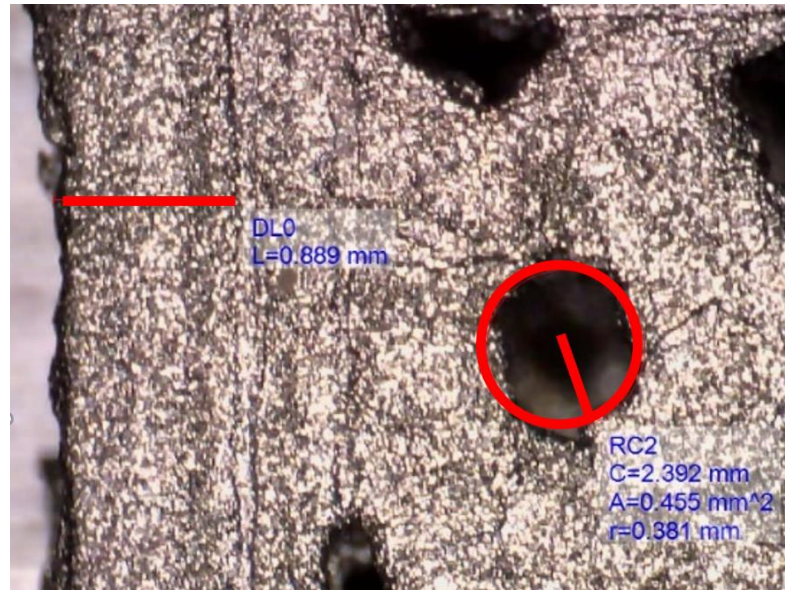
Figure 87 - Measurements were done through microscopic analysis

The graph "Line Width" in Figure 88 shows that all of the sintered cubes have a smaller dimension than the non-sintered cubes, as expected. It can also be observed that the quarter cubic infill proved to be the infill that suffered the most shrinkage with a percentage of 25.53%, followed by the gyroid infill with 10.6%, and lastly, tri-hexagon infill with 6.4%.
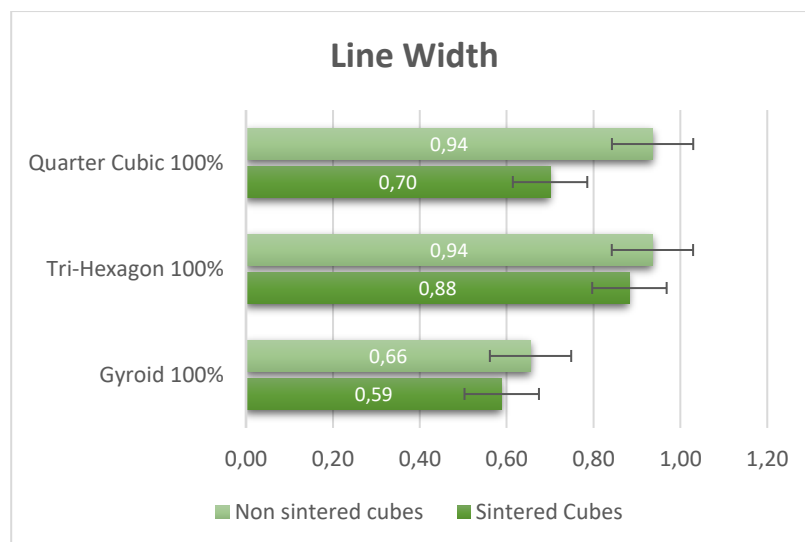
Figure 88 - Line width of the printed cubes

In the "Orifice Dimension" graph in Figure 89, the quarter-cubic and tri-hexagon infill showed a shrinkage percentage of +/-23%, while the gyroid infill was 27,3%. The latter proved to be the infill with minor porosity.
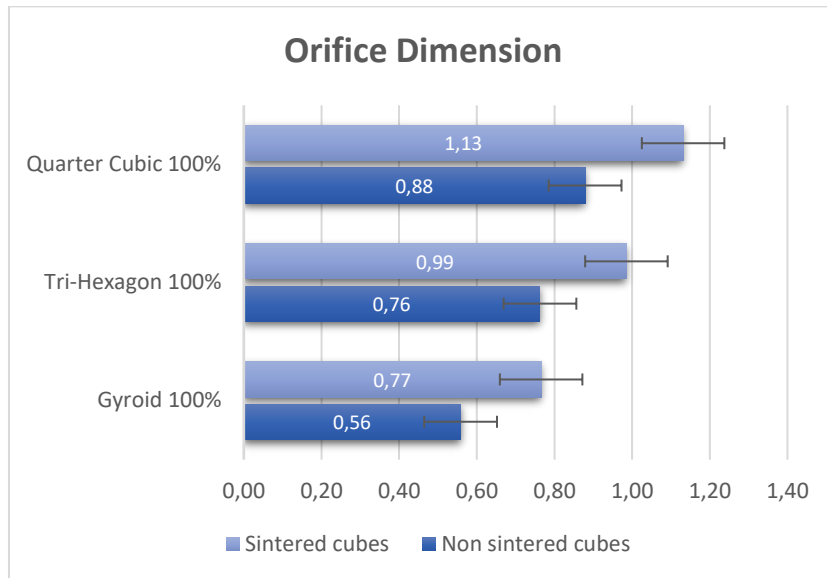
Figure 89 - Orifice dimension of the printed cubes

In the "Cube Length" graph, Figure 90, it is again noticeable that the gyroid infill showed the one with the highest shrinkage rate, with 14.6%. In the last graphic, "Cube Height", Figure 91, the shrinkage rate was similar in all infills.
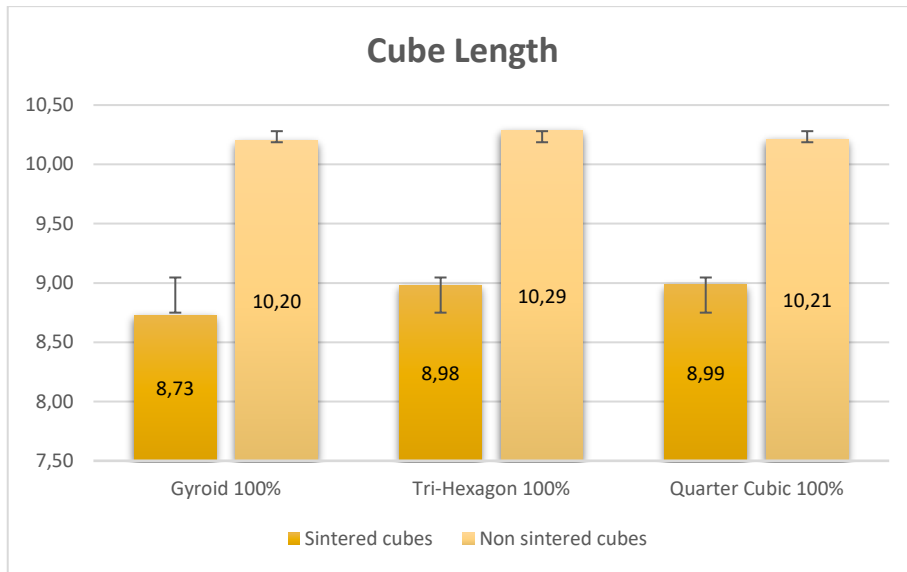
Figure 90 - Cube Length
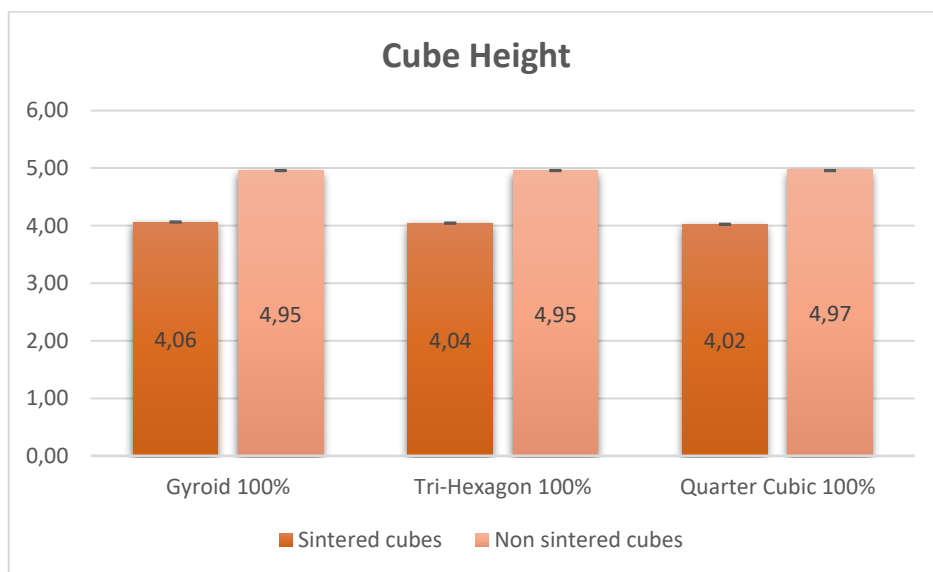
Figure 91 - Cube Height

4.6. Surface Roughness Test

After performing the surface roughness test, the programme provides the results through a sheet of graphs and values for each specimen tested, as shown in Figure 92. The remaining results can be found in Attachment VIII.

Prüfprotokoll

ACCRETECH

Seriennummer:		Kommentar		Messdatum	08.07.2022
Teilenummer		Prüfer	Kalhöfer	Messzeit	08:08:27

Messbedingung

Messtyp	Roughness measurement	Cutoff	0,8mm	λs Filter	2,5um
Berechnungsstandard	ISO1997/2009	Filtermethode	Gaussian	Einheit	mm/um
Auswertelänge	4,00mm	Messbereich	500,0um		
Messgeschwindigkeit	0,30mm/s	Entfernen der Form	Straight		

Messergebnis

Pt	54,292	Ra_5	2,179	Rz_5	13,079
Ra	2,744	Rz	17,185	Rp	8,766
Ra_1	2,684	Rz_1	17,211	Rp_1	9,380
Ra_2	3,529	Rz_2	19,453	Rp_2	9,315
Ra_3	2,658	Rz_3	19,021	Rp_3	9,895
Ra_4	2,670	Rz_4	17,163	Rp_4	8,087

Profilkurve

BAC(P)

BAC(R)

Figure 92 - Surface roughness test - specimen AA

All the results were treated and organized in Table 13, where the average of three specimens of each category (infill+density) was calculated and tested three times. Table 12 shows the averages obtained for Ra, the mean roughness value in micrometres, and Rz, the measured roughness depth. All the values obtained can be found in Attachment IX.

Table 12 - Average of the results obtained on the surface roughness test

SURFACE ROUGHNESS TEST - AVERAGE				
DENSITY	PARAMETER	GYROID	TRI-HEXAGON	QUARTER CUBIC
60%	Ra Average (µm)	3,34	2,97	3,91
60%	Rz Average (µm)	19,47	22,47	28,66
80%	Ra Average (µm)	3,19	3,04	4,74
80%	Rz Average (µm)	20,12	30,07	33,28

To better interpret the results, graphs were created for the parameters under study. Ra measures the average length between the peaks and valleys and the deviation from the mean line on the entire surface within the sampling length. Moreover, Rz measures the vertical distance from the highest peak to the lowest valley within five sampling lengths and averages the distances. Figure 93 shows the graph of the Ra values, and Figure 94 shows the graph of Rz values.
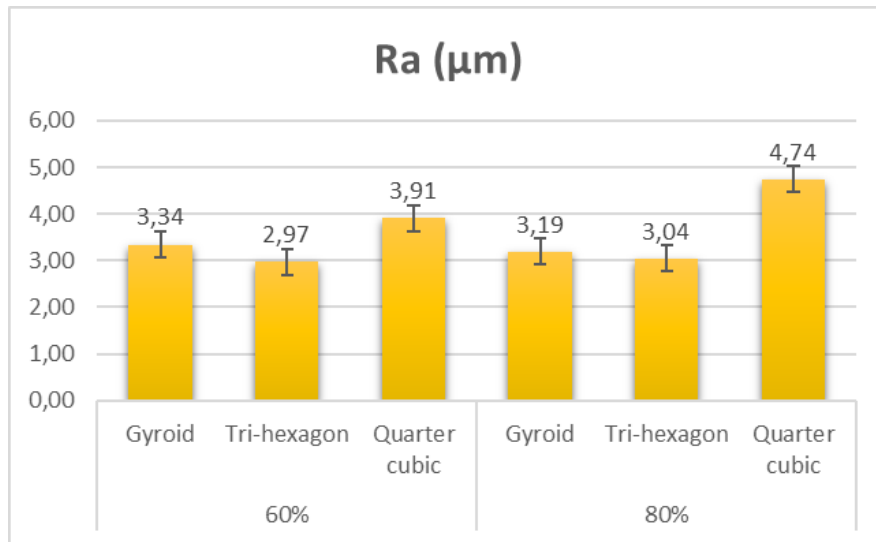
Figure 93 - Ra values obtained for the different types of specimens

In the graph of Ra, it is possible to see that the infill pattern quarter cubic presents the highest value for the specimens with 60% density and 80. Which means that this infill presents the most significant variation in average length between the peaks and valleys specimens' surface. The specimens with 60% density show values of 3.91 µm, and those with 80% density, 4.74 µm. On the contrary, the infill pattern tri-hexagon shows the lowest values. For this parameter, 2.97 µm for the specimens with 60% and 3.04 µm for those with 80%. Thus, the infill gives a smaller amount of rough parts on the surface along the length of the specimen.
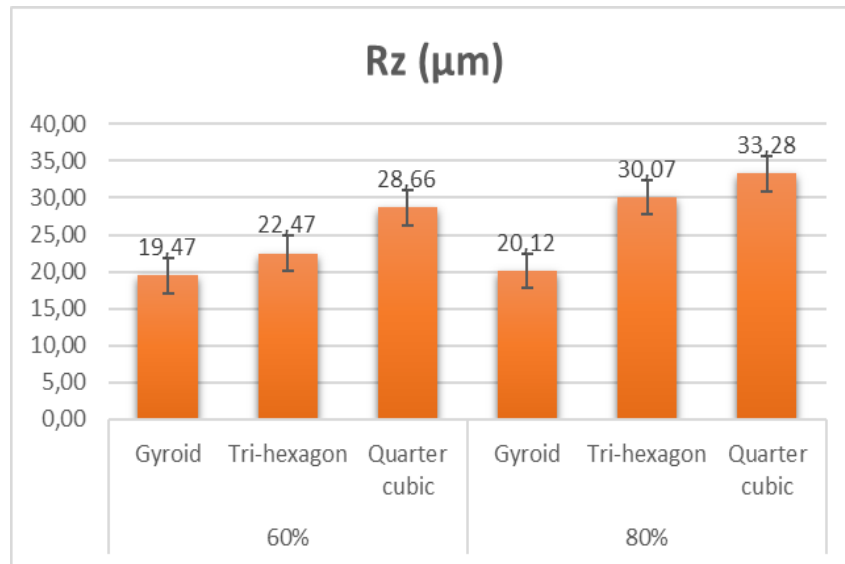
Figure 94 - Rz values obtained for the different types of specimens

In the Rz graph, the quarter cubic infill remains the infill with the highest values compared to the others, for the 60% specimens 28.66 µm and the 80% specimens 33.28 µm. This parameter means that this infill has a greater vertical distance between the peaks and valleys of the specimen surface. In other words, more roughness across the surface. However, for this parameter, the infill with the best results is not the tri-hexagon as it had been in the Ra plot but the pattern infill gyroid. This presents the smallest vertical distance between peaks and valleys. For specimens with 60% density, it is 19.47 µm; for those with 80%, it is 20.12 µm.

In the following graph, Figure 95, it is possible to compare the obtained values of Ra and Rz.
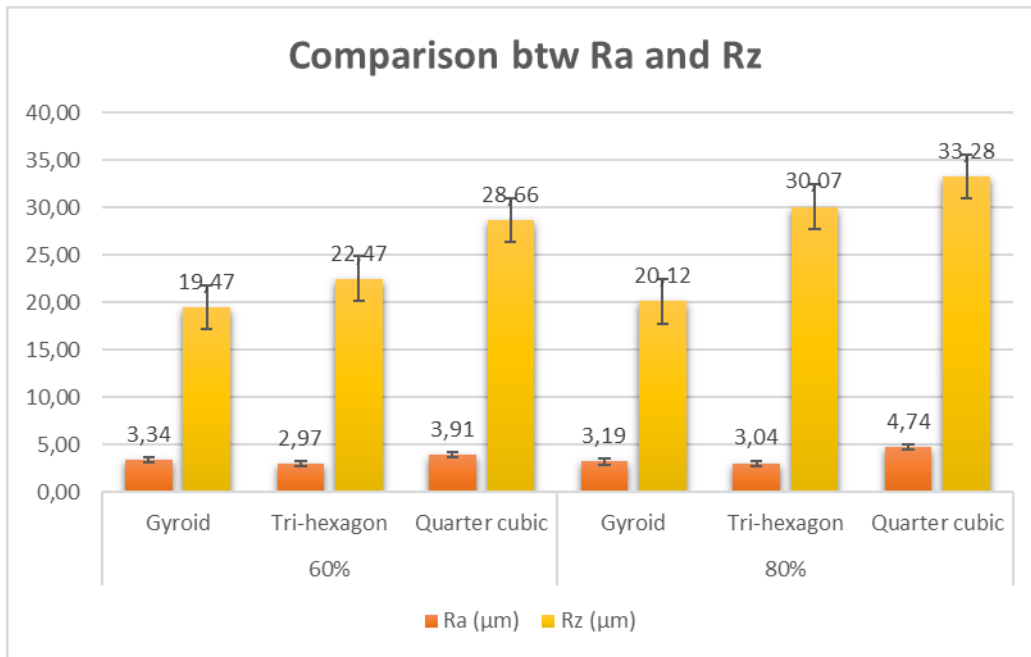
Figure 95 - Comparison between Ra and Rz values

Although the infill pattern gyroid has more peaks and valleys along the length of the specimen than the tri-hexagon infill specimens, they present a smaller vertical distance. Thus, the infill pattern gyroid is the best surface roughness.

5. **Printed Part**

As a case study, it was decided to print a component from the automotive industry to understand the influence of Fused Filament Fabrication technology in the production of parts and the cost of it compared with other technologies. Thus, the chosen part was the car cylinder head that sits on the engine and closes off the combustion chamber. This part was modelled using *Solidworks* software, and the final result is shown in Figure 96; a) top view b) bottom view.
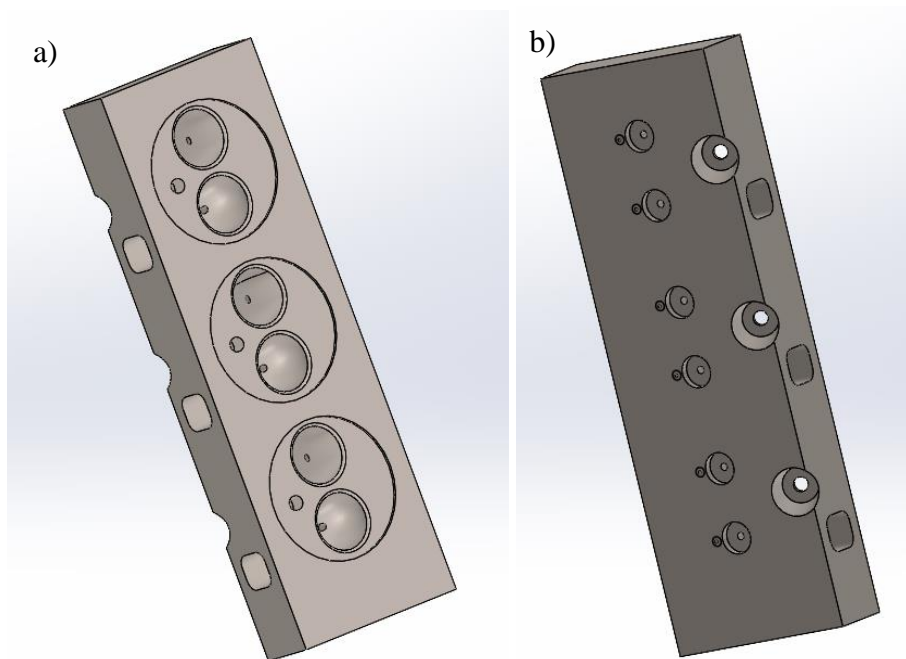
Figure 96 - Car cylinder head

After modelling, the design must be passed to the *CURA* software, where the parameterisation will be done. The parameters for printing this part are gyroid pattern, 60% density, 0º angle and without support material. The car cylinder head presents angles greater than 45º, so support material is required to print the part. However, no support structures will be used since the joining of PVA, and 316L stainless steel does not print the part correctly, as verified earlier in this work.

The original modelled part was oversized for the printer platen, so the part was scaled to 20% of its original size, the new dimensions are presented in Figure 97. It is with this new

dimension that the cost comparison between FFF and SLM will be carried out. In Figure 98, it is possible to see the preview version of the printed part in *CURA*.
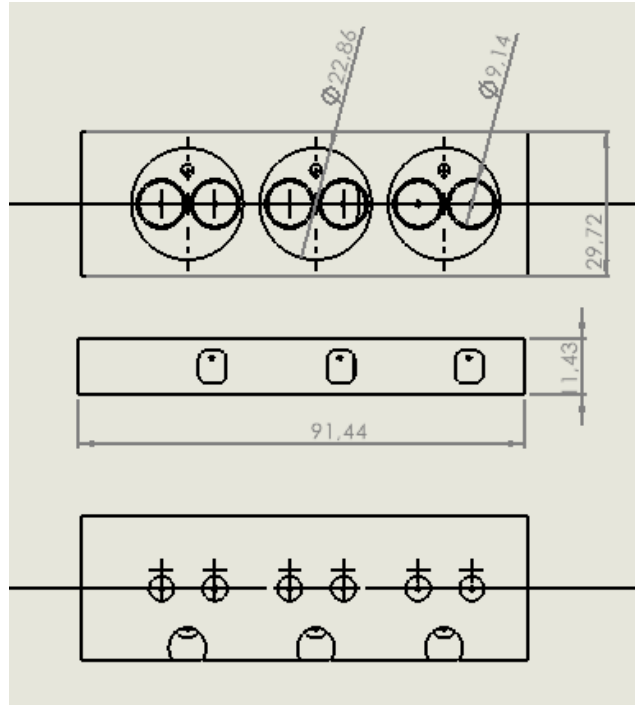
Figure 97 - Car cylinder head 2D drawing - dimensions
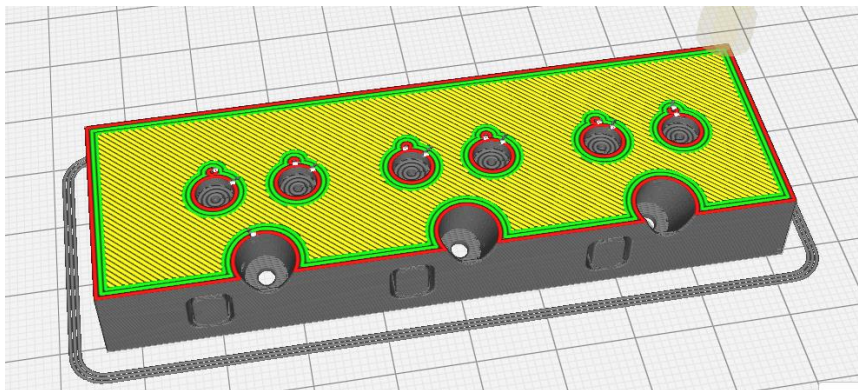
Figure 98 - Car cylinder head sliced on CURA

In Figure 99, the inside of the part is printed with a gyroid pattern only with 60% density. It is possible to see that no support structures are needed for the holes that the part has.

Figure 99 - Car cylinder head being printed

After printing, the appearance of the part is shown in Figure 100, a) corresponds to the side view of the part, b) the top view and c) the bottom view

a)

b)

c)
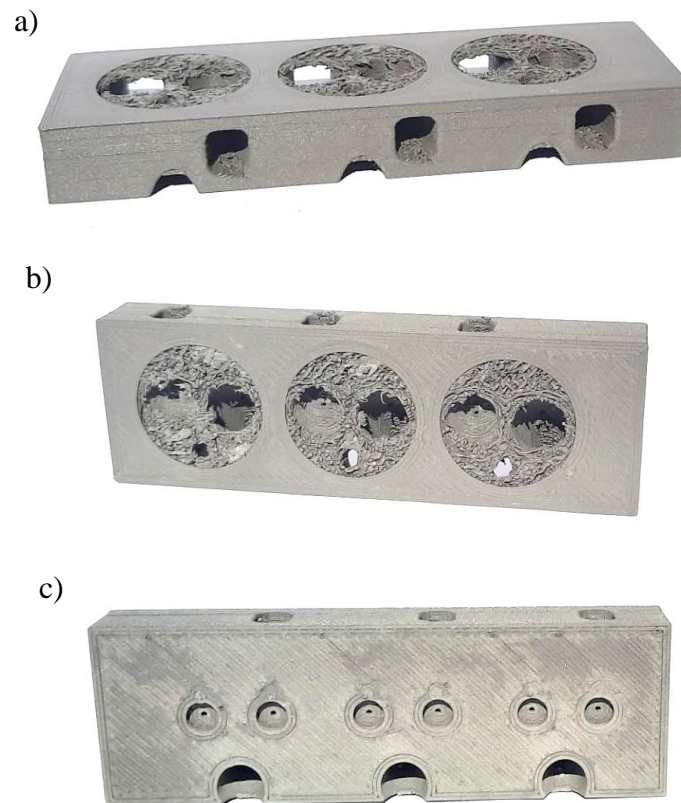
Figure 100 - Car cylinder head printed with FFF technology

This part is designed by additive manufacturing and not conventional processes, making it possible to save much material. Through the FFF technology, the infill may have a percentage lower than 100%, in this case, 60%, which would not be possible using a CNC. Nowadays, the weight of automotive and aerospace parts is an essential factor, as the final weight of the car or aircraft can be much lower than the original. For the cars, this can ensure more speed attainable, and for aircraft's fuel efficiency and allow an aircraft to carry more weight.

5.1. Cost Analysis

In the following chapters, all the values obtained through calculations for cost comparison between Fused Fillament Fabrication technology and Selective Laser Melting technology are estimated. Costs such as maintenance, set up and labour are not included in the calculations.

5.1.1. Cost Analysis - Fused Filament Fabrication

Printer Cost -The Ultimaker S3 printer has a useful life of 5 years. Considering 280 working days of work, and considering that the printer will always be working, in five years the printer will work 33600 hours. The printer cost 4969,20€ as shown in Attachment X of the budget the company Fan 3D gave. Knowing that it takes 3,52 hours to print the car cylinder head, we can determine the cost of the equipment for this operation. It takes 0,76€ to print this part which is possible to see in the following calculation.

$$\text{€} Printer\ to\ print\ the\ part = \frac{Printer\ cost\ \times Time\ to\ print\ the\ part}{Printer\ useful\ life}$$

$$= \frac{4969,20 \times 3,51}{33600} = 0,52\text{€}$$

Electricity Cost - It is known that the maximum output power of the Ultimaker S3 printer is 350 W, and the cost of electricity is 0,32 euros per Kw/h. This data makes it possible to know how much electricity the machine spends per hour.

$$Cost\ energy\ per\ hour = Printer\ maximum\ power \times Cost\ of\ electricity\ per\ hour$$

$$= 0,35 \times 0,32 = 0,112€$$

After calculating the energy consumption per hour, obtaining the energy consumption for the 3:51 hours required to print the part is already possible. Therefore, it takes 0,79€ of electricity to print the car cylinder head, like shows in the next equation.

$$Cost\ energy\ for\ the\ part = Time\ to\ print \times cost\ energy\ per\ hour$$

$$= 3,51 \times 0,112 = 0,40\ €$$

Material Cost - A 3kg roll of BASF Ultrafuse 316L costs around 460€, and the quantity of material needed to print the part is just 71g, given by the software CURA. With this data, it is possible to calculate the cost of material needed to print the part. For example, printing the car cylinder head spends 16,56€, like it is demonstrated in the following equation.

$$Material\ Cost\ for\ the\ part = \frac{Material\ needed\ \times Cost\ of\ 3kg\ roll}{3\ kg\ roll}$$

$$= \frac{71 \times 460}{3000} = 10,89€$$

Sintering Cost – an external company carries out the sintering and debinding processes. The price that the company charges for these processes are 68,60 €/kg. Having this value and knowing the mass of the piece, 108g, it is possible to calculate the sintering cost for this part.

$$Sintering\ Cost\ for\ the\ part = \frac{Part\ mass\ \times Sintering\ cost\ per\ kg}{1\ kg}$$

$$= \frac{71 \times 68{,}60}{1000} = 4{,}87€$$

In this way, producing this piece using FFF technology costs 16,67€.

5.1.2. Cost Analysis – Selective Laser Melting

The material AISI Type 316L Stainless Steel was selected in Solidworks software to know the part's mass with 100% density, Figure 101. The mass is 202,31g. If the piece with only 60% density is printed, its mass will be 121,39g.
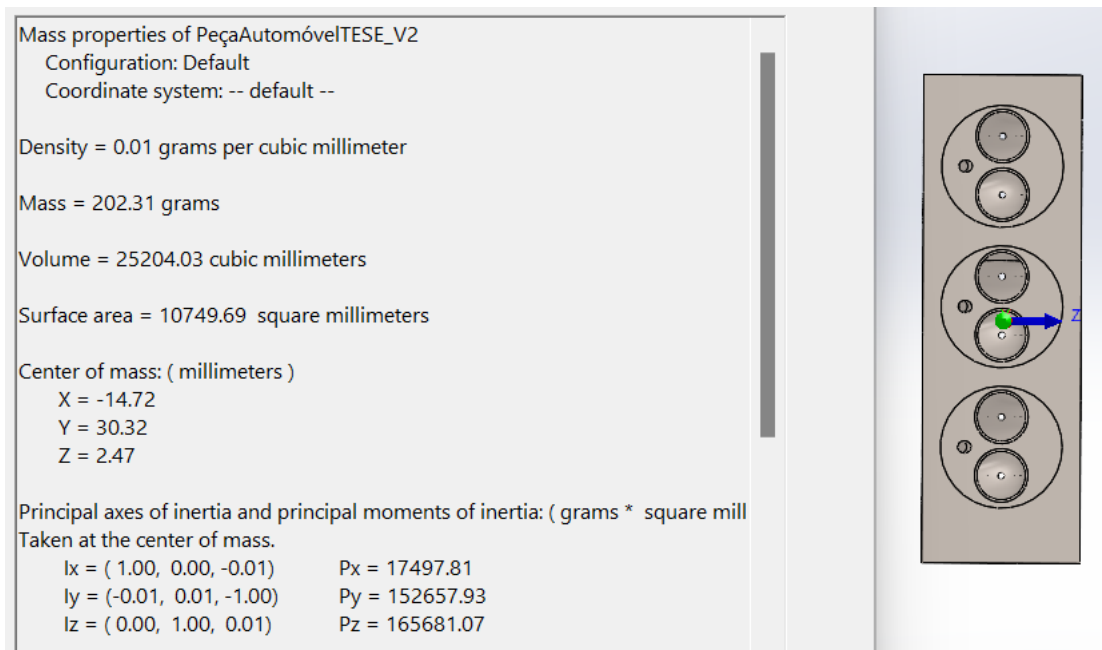
Figure 101 - Mass of the piece with 100% density

The machine selected to do the cost analysis for the Selective Laser Melting technology is the Kurtz Ersa Alpha 140 from Laser Melting Innovations, Figure 102, available in the mechanical lab of Aalen University.

Figure 102 - Kurtz ersa ALPHA 140 Printer

The print speed of this machine is 50mm/s. Therefore, the following calculations had to be made to determine how long it would take to print the part using SLM technology. First, it was necessary to calculate the number of layers the part has. Each layer has 0,05 mm; as can be seen in the following equation, 203 layers are needed.

$$Number\ of\ Layers = \frac{Part\ height}{1\ layer\ height} = \frac{10,16}{0,05} = 203\ layers$$

Next, it is essential to know the area of each layer and, consecutively, the time it takes to print it. For example, in the following equations, each layer is about 2146.42 mm long and takes 42.95s to print it.

$$Average\ area\ of\ a\ layer = Part\ length \times Part\ width = 2147,42\ mm^2$$

$$Printing\ time\ for\ 1\ layer = \frac{Average\ area\ of\ 1\ layer}{Speed\ to\ print\ 1\ mm} = \frac{2147,42}{50} = 42,95s$$

Finally, to know the time it takes to print all the layers of the piece. In the following equation, we arrive at the value of 4337.79s corresponding to 1,20 hours.

$$Printing\ time\ for\ the\ whole\ part$$
$$= Printing\ time\ for\ 1\ layer \times Number\ of\ layers = 42,95 \times 203$$
$$= 8718,85\ s = 2,42\ hours$$

Printer Cost – The Kurtz Ersa Alpha 140 has a useful life of 7 years. Considering 280 working days of work and considering that the printer will work 24 hours per day, in seven years the printer will work 47040 hours. The printer cost is around 85000€. Knowing that it takes 1,20 hours to print the car cylinder head, we can determine the cost of the equipment for this operation. It costs 1,66€ to print this part, as it is possible to see in the following calculation.

$$€Printer\ to\ print\ the\ part = \frac{Printer\ cost \ \times Time\ to\ print\ the\ part}{Printer\ useful\ life}$$

$$= \frac{85000 \times 1,20}{47040} = 2,17€$$

Electricity Cost - It is known that the maximum output power of the printer is 450 W, and the cost of electricity is 0,32 euros per Kw/h. Therefore, with this data, it is possible to know how much electricity the machine spends per hour.

$$Cost\ energy\ per\ hour = Printer\ maximum\ power \times Cost\ of\ electricity\ per\ hour$$

$$= 0,45 \times 0,32 = 0,144€$$

After calculating the energy consumption per hour, obtaining the energy consumption for the 1,20 hours required to print the part is already possible. It spends 0,17€ of electricity to print the car cylinder head as shown in the following equation.

$$Cost\ energy\ for\ the\ part = Time\ to\ print \times cost\ energy\ per\ hour$$

$$= 1,20 \times 0,144 = 0,17\ €$$

Material Cost - A 1kg powder of BASF Ultrafuse 316L costs around 68,74€, and the quantity of material needed to print the part is just 121,39 g. With this data, it is possible to calculate the cost of material needed to print the part. For example, the following equation demonstrates that printing the car cylinder head spends 8,34€ like it.
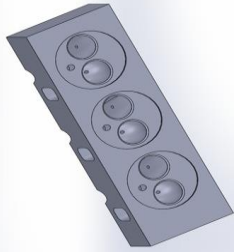
$$Material\ Cost\ for\ the\ part = \frac{Material\ needed\ \times Cost\ of\ 1kg\ powder}{1\ kg\ powder}$$

$$\frac{121,39 \times 68,74}{1000} = 8,34€$$

Sintering Cost – the company that executes the sintering and debinding process charges 68,60€/kg. Thus, knowing the part's mass, 121,39 is possible to calculate the sintering cost for this part.

$$Sintering\ Cost\ for\ the\ part = \frac{Part\ mass\ \times Sintering\ cost\ per\ kg}{1\ kg}$$

$$= \frac{121,39 \times 68,60}{1000} = 8,33€$$

In total, producing the car cylinder head with SLM technology costs 18,70€. In Table 13 it is possible to compare the cost of producing the part with FFF and with SLM. It must be taken into account that the values obtained are estimates.

Table 13 - Cost comparison between FFF and SLM technologies

CAR CYLINDER HEAD COST ANALYSIS						
Part	Technology	Printer Cost	€/Electricity	Material Cost	€/Sintering	TOTAL
	FFF	0,52€	0,40€	10,89€	4,87€	16,68€
	SLM	2,17€	0,17€	8,34€	8,33€	19,01€

6. **Conclusion**

This work aimed to optimise the production of components in 316L Stainless Steel through the parameters using the FFF process. One of the main objectives was to test different parameters in the production of specimens, from infill pattern, density, print angle and support structures, and then find the best way to produce parts with this technology and material. Furthermore, to optimise all these parameters was necessary to understand the mechanical and microstructural properties of the parts produced. For this purpose, tests were carried out, from the tensile test, microscopic analysis and roughness analysis.

The tensile tests showed that the tensile strength increases with the component's density and the type of infill pattern used, being the gyroid with the best values. Furthermore, the highest experimental tensile strength was 471,78 MPa representing 84% of the theoretical value, 561 MPa, presented in the material data sheet. Thus, the values obtained were lower than expected

The microscopic analysis showed that the infill pattern gyroid has less porosity than the other ones, which may explain why the pattern presents the best result in terms of tensile strength. Besides this, the surface roughness test also showed that the infill pattern gyroid presents the lowest Rz values, presenting less variation between high and low points along the specimen. This can also explain the results obtained in the tensile test.

Concerning the support structures developed, it is inferred that using PVA as a support material is not the best solution when printing 316L Stainless Steel, as these materials do not stick to each other. Better results were presented when the printing was done only with metal.

Although the mechanical properties of the parts produced by Selective Laser Melting technology are superior to those produced by Fused Filament Fabrication technology, this technology is competitive in terms of production costs. Through this technology, it is possible to create a part using 89% of the SLM cost.

This technology also proved to have many advantages compared with conventional processes, promoting significant advantages such as choosing the infill density and making the parts produced lighter, which nowadays is a significant factor for industries such as aerospace and automotive. In addition to this advantage, there is also a significant reduction

in waste since only the material used to produce the part is practically spent with additive manufacturing.

Bibliography

3Dnatives. (2022). ExOne M-Flex. Retrieved from https://www.3dnatives.com/3D-compare/de/3d-drucker/exone-m-flex/

3druck. (2021). Carmel 1400: XJet stellt neue 3D-Drucker bei der Formnext vor. Retrieved from https://3druck.com/drucker-und-produkte/carmel-1400-xjet-0485679/

3m3drobotics. (2022a). Overview: How SLS 3D printing works? Retrieved from https://www.3m3drobotics.com/selective-laser-sinteringsls/

3m3drobotics. (2022b). Stereolithography (SLA/DLP). Retrieved from https://www.3m3drobotics.com/stereolithography-sla-dlp/

Advanced Additive Manufacturing. (2018). 3D printing vs CNC Machining – Key differences. Retrieved from https://www.advancedadditivemanufacturing.co.uk/blog/3d-printing-vs-cnc-machining-key-differences/

Ait-Mansour, I., Kretzschmar, N., Chekurov, S., Salmi, M., & Rech, J. (2020). Design-dependent shrinkage compensation modeling and mechanical property targeting of metal FFF. *Progress in Additive Manufacturing*, *5*(1), 51–57. https://doi.org/10.1007/s40964-020-00124-8

Alkaios Bournias Varotsis. (2022). What is SLA 3D printing? Retrieved from https://www.hubs.com/knowledge-base/what-is-sla-3d-printing/

ANDY. (2022). No TitleDrop on Demand (DOD) – THE Inkjet Technology of the Future? Retrieved from https://www.andy-machinery.com/news/drop-on-demand-dod-the-inkjet-technology-of-the-future/

Aniwaa. (2022). EBAM 300 Series. Retrieved from https://www.aniwaa.com/product/3d-printers/sciaky-ebam-300-series/

ArtiBoyut. (2022). Como funciona uma impressora 3D? - Métodos de Fabricação Aditiva. Retrieved from https://www.artiboyut.com/index.php/tr/egitim/63-3d-yazici-nasil-calisir-katmanli-uretim-yontemleri

B FOXDOC. (2022). SLA vs DLP. Retrieved from https://facfox.com/docs/kb/what-is-a-dlp-3d-printer-simply-explained

BASF 3D Printing Solutions. (2019a). Ultrafuse 316L: User guidelines for 3D printing metal parts. *BASF 3D Printing Solutions*, *process in*(2), 1. Retrieved from https://www.basf.com/global/en/who-we-are/organization/locations/europe/german-companies/basf-3d-printing-solutions-gmbh/metal-solutions/Ultrafuse_316L.html

BASF 3D Printing Solutions. (2019b). Ultrafuse 316L. *BASF 3D Printing Solutions*, *process in*(2), 1. Retrieved from https://www.basf.com/global/en/who-we-are/organization/locations/europe/german-companies/basf-3d-printing-solutions-gmbh/metal-solutions/Ultrafuse_316L.html

Beamler. (2019). Post-processing in 3D printing. Retrieved from https://www.beamler.com/post-processing-3d-printing/

Burgués-Ceballos, I., Stella, M., Lacharmoise, P., & Martínez-Ferrero, E. (2014). Towards industrialization of polymer solar cells: Material processing for upscaling. *Journal of Materials Chemistry A*, *2*(42), 17711–17722. https://doi.org/10.1039/c4ta03780d

Cheng, L., Liang, X., Bai, J., Chen, Q., Lemon, J., & To, A. (2019). On utilizing topology optimization to design support structure to prevent residual stress induced build failure in laser powder bed metal additive manufacturing. *Additive Manufacturing*, *27*, 290–304. https://doi.org/10.1016/j.addma.2019.03.001

Clevercreations. (2022). FDM vs FFF: What is the difference? Retrieved from https://clevercreations.org/fff-vs-fdm-difference-3d-printing/

Conspir3D. (2022). Conspir3D - Debinding und Sintering. Retrieved from https://conspir3d.com/wissen/ultrafuse-debinding-sinteringprocess/

Dubert, P. (2020). The ISO / ASTM 52941 standards for additive manufacturing has been published. Retrieved from https://3dprintingcenter.net/the-iso-astm-52941-standards-for-additive-manufacturing-has-been-published/

EOS. (2022). INTEGRA P 450 A mid range polymer additive manufacturing System. Retrieved from https://www.eos.info/en/additive-manufacturing/3d-printing-plastic/eos-polymer-systems/integra-p-450

ETEC. (2021). Envision One. Retrieved from https://etec.desktopmetal.com/product/envisionone/

Experience, M. 3D. (2022). Introduction to 3D printing - additive processes. Retrieved from https://make.3dexperience.3ds.com/processes/material-jetting

FACFOX. (2022). Selective Laser Melting (SLM) – 3D Printing Simply Explained. Retrieved from https://facfox.com/docs/kb/selective-laser-melting-slm-3d-printing-simply-explained

Fast Radius. (2022). Fused deposition modeling advantages and disadvantages. Retrieved from https://www.fastradius.com/resources/fused-deposition-modeling-advantages-and-disadvantages/

Formlabs. (2022). Additive vs. Subtractive Manufacturing. Retrieved from https://formlabs.com/eu/blog/additive-manufacturing-vs-subtractive-manufacturing/

GE Additive. (2022). Arcam EBM Q10plus. Retrieved from https://www.ge.com/additive/additive-manufacturing/machines/ebm-machines/arcam-ebm-q10plus

Gonabadi, H., Yadav, A., & Bull, S. J. (2020). The effect of processing parameters on the mechanical characteristics of PLA produced by a 3D FFF printer. *International Journal of Advanced Manufacturing Technology*, *111*(3–4), 695–709. https://doi.org/10.1007/s00170-020-06138-4

Gonzalez-Gutierrez, J., Cano, S., Schuschnigg, S., Kukla, C., Sapkota, J., & Holzer, C. (2018). Additive manufacturing of metallic and ceramic components by the material extrusion of highly-filled polymers: A review and future perspectives. *Materials*, *11*(5). https://doi.org/10.3390/ma11050840

González, C. M. (2020). Infographic: The History of 3D Printing. Retrieved from https://www.asme.org/topics-resources/content/infographic-the-history-of-3d-printing

Gornet, T. (2017). *History of Additive Manufacturing*. 1–24. https://doi.org/10.4018/978-1-5225-2289-8.ch001

Hendrixson, S. (2022). AM 101: NanoParticle Jetting (NPJ). Retrieved from

https://www.additivemanufacturing.media/articles/am-101-nanoparticle-jetting-npj

HUBS. (n.d.). Additive Manufacturing Technologies. Retrieved from 2022 website: https://www.hubs.com/get/am-technologies/

HUBS. (2022a). *What are supports in 3D printing?* Retrieved from https://www.hubs.com/knowledge-base/supports-3d-printing-technology-overview/

HUBS. (2022b). What is Binder Jetting 3D printing? Retrieved from https://www.hubs.com/knowledge-base/introduction-binder-jetting-3d-printing/

i.materialise. (2022). Fused Deposition Modeling. Retrieved from https://i.materialise.com/en/3d-printing-technologies/fused-deposition-modeling

Ibsen. (2022). DMD spectrometers. Retrieved from https://ibsen.com/resources/spectrometer-resources/dmd-spectrometers/

IGO3D. (2020). *IGO3D Webinar: Ultrafuse 316L.* Retrieved from https://www.youtube.com/watch?v=OOYlwkNJt5g&ab_channel=IGO3D

IGO3D. (2022). BASF Ultrafuse 316L. Retrieved from https://www.igo3d.com/basf-ultrafuse-316l-175mm-3000g?curr=EUR&utm_term=&utm_campaign=0.2+%5Bcb+-+MaxPerformance+-+shopping+-+DACH%5D+3D+Druckmaterialien&utm_source=adwords&utm_medium=ppc&hsa_acc=2959589712&hsa_cam=17785764658&hsa_grp=&hsa_ad=&hsa_src=x&h

Ile Kauppila. (2022). Selective Laser Melting / SLM 3D Printing – The Ultimate Guide. Retrieved from https://all3dp.com/1/selective-laser-melting-guide/

Industrial Heating. (2022). Sintering and Additive Manufacturing. Retrieved from https://www.industrialheating.com/articles/94932-sintering-and-additive-manufacturing

ISO/ASTM. (2015). ISO/ASTM 52900:2015(en) Additive manufacturing — General principles — Terminology. Retrieved from https://www.iso.org/obp/ui/#iso:std:iso-astm:52900:ed-1:v1:en

ISO/ASTM. (2021). ISO/ASTM 52900:2021. Retrieved from https://www.iso.org/obp/ui/#iso:std:iso-astm:52900:ed-2:v1:en

Jiang, J., Xu, X., & Stringer, J. (2018). Support structures for additive manufacturing: A review. *Journal of Manufacturing and Materials Processing*, 2(4). https://doi.org/10.3390/jmmp2040064

Kumar, S. A. (2021). No TitleBasic principles of additive manufacturing: different additive manufacturing technologies. Retrieved from https://www.sciencedirect.com/topics/engineering/laser-engineered-net-shaping

L.E. Murr, S. M. G. (2014). Electron Beam Melting. Retrieved from https://www.sciencedirect.com/topics/chemistry/electron-beam-melting

Lahaie, R. (2020). *FUSED DEPOSITION MANUFACTURING OF MULTIPLE MATERIALS VIA CO- FUSED DEPOSITION MANUFACTURING OF MULTIPLE MATERIALS VIA CO-EXTRUSION BY SUBMITTED TO THE COLLEGE OF ENGINEERING FOR THE DEGREE OF MECHANICAL ENGINEERING*. (August). https://doi.org/10.13140/RG.2.2.16367.87206

Liu, B., Wang, Y., Lin, Z., & Zhang, T. (2020). Creating metal parts by Fused Deposition Modeling and Sintering. *Materials Letters*, Vol. 263. https://doi.org/10.1016/j.matlet.2019.127252

Machining. (2022). Differences between additive and subtractive manufacturing. Retrieved from http://www.difference.minaprem.com/machining/difference-between-additive-and-subtractive-manufacturing/

Manufacturing, A. (2018). 3D Printing Support Structures: A Complete Guide. Retrieved from https://amfg.ai/2018/10/17/3d-printing-support-structures-guide/

Martin. (2022). Tri-Hexagon Infill Pattern | Stability, Uses, Density & More. Retrieved from https://the3dprinterbee.com/tri-hexagon-infill/

Michael Dwamena. (2022). What is the Best Infill Pattern for 3D Printing? Retrieved from https://3dprinterly.com/what-is-the-best-infill-pattern-for-3d-printing/

Mierzejewska, Ż. A., & Markowicz, W. (2015). Selective Laser Sintering – Binding

Mechanism And Assistance In Medical Applications. *Advances in Materials Science*, *15*(3), 5–16. https://doi.org/10.1515/adms-2015-0011

Negi, S., Nambolan, A. A., Kapil, S., Joshi, P. S., R, M., Karunakaran, K. P., & Bhargava, P. (2020). Review on electron beam based additive manufacturing. *Rapid Prototyping Journal*, *26*(3), 485–498. https://doi.org/10.1108/RPJ-07-2019-0182

Nohut, S., & Schwentenwein, M. (2022). Vat Photopolymerization Additive Manufacturing of Functionally Graded Materials: A Review. *Journal of Manufacturing and Materials Processing*, *6*(1). https://doi.org/10.3390/jmmp6010017

OPTOMEC. (2020). Optomec 3D Printers. Retrieved from https://optomec.com/additive-manufacturing/

Pagac, M., Hajnys, J., Ma, Q. P., Jancar, L., Jansa, J., Stefek, P., & Mesicek, J. (2021). A review of vat photopolymerization technology: Materials, applications, challenges, and future trends of 3d printing. *Polymers*, *13*(4), 1–20. https://doi.org/10.3390/polym13040598

Palčič, I. et al. (2009). Potential of laser engineered net shaping (LENS) technology. *Materials and Manufacturing Processes*, *24*(7–8), 750–753. https://doi.org/10.1080/10426910902809776

Peels, J. (2020). BASF Launches 17-4 Stainless Steel Metal 3D Printing Filament for FDM Printers. Retrieved from https://3dprint.com/276408/basf-launches-17-4-stainless-steel-metal-3d-printing-filament-for-fdm-printers-d/

Perry Cain. (2022). Supports in 3D Printing: A technology overview. Retrieved from https://www.hubs.com/knowledge-base/supports-3d-printing-technology-overview/

Pollen. (2022). Infill. Retrieved from https://www.pollen.am/design_guidelines_wall_infill/

Prata, I. S. (2019). *Desenvolvimento de parâmetros do processo Fusão Seletiva a Laser para a liga de Inconel 625*.

Proto, 3000. (2022). Continuous Digital Light Processing (cDLP) 3D Printing Technology. Retrieved from https://proto3000.com/service/3d-printing-services/technologies/cdlp-3d-printing-technology/

Radius, F. (2022). Additive manufacturing support structures: Why they matter and how to design for them. Retrieved from https://www.fastradius.com/resources/support-structures-why-they-matter-and-how-to-design-for-them/

RAMLAB. (2022). MaxQ ROBOT TURN KEY WAAM SYSTEM. Retrieved from https://www.ramlab.com/maxq-robot/

Razavykia, A., Brusa, E., Delprete, C., & Yavari, R. (2020). An overview of additive manufacturing technologies-A review to technical synthesis in numerical study of selective laser melting. *Materials*, *13*(17). https://doi.org/10.3390/ma13173895

Riecker, S., Hein, S. B., Lehmann, M., Studnitzky, T., Andersen, O., & Kieback, B. (2018). *Fused Filament Fabrication With Highly Loaded Filaments – a new AM Approach for the Production of Metal Parts*. (March), 1–5.

Robinson, T. (2022). SLS 3D printing. Retrieved from https://3d-print-lab.com/qa/who-invented-sls-3d-printing.html

Silva, C., Pais, A. I., Caldas, G., Gouveia, B. P. P. A., Alves, J. L., & Belinha, J. (2021). Study on 3D printing of gyroid-based structures for superior structural behaviour. *Progress in Additive Manufacturing*, *6*(4), 689–703. https://doi.org/10.1007/s40964-021-00191-5

SLM Solutions. (2022). Industrial Metal AM Machines. Retrieved from https://www.slm-solutions.com/products-and-solutions/machines/

Stratasys. (2022). J850 Digital Anatom 3D Printer. Retrieved from https://www.stratasys.com/de/3d-printers/printer-catalog/polyjet/j850-digital-anatomy/

Systems, 3D. (2022). ProX 800. Retrieved from https://de.3dsystems.com/3d-printers/prox-800

Tan, J. H., Wong, W. L. E., & Dalgarno, K. W. (2017). An overview of powder granulometry on feedstock and part performance in the selective laser melting process. *Additive Manufacturing*, *18*(October), 228–255. https://doi.org/10.1016/j.addma.2017.10.011

Team, I. E. (2022). The critical role of 3D printing support material. Retrieved from

https://infinitematerialsolutions.com/us/en/learn/article/critical-role-of-support-materials

ThomasNet. (2022). All About Electron Beam Additive Manufacturing (EBAM) 3D Printing. Retrieved from https://www.thomasnet.com/articles/custom-manufacturing-fabricating/electron-beam-additive-manufacturing-ebam-3d-printing/

Top 3D Blog. (2022). FFF vs FDM: Difference and Best Printers. Retrieved from https://top3dshop.com/blog/fff-vs-fdm-difference-and-best-printers

Treatstock. (2022a). EnvisionTec Micro Plus Advantage. Retrieved from https://www.treatstock.com/machines/item/353-micro-plus-advantage

Treatstock. (2022b). Mcor IRIS HD. Retrieved from https://de.treatstock.com/machines/item/101-mcor-iris-hd

Valérie, H. (2021). *3D PRINTING OF INCONEL 718 BY MEAM (METAL EXTRUSION ADDITIVE MANUFACTURING) Dissertation and Annexes*. (February).

Weber, S. et al. (2020). PARAMETERS on SUPPORT STRUCTURE DESIGN for METAL ADDITIVE MANUFACTURING. *Proceedings of the Design Society: DESIGN Conference*, *1*(May), 1145–1154. https://doi.org/10.1017/dsd.2020.14

Wikipedia. (2022). Fused Fillament Fabrication. Retrieved from https://en.wikipedia.org/wiki/Fused_filament_fabrication

Xometry. (2022). Subtractive Manufacturing vs. Additive Manufacturing. Retrieved from https://xometry.eu/en/subtractive-manufacturing-vs-additive-manufacturing/

Attachments

Attachment I

Planning of parts to be printed with 60% of density. Printing time. Weight of the parts before and after sintering. Photos of the printed parts.

| | | | | | | | | | | | | | | |
|---|---|---|---|---|---|---|---|---|---|---|---|---|---|
| **3D PRINTING PLAN** | | | | | | | | | | | | | |
| **TENSILE SAMPLES** | | | | | | | | | | | | | |
| DENSITY | ANGLE | PATTERN | QTT | TIME | TENSILE NUMBER | REF. | WEIGHT BEFORE SINT. (g) | WEIGHT BF AVERAGE (g) | WEIGHT AFTER SINT. (g) | WEIGHT AT AVERAGE (g) | THICKNESS (mm) | WIDTH MIDDLE (mm) | WIDTH TIPS (mm) | PHOTO |
| 60% | 0º | Gyroid 60% | 7 | 10 | 1 | AA | 31,328 | 31,13 | 27,959 | 27,74 | 5,14 | 6,26 | 10,3 | |
| | | | | | 2 | AB | 31,156 | | 27,78 | | 5,11 | 6,22 | 10,3 | |
| | | | | | 3 | AC | 31,479 | | 28,07 | | 5,1 | 6,32 | 10,37 | |
| | | | | | 4 | AD | 31,331 | | 27,936 | | 5,09 | 6,25 | 10,27 | |
| | | | | | 5 | AE | 31,346 | | 27,945 | | 5,08 | 6,31 | 10,35 | |
| | | | | | 6 | AF | 31,202 | | 27,81 | | 5,08 | 6,25 | 10,31 | |
| | | | | | 7 | AG | 30,063 | | 26,704 | | 5,04 | 6,29 | 10,28 | |
| | | Tri Hexagon 60% | 4 | 5,53 | 1 | BA | 30,426 | 30,76 | 27,12 | 27,43 | 5,07 | 6,33 | 10,35 | |
| | | | | | 2 | BB | 30,795 | | 27,454 | | 5,12 | 6,29 | 10,23 | |
| | | | | | 3 | BC | 30,624 | | 27,322 | | 5,09 | 6,28 | 10,24 | |
| | | | | | 4 | BD | 31,072 | | 27,718 | | 5,17 | 6,29 | 10,2 | |
| | | | 3 | 4,28 | 5 | BE | 30,718 | | 27.384 | | 5,07 | 6,39 | 10,24 | |
| | | | | | 6 | BF | 30,873 | | 27,524 | | 5,08 | 6,22 | 10,23 | |
| | | | | | 7 | BG | 30,79 | | 27,449 | | 5,1 | 6,26 | 10,2 | |
| | | Quater cubic 60% | 7 | 10,2 | 1 | CA | 29,133 | 29,14 | 25,967 | 25,98 | 4,95 | 6,29 | 10,18 | |
| | | | | | 2 | CB | 29,113 | | 25,922 | | 5,04 | 6,26 | 10,3 | |
| | | | | | 3 | CC | 29,05 | | 25,894 | | 4,96 | 6,27 | 10,28 | |
| | | | | | 4 | CD | 29,162 | | 26,011 | | 5,02 | 6,24 | 10,28 | |
| | | | | | 5 | CE | 29,356 | | 26,16 | | 5,09 | 6,31 | 10,27 | |
| | | | | | 6 | CF | 29,264 | | 26,111 | | 5,05 | 6,23 | 10,3 | |
| | | | | | 7 | CG | 28,923 | | 25,789 | | 4,93 | 6,34 | 10,34 | |

Planning of parts to be printed with 80% of density. Printing time. Weight of the parts before and after sintering. Photos of the printed parts.

DENSITY	ANGLE	PATTERN	QTT	TIME	TENSILE NUMBER	REF.	WEIGHT BEFORE SINT. (g)	WEIGHT BF AVERAGE (g)	WEIGHT AFTER SINT. (g)	WEIGHT AT AVERAGE (g)	THICKNESS (mm)	WIDTH MIDDLE (mm)	WIDTH TIPS (mm)	PHOTO
80%	0º	Gyroid 80%	7	12,15	1	AH	35,042	35,09	31,258	31,30	5,08	6,23	10,23	
					2	AI	35,093		31,313		5,11	6,28	10,31	
					3	AJ	35,022		31,221		5,13	6,26	10,29	
					4	AK	35, 091		31,313		5,09	6,26	10,3	
					5	AL	35,205		31,422		5,15	6,2	10,24	
					6	AM	35,256		31,442		5,16	6,3	10,2	
					7	AN	34,924		31,162		5,04	6,25	10,3	
		Tri Hexagon 80%	7	11,34	1	BH	34,96	34,81	31,219	31,05	5,17	6,56	10,84	
					2	BI	34,685		30,943		5,11	6,6	10,63	
					3	BJ	34,695		30,953		5,06	6,65	10,82	
					4	BK	34,766		31,018		5,15	6,55	10,63	
					5	BL	34,683		30,909		5,16	6,52	10,62	
					6	BM	35,069		31,26		5,2	6,49	10,35	
					7	BN	34,803		31,05		5,15	6,64	10,55	
		Quater cubic 80%	7	11,31	1	CH	32,495	32,71	28,915	29,03	5,06	6,25	10,35	
					2	CI	33,125		29,084		5,16	6,31	10,35	
					3	CJ	32,794		28,902		5,11	6,26	10,25	
					4	CK	32,581		29,035		5,04	6,25	10,26	
					5	CL	32,743		29,33		5,12	6,26	10,29	
					6	CM	32,68		29,021		5,08	6,29	10,35	
					7	CN	32,531		28,888		4,99	6,29	10,34	

Attachment II - Graph obtained in the tensile test 0º parts, gyroid 60% and 80%.
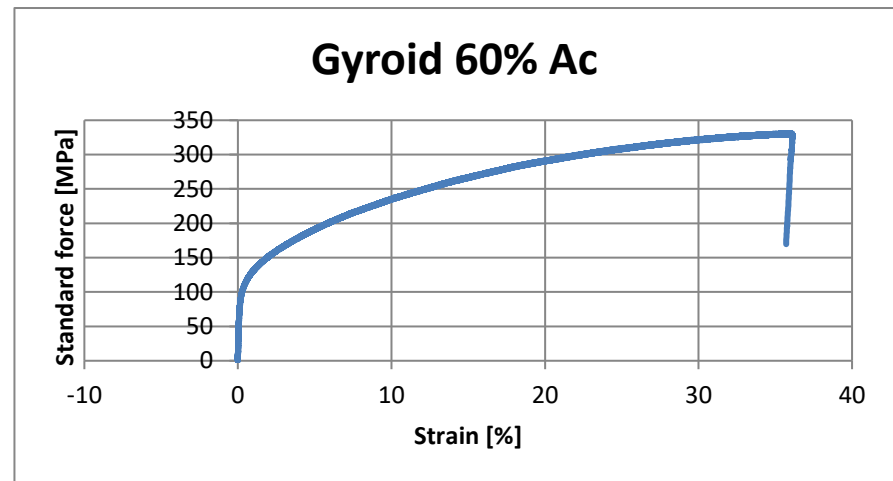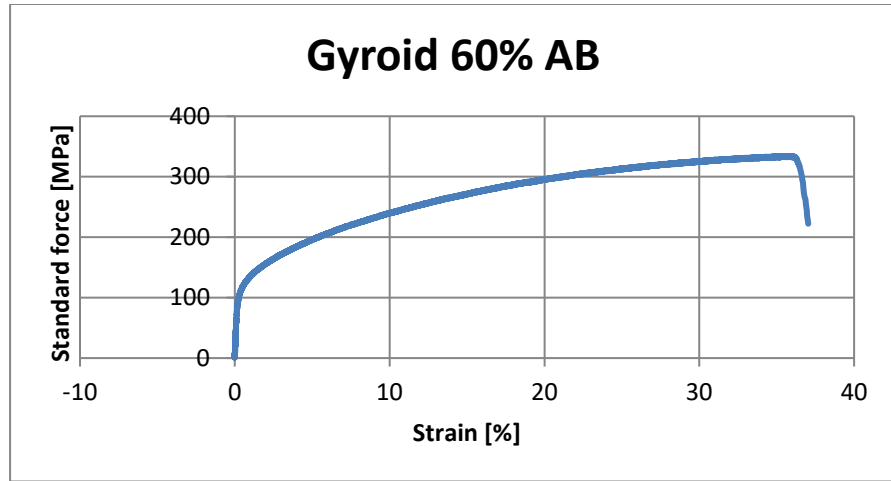
Attachment III - Graph obtained in the tensile test 0º parts, tri-hexagon 60% and 80%.
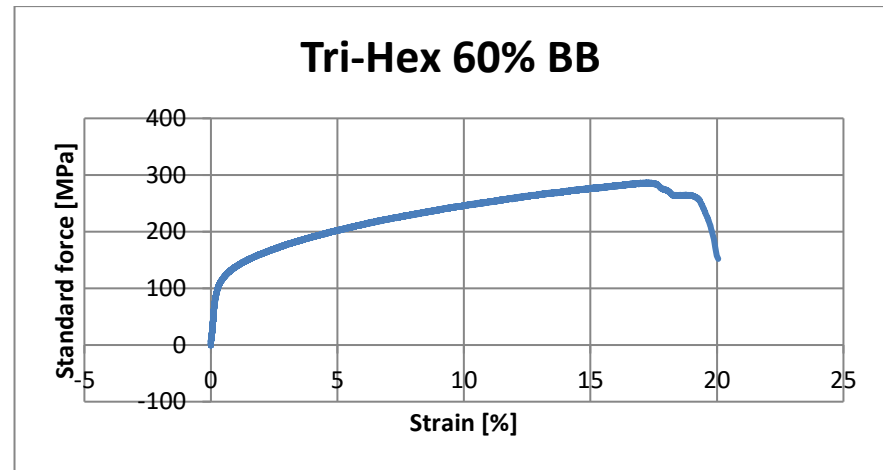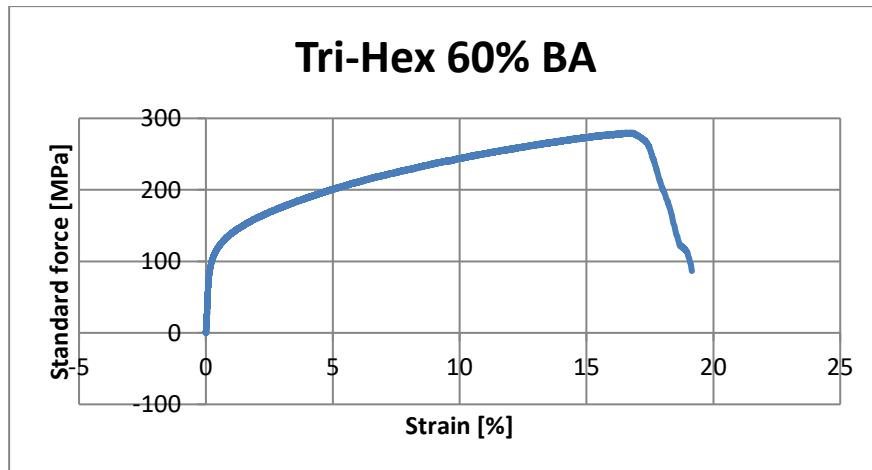
Attachment IV - Graph obtained in the tensile test 0º parts, quarter cubic 60% and 80%.

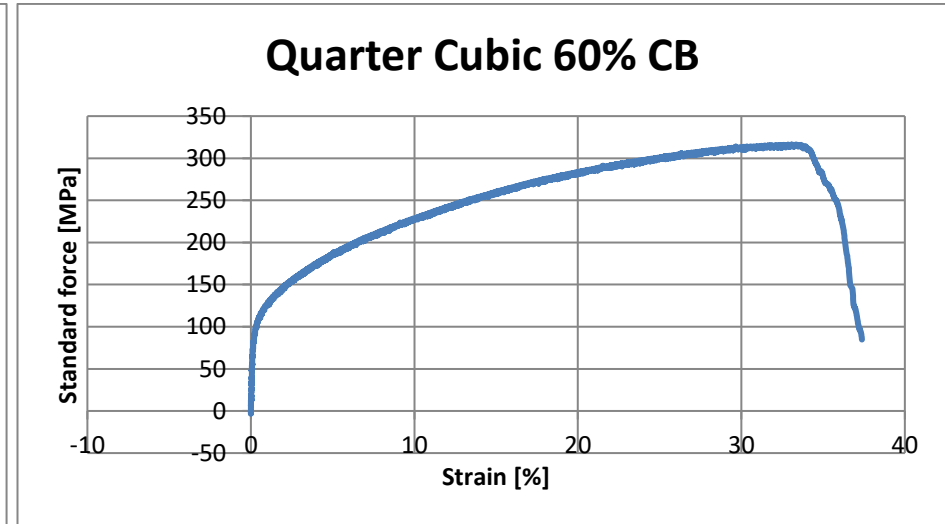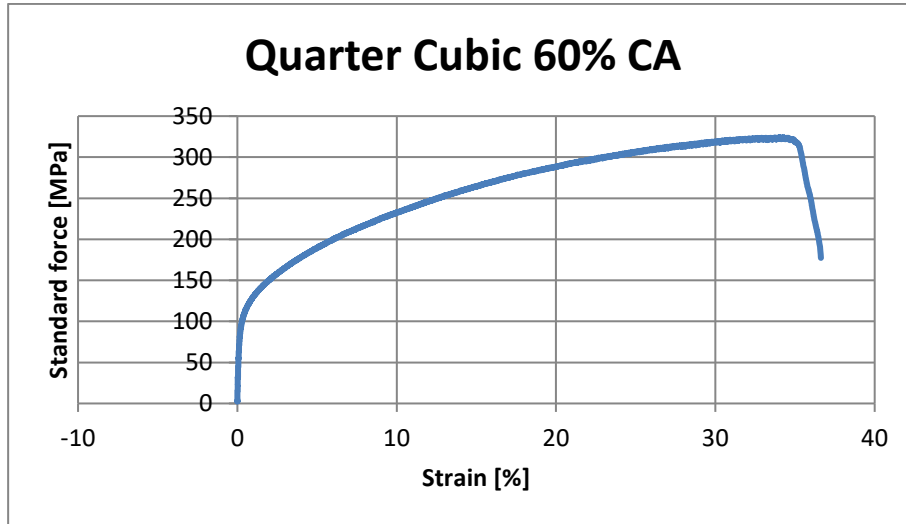Attachment V

Results obtained in the tensile test 0º parts. Calculation of averages Rm and Rp2.

TENSILE TEST RESULTS						
DENSITY	60%			80%		
INFILL	SAMPLE	Rm	Rp02	SAMPLE	Rm	Rp02
GYROID	AA	331,70	108,66	AH	307,13	104,85
	AB	334,13	110,64	AI	368,30	127,42
	AC	331,24	105,93	AJ	368,37	125,17
	AD	343,33	113,89	AK	389,91	-
	AE	348,77	-	AL	387,55	-
	AF	337,92	-	AM	380,10	-
	AG	329,00	106,66	AN	388,12	128,87
	SD	6,672	2,881	SD	26,975	9,748
	AVERAGE	336,583	109,156	AVERAGE	369,928	121,575
TRI-HEXAGON	BA	280,03	111,44	BH	292,53	122,15
	BB	286,73	115,20	BI	308,74	122,63
	BC	264,99	114,22	BJ	293,48	121,12
	BD	282,01	110,75	BK	317,15	121,23
	BE	274,84	113,32	BL	311,77	-
	BF	277,33	113,33	BM	307,23	-
	BG	281,34	115,31	BN	286,81	121,69
	SD	6,403	1,622	SD	10,615	0,569
	AVERAGE	278,181	113,367	AVERAGE	302,529	121,765
QUARTER CUBIC	CA	324,27	106,12	CH	387,82	-
	CB	316,34	103,55	CI	384,57	-
	CC	325,59	103,76	CJ	383,43	115,49
	CD	324,51	105,89	CK	-	-
	CE	320,81	105,04	CL	381,56	117,70
	CF	323,92	-	CM	388,73	-
	CG	325,63	102,56	CN	406,37	-
	SD	3,108	1,296	SD	8,255	1,105
	AVERAGE	323,010	104,485	AVERAGE	388,745	116,592

Attachment VI

Plan and parameters of the cubes used for microscopic analysis.

3D PRINTING PLAN							
CUBES SAMPLES							
% INFILL	PATTERN	QTT	TIME	TENSILE NUMBER	REF.	WEIGHT (g)	FOTO
100%	Gyroid	3	0,25	1	DA	2,484	
				2	DB	2,49	
				3	DC	2,489	
	Tri Hexagon	3	0,24	1	EA	2,454	
				2	EB	2,467	
				3	EC	2,448	
	Quatercubic	3	0,24	1	FA	2,494	
				2	FB	2,48	
				3	FC	2,49	

Attachment VII

Microscopic Analysis Sintered and non-sintered cubes.
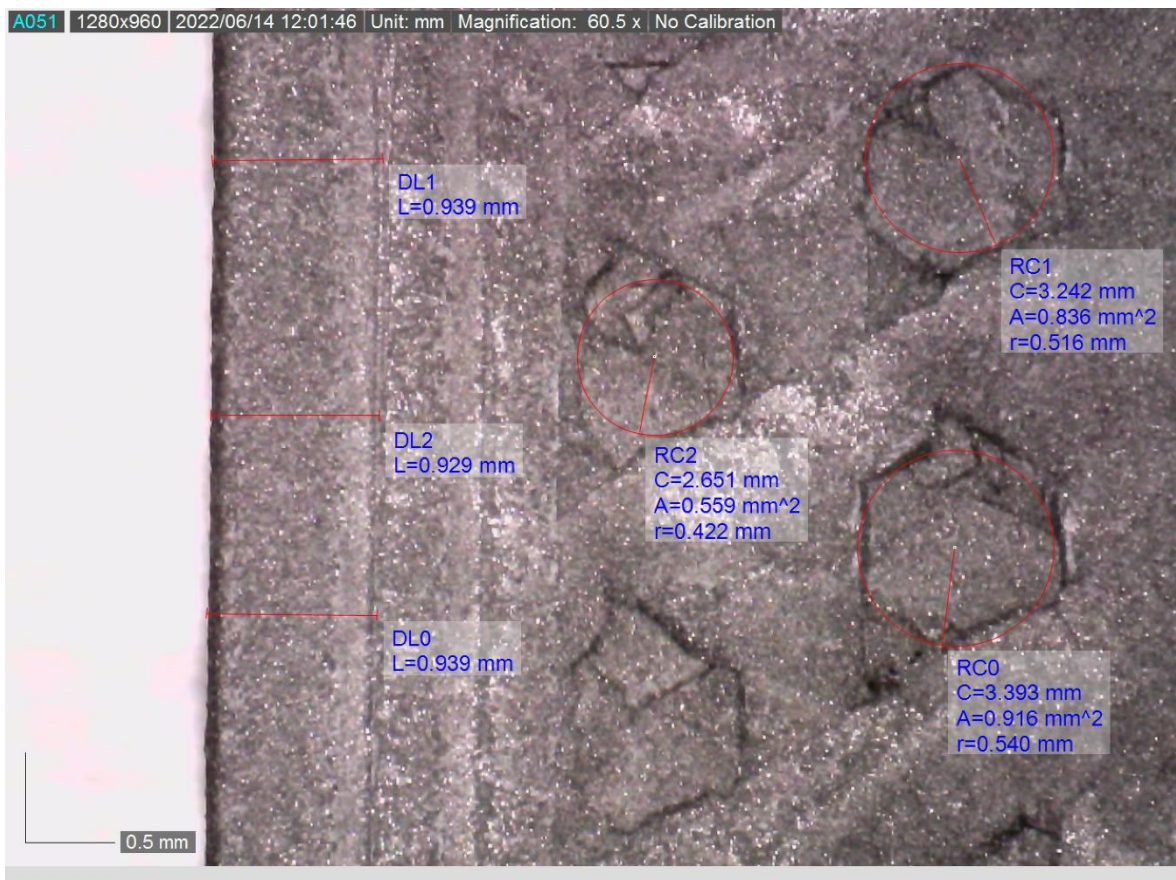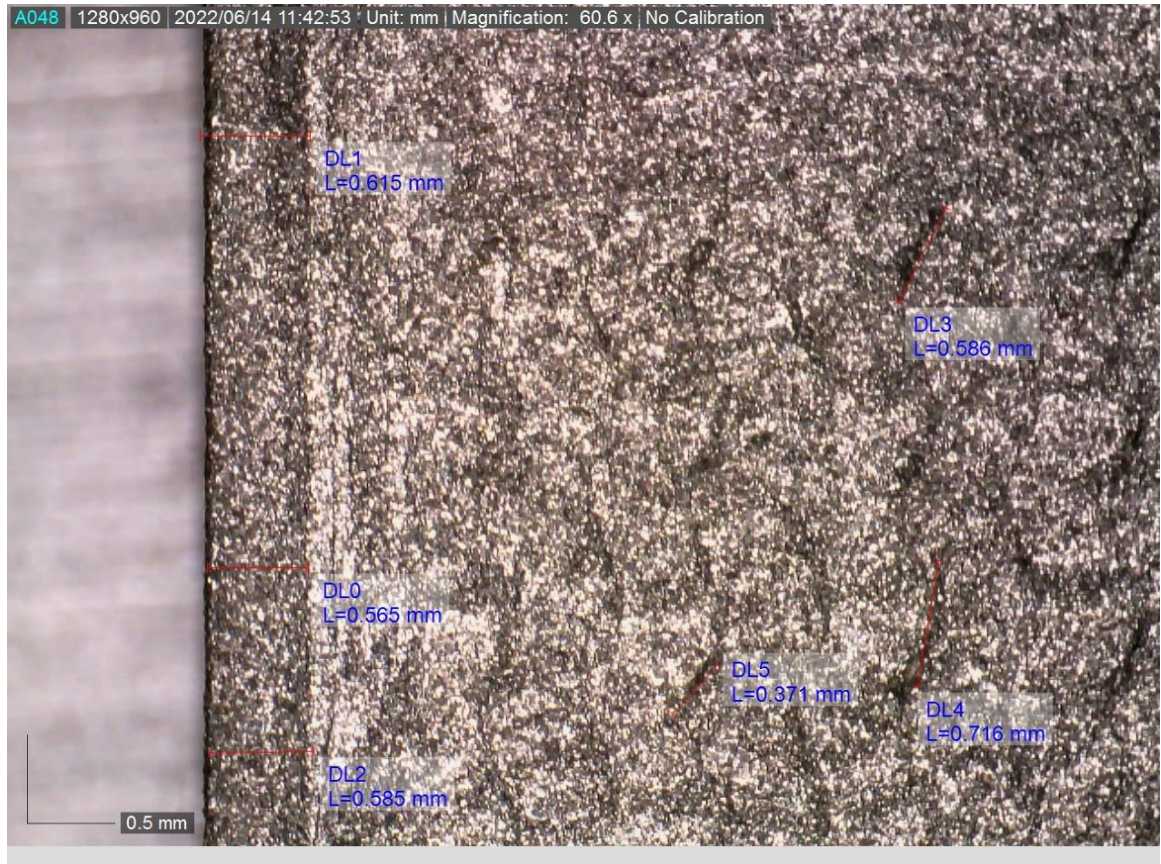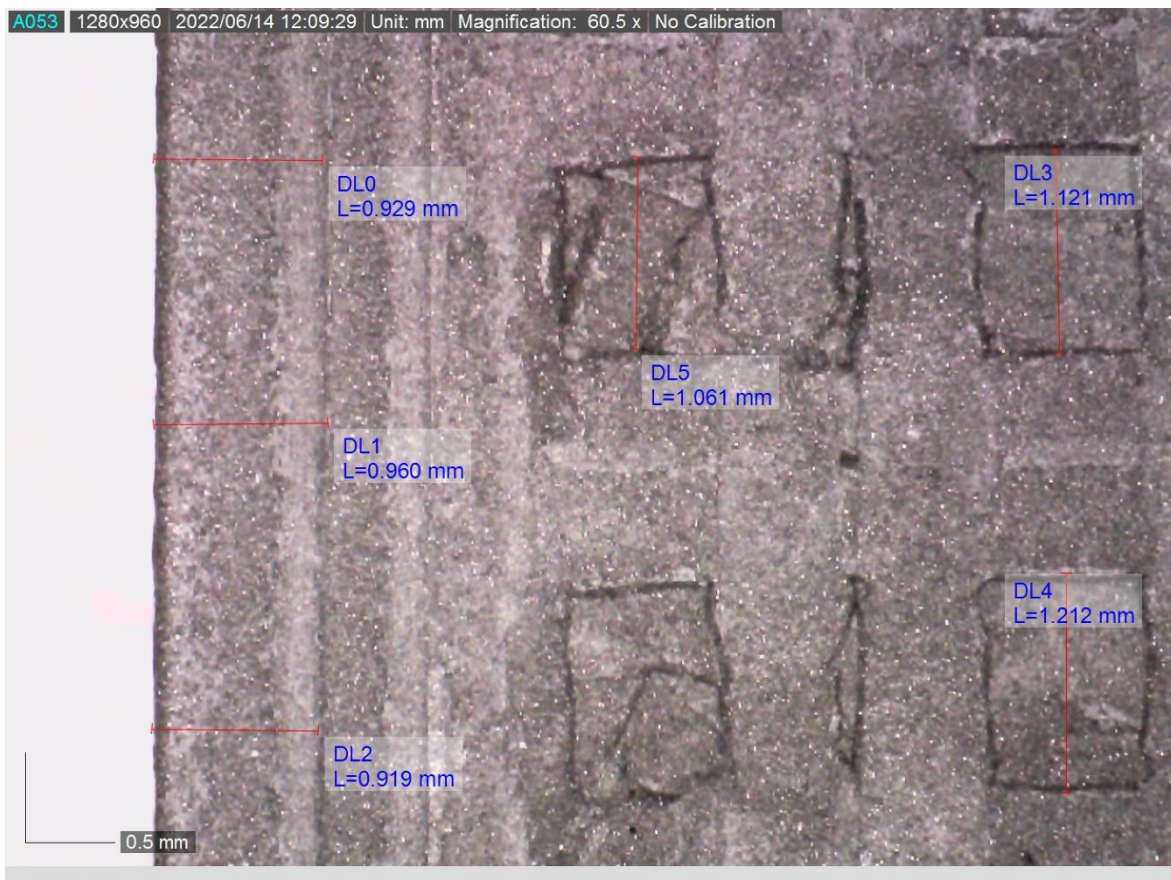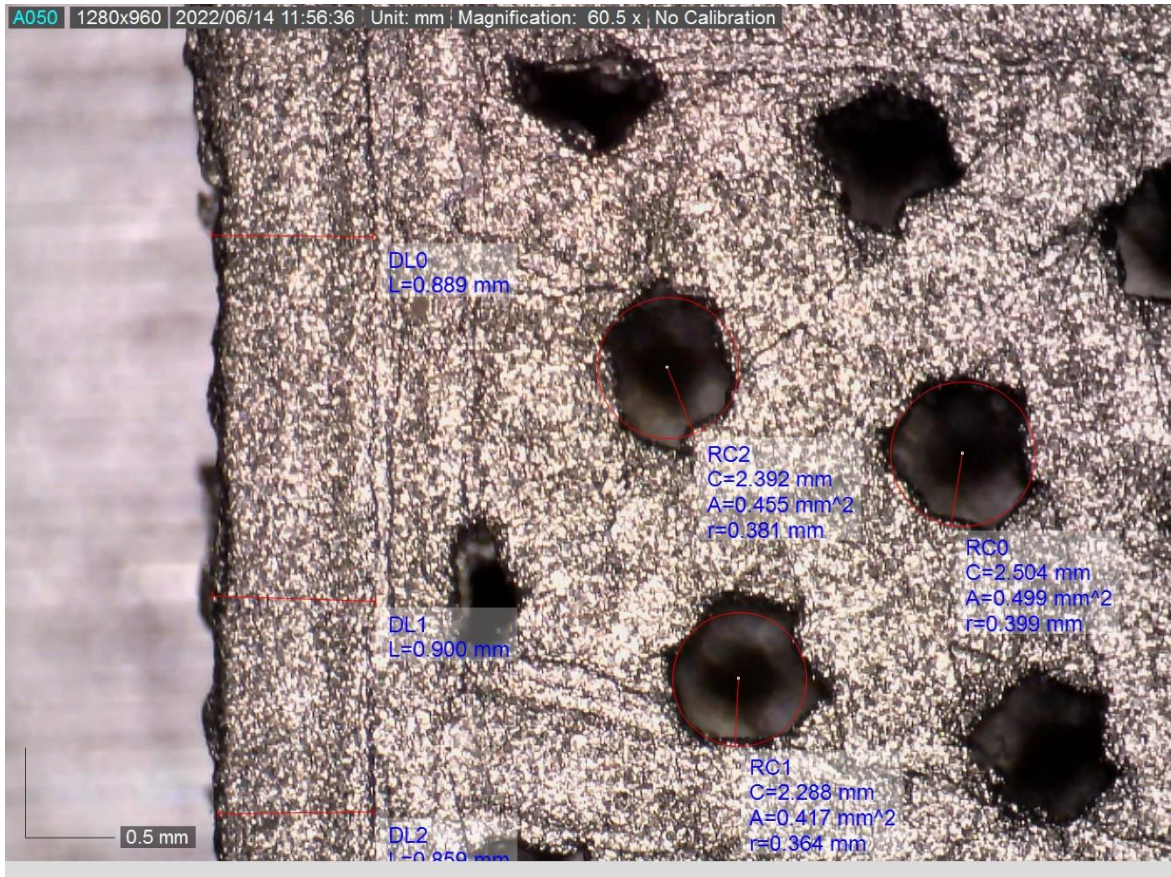
Attachment VIII

Surface roughness results for AA2 sample of Gyroid 60%.

		Prüfprotokoll					ACCRETECH
Seriennummer:		Kommentar		Messdatum	08.07.2022		
Teilenummer		Prüfer	Kalhöfer	Messzeit	08:10:29		
Messbedingung							
Messtyp	Roughness measurement	Cutoff	0,8mm	λs Filter	2,5um		
Berechnungsstandard	ISO1997/2009	Filtermethode	Gaussian	Einheit	mm/um		
Auswertelänge	4,00mm	Messbereich	500,0um				
Messgeschwindigkeit	0,30mm/s	Entfernen der Form	Straight				
Messergebnis							
Pt	37,716	Ra_5	2,720	Rz_5	25,298		
Ra	2,899	Rz	21,822	Rp	8,453		
Ra_1	3,148	Rz_1	19,427	Rp_1	10,599		
Ra_2	3,492	Rz_2	27,921	Rp_2	8,259		
Ra_3	2,369	Rz_3	13,088	Rp_3	7,822		
Ra_4	2,768	Rz_4	23,377	Rp_4	8,908		

Attachment IX

Results obtained in the surface roughness test. Calculation of averages.

SAMPLE TYPE	REF	Ra μm	Ra AVERAGE μm	TOTAL Ra AVERAGE μm	SD μm	Rz μm	Rz AVERAGE μm	TOTAL Rz AVERAGE μm	SD μm
SURFACE ROUGHNESS									
Gyroid 60%	AA	2,744	2,844	3,340	0,360	17,185	20,611	19,468	1,808
		2,899				21,822			
		2,890				22,825			
	AB	3,606	3,658			20,310	19,476		
		3,663				19,912			
		3,706				18,205			
	AC	3,567	3,518			19,074	18,317		
		3,539				17,753			
		3,448				18,125			
Gyroid 80%	AI	3,953	3,693	3,189	0,483	22,690	21,332	20,124	3,122
		3,853				21,885			
		3,273				19,420			
	AJ	2,803	2,982			22,378	22,521		
		3,087				24,560			
		3,057				20,625			
	AM	3,539	2,892			19,405	16,518		
		2,531				14,357			
		2,606				15,793			
Tri-Hexagon 60%	BA	2,837	2,837	2,965	0,205	29,322	22,624	22,469	4,461
		2,841				17,767			
		2,832				20,783			
	BB	2,681	2,826			17,272	18,722		
		2,832				16,199			
		2,965				22,694			
	BC	3,174	3,232			27,167	26,061		
		3,335				25,873			
		3,188				25,143			

SURFACE ROUGHNESS									
SAMPLE TYPE	REF	Ra μm	Ra AVERAGE μm	TOTAL Ra AVERAGE μm	SD μm	Rz μm	Rz AVERAGE μm	TOTAL Rz AVERAGE μm	SD μm
Tri-Hexagon 80%	BH	3,055	3,034	3,040	0,151	22,636	21,264	30,071	9,605
		3,141				22,201			
		2,907				18,956			
	BI	2,706	2,998			21,328	28,559		
		3,251				33,064			
		3,038				31,284			
	BJ	3,136	3,087			45,915	40,391		
		3,136				45,915			
		2,988				29,342			
Quarter Cubic 60%	CA	3,870	3,783	3,906	0,509	28,712	26,841	28,656	2,860
		3,560				25,780			
		3,919				26,031			
	CB	3,708	4,403			35,022	30,217		
		5,012				28,717			
		4,488				26,912			
	CC	3,798	3,533			28,662	28,911		
		3,610				31,736			
		3,190				26,334			
Quarter Cubic 80%	CH	5,722	5,869	4,739	0,868	32,199	32,874	33,275	6,154
		6,494				39,435			
		5,392				26,988			
	CI	3,781	4,169			30,718	31,474		
		4,214				29,986			
		4,511				33,717			
	CJ	4,265	4,178			47,661	35,478		
		3,908				31,316			
		4,361				27,457			

Attachment X

Budget Ultimaker S3

FAVORITANSWER - Consultoria em Engenharia, Lda.

Av. Dr. Mário Soares, Lote 35

2740-119 Porto Salvo

Telefone: 215 815 201

Email: fan3d@amfan3d.com

Nº de Contribuinte: 515575720

Carolina Costa

Orçamento 2022.08.08

Código	Quantidade	Artigo	Preço Unitário	Preço Total
216931	1	Ultimaker S3	3 950,00 €	3 950,00 €
		Transporte		90,00 €
			Sub-total	4 040,00 €
			IVA - 23%	929,20 €
			TOTAL	4 969,20 €